GEOSPHERE

GEOSPHERE, v. 15

https://doi.org/10.1130/GES02014.1

23 figures; 3 tables; 1 set of supplemental files

CORRESPONDENCE: jtrop@bucknell.edu

CITATION: Trop, J.M., Benowitz, J., Cole, R.B., and O'Sullivan, P., 2019, Cretaceous to Miocene magmatism, sedimentation, and exhumation within the Alaska Range suture zone: A polyphase reactivated terrane boundary: Geosphere, v. 15, https://doi.org/10.1130/GES02014.1.

Science Editors: Andrea Hampel, Raymond M. Russo
Guest Associate Editor: James V. Jones, III

Received 27 May 2018
Revision received 16 February 2019
Accepted 15 April 2019

Cretaceous to Miocene magmatism, sedimentation, and exhumation within the Alaska Range suture zone: A polyphase reactivated terrane boundary

Jeffrey M. Trop[1], Jeff Benowitz[2], Ronald B. Cole[3], and Paul O'Sullivan[4]

[1]Department of Geology and Environmental Geosciences, Bucknell University, 701 Moore Avenue, Lewisburg, Pennsylvania 17837, USA
[2]Geophysical Institute and Geochronology Laboratory, University of Alaska Fairbanks, Fairbanks, Alaska 99775, USA
[3]Department of Geology, Allegheny College, 520 N. Main Street, Meadville, Pennsylvania 16335, USA
[4]GeoSeps Services, Moscow, Idaho 83843, USA

ABSTRACT

The Alaska Range suture zone exposes Cretaceous to Quaternary marine and nonmarine sedimentary and volcanic rocks sandwiched between oceanic rocks of the accreted Wrangellia composite terrane to the south and older continental terranes to the north. New U-Pb zircon ages, $^{40}Ar/^{39}Ar$, ZHe, and AFT cooling ages, geochemical compositions, and geological field observations from these rocks provide improved constraints on the timing of Cretaceous to Miocene magmatism, sedimentation, and deformation within the collisional suture zone. Our results bear on the unclear displacement history of the seismically active Denali fault, which bisects the suture zone. Newly identified tuffs north of the Denali fault in sedimentary strata of the Cantwell Formation yield ca. 72 to ca. 68 Ma U-Pb zircon ages. Lavas sampled south of the Denali fault yield ca. 69 Ma $^{40}Ar/^{39}Ar$ ages and geochemical compositions typical of arc assemblages, ranging from basalt-andesite-trachyte, relatively high-K, and high concentrations of incompatible elements attributed to slab contribution (e.g., high Cs, Ba, and Th). The Late Cretaceous lavas and bentonites, together with regionally extensive coeval calc-alkaline plutons, record arc magmatism during contractional deformation and metamorphism within the suture zone. Latest Cretaceous volcanic and sedimentary strata are locally overlain by Eocene Teklanika Formation volcanic rocks with geochemical compositions transitional between arc and intraplate affinity. New detrital-zircon data from the modern Teklanika River indicate peak Teklanika volcanism at ca. 57 Ma, which is also reflected in zircon Pb loss in Cantwell Formation bentonites. Teklanika Formation volcanism may reflect hypothesized slab break-off and a Paleocene–Eocene period of a transform margin configuration. Mafic dike swarms were emplaced along the Denali fault from ca. 38 to ca. 25 Ma based on new $^{40}Ar/^{39}Ar$ ages. Diking along the Denali fault may have been localized by strike-slip extension following a change in direction of the subducting oceanic plate beneath southern Alaska from N-NE to NW at ca. 46–40 Ma. Diking represents the last recorded episode of significant magmatism in the central and eastern Alaska Range, including along the Denali fault. Two tectonic models may explain emplacement of more primitive and less extensive Eocene–Oligocene magmas: delamination of the Late Cretaceous–Paleocene arc root and/or thickened suture zone lithosphere, or a slab window created during possible Paleocene slab break-off. Fluvial strata exposed just south of the Denali fault in the central Alaska Range record synorogenic sedimentation coeval with diking and inferred strike-slip displacement. Deposition occurred ca. 29 Ma based on palynomorphs and the youngest detrital zircons. U-Pb detrital-zircon geochronology and clast compositional data indicate the fluvial strata were derived from sedimentary and igneous bedrock presently exposed within the Alaska Range, including Cretaceous sources presently exposed on the opposite (north) side of the fault. The provenance data may indicate ~150 km or more of dextral offset of the ca. 29 Ma strata from inferred sediment sources, but different amounts of slip are feasible.

Together, the dike swarms and fluvial strata are interpreted to record Oligocene strike-slip movement along the Denali fault system, coeval with strike-slip basin development along other segments of the fault. Diking and sedimentation occurred just prior to the onset of rapid and persistent exhumation ca. 25 Ma across the Alaska Range. This phase of reactivation of the suture zone is interpreted to reflect the translation along and convergence of southern Alaska across the Denali fault driven by highly coupled flat-slab subduction of the Yakutat microplate, which continues to accrete to the southern margin of Alaska. Furthermore, a change in Pacific plate direction and velocity at ca. 25 Ma created a more convergent regime along the apex of the Denali fault curve, likely contributing to the shutting off of near-fault extension-facilitated arc magmatism along this section of the fault system and increased exhumation rates.

INTRODUCTION

Collision and accretion of allochthonous terranes along convergent plate margins are considered to be primary contributors to the expansion of continental crust (Condie, 1998; Cawood et al., 2009; Stern and Scholl, 2010; Tetreault and Buiter, 2014). Island arcs, oceanic plateaus, submarine ridges, seamounts, and continental fragments that are too thick and buoyant to subduct have accreted

to continental margins throughout much of Earth's history (Cloos, 1993; Karabinos et al., 2017). During terrane accretion, a suture zone typically develops between the colliding terrane and the former continental margin. Suture zones are syncollisional features but often also serve as postcollisional zones of crustal weakness prone to reactivation (Hendrix et al., 1996; Holdsworth et al., 2001; Cavazza et al., 2015; Laskowski et al., 2017). Thus, geologic records preserved within suture zones provide an archive of the evolution of tectonic processes in part influenced by inherited and developed lithospheric heterogeneity, including deformation, magmatism, and sedimentation, during and following collision.

Southern Alaska is a prime location to study accretionary tectonic processes given that it consists of a collage of accreted terranes that were added progressively to the former continental margin, and terrane accretion is actively occurring (Coney et al., 1980; Plafker and Berg, 1994; Worthington et al., 2012). In particular, the Alaska Range suture zone is an ideal location to examine the long-term evolution of a collisional boundary that resulted from terrane accretion and was subsequently shaped by diverse processes following collision. The suture zone initially formed from collision and accretion of the Wrangellia composite terrane during Mesozoic time and was reactivated and overprinted during collision of the Yakutat terrane during Cenozoic time (Plafker and Berg, 1994; Trop and Ridgway, 2007). The surface geology reveals a distinct north to south transition from continental crust of the Yukon composite terrane to oceanic crust of the Wrangellia composite terrane (Jones et al., 1982); this transition correlates with variations in geophysical parameters (Veenstra et al., 2006; Saltus et al., 2007; Brennan et al., 2011). Continental-affinity metamorphic and granitoid rocks of the Yukon composite terrane crop out outboard (south) of autochthonous or slightly displaced North American crust (Fig. 1; Foster et al., 1994; Dusel-Bacon et al., 2006; Dusel-Bacon and Williams, 2009). The suture zone juxtaposes these continental rocks with the Wrangellia composite terrane, which includes the Wrangellia, Peninsular, and Alexander terranes. Wrangellia is an assemblage of chiefly late Paleozoic–Jurassic igneous rocks and marine sedimentary strata that originated as an oceanic island arc and evolved into an oceanic plateau (Greene et al., 2008; Israel et al., 2014). The Peninsular terrane is an assemblage of late Paleozoic–Jurassic igneous rocks and marine sedimentary strata interpreted as an accreted oceanic island arc (Rioux et al., 2007). The Alexander terrane consists chiefly of metamorphosed volcanic arc igneous and sedimentary rocks (Berenak et al., 2014). Analysis of geologic data sets indicates the Wrangellia, Peninsular, and Alexander terranes were juxtaposed by late Paleozoic time (Beranek et al., 2014; Israel et al., 2014) and collided with the former continental margin during mid-Jurassic to mid-Cretaceous time (Haeussler, 1992; Kalbas et al., 2007; Manuszak et al., 2007; Gehrels et al., 2009; Hampton et al., 2010; Stevens Goddard et al., 2018).

The mapped surface geology of the Alaska Range suture zone spans a region as much as 100 km wide in the eastern and central Alaska Range and northern Talkeetna Mountains (Fig. 1; Csejtey et al., 1992; Nokleberg et al., 1992a, 1992b; Ridgway et al., 2002). Geophysical data sets indicate that the suture zone is a crustal-scale feature between the Hines Creek fault on the north and the Talkeetna fault on the south (Fig. 1; Brennan et al., 2011), although deformation extends outside the region between these major faults (Ridgway et al., 2002). Originally identified from rock types and deformation patterns at the surface (Jones et al., 1982; Ridgway et al., 2002), geophysical studies demonstrate that the suture zone proper extends through the crust and is bound by significant steps in the Moho. The Hines Creek and Talkeetna faults appear to continue through the crust nearly vertically and extend into the mantle (Brennan et al., 2011), and the Denali fault also appears to vertically offset the Moho 10–15 km (Allam et al., 2017).

The suture zone formed initially as a result of mid-Cretaceous collision of the oceanic Wrangellia composite terrane with the former North American continental margin (e.g., Jones et al., 1982; Ridgway et al., 2002; Hampton et al., 2010). Late Jurassic to Late Cretaceous sedimentary strata (Kahiltna assemblage) exposed between the Hines Creek fault and Talkeetna fault record erosion of both the former continental margin and the accreted oceanic terrane during collision (Ridgway et al., 2002; Kalbas et al., 2007; Hampton et al., 2010). Kahiltna assemblage strata exposed in the central Alaska Range represents a Kimmeridgian–Cenomanian marine basin filled by west-southwestward–flowing submarine deposystems that transported sediment derived from Paleozoic continental margin strata uplifted in the along-strike suture zone (Ridgway et al., 2002; Kalbas et al., 2007; Hampton et al., 2010; Hults et al., 2013; Romero, 2018). Kahiltna assemblage deposits exposed in the northern Talkeetna Mountains represent a Kimmeridgian–Valanginian marine basin that was filled by northwestward-flowing submarine-fan systems that transported sediment derived from the Wrangellia and Yukon composite terrane (Hampton et al., 2010; Hults et al., 2013). A belt of retrograde metamorphism and a regional anticlinorium developed along the continental margin just north of the Hines Creek fault from ca. 115 to ca. 106 Ma, approximately coeval with cessation of widespread deposition in the Kahiltna sedimentary basins (Ridgway et al., 2002). Folding and metamorphism of Kahiltna assemblage strata exposed along the Valdez Creek shear zone in the northern Talkeetna Mountains occurred during Late Cretaceous time (Csejtey et al., 1992; Ridgway et al., 2002). Coeval with metamorphism of Kahiltna basin strata in the southern part of the suture zone was development of a thrust-top basin, the Cantwell basin, which is presently exposed between the Hines Creek and Denali fault systems. Compositional, detrital geochronologic, and geologic mapping data indicate that the ~4 km of Upper Cretaceous nonmarine and marginal marine sedimentary strata in the Cantwell basin record regional subaerial uplift of the suture zone (Ridgway et al., 1997; Trop and Ridgway, 1997).

Following mid- to Late Cretaceous collision and subaerial uplift of the suture zone, continued plate convergence persisted well south of the suture zone and overprinted the suture zone, producing complexly deformed, heterogeneous lithosphere. Latest Cretaceous to Holocene plate convergence included persistent subduction of oceanic crust, including subduction of the Yakutat microplate since ca. 30 Ma (Finzel et al., 2011; Brueseke et al., 2019). The Yakutat microplate is interpreted as an oceanic plateau that has been subducting at a shallow angle beneath Alaska, reaching a maximum geophysically imaged depth of ~100–150 km beneath the Alaska Range (Stachnik et al., 2004; Eberhart-Philips et al., 2006).

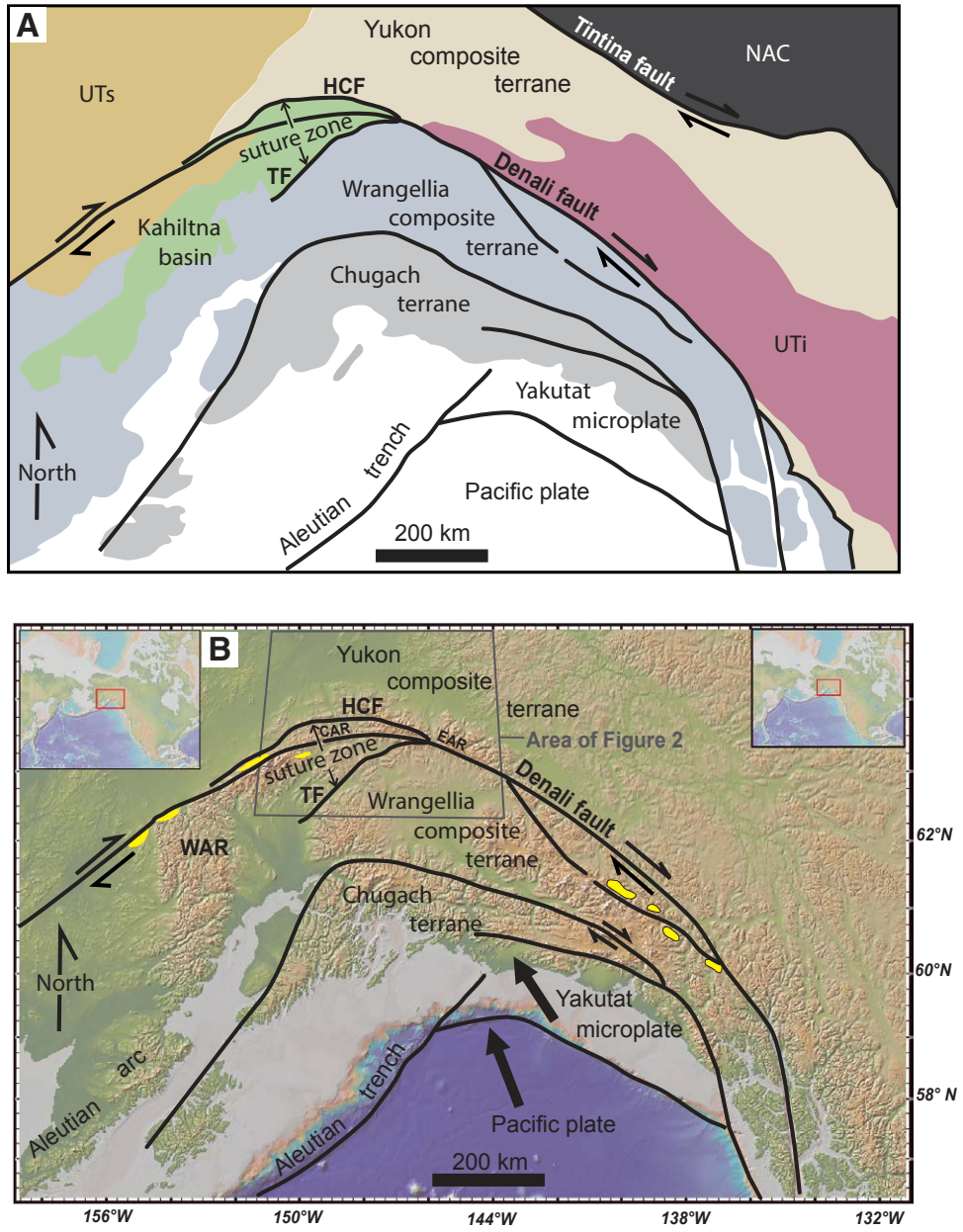

Figure 1. Regional maps of south-central Alaska and adjacent parts of Canada showing major terranes (A) and topography (B). The Alaska Range suture zone is defined as the broad region (>100 km in places) that occurs between oceanic rocks of the Wrangellia composite terrane and continental rocks of the Yukon composite terrane. Yellow polygons represent Eocene–Oligocene sedimentary strata interpreted as strike-slip basins related to dextral slip along the Denali fault (Dickey, 1984; Ridgway and DeCelles, 1993; Trop et al., 2004; this study). Abbreviations: CAR—Central Alaska Range; EAR—Eastern Alaska Range; HCF—Hines Creek fault; NAC—North American continent; TF—Talkeetna fault; WAR—Western Alaska Range; UTi—undifferentiated terranes and igneous rocks; UTs—unidentified terranes and sedimentary rocks. Gray rectangle marks location of Figure 2. Adapted from Brennan et al. (2011) and Fitzgerald et al. (2014).

Latest Cretaceous–Cenozoic sedimentary basins and volcano-plutonic complexes provide a geologic record of the evolution of the suture zone during this more recent, postcollisional tectonic phase (e.g., Cole et al., 1999; Ridgway et al., 2007; Benowitz et al., 2011, 2014; Riccio et al., 2014; Fitzgerald et al., 2014). Along the north flank of the central Alaska Range, deformed Oligocene–Pliocene fluvial-lacustrine sedimentary strata record transpressional foreland basin development (Tanana basin on Fig. 2; Ridgway et al., 2007). Along the south flank of the central and eastern Alaska Range, Oligocene–Miocene fluvial-lacustrine sedimentary strata record strike-slip basin development and deformation related to dextral slip along the Denali fault (Colorado Creek and McCallum basins, Trop et al., 2004; Allen, 2016; Waldien et al., 2018). In the central and eastern Alaska Range and northern Talkeetna Mountains, ca. 72–50 Ma volcanics and intrusions reflect subduction-related arc magmatism and collisional magmatism influenced by slab window or delamination processes (Moll-Stalcup, 1994; Cole et al., 2006b, 2007, 2016). A younger suite of ca. 42–34 Ma intrusions are also attributable to subduction-related processes (Reed and Lanphere, 1973; Moll-Stalcup, 1994; Cole and Layer, 2002; Jicha et al., 2006). Post–25 Ma magmatic products in the Alaska Range suture zone are limited to isolated occurrences of very spatially restricted basaltic rocks (e.g., Buzzard Creek, Jumbo Dome; Andronikov and Mukasa, 2010; Cameron et al., 2015). This essential cessation of Alaska Range suture zone subduction-related magmatism is likely reflecting initiation of shallow subduction of the thick Yakutat microplate at ca. 30 Ma (Eberhart-Phillips et al., 2006; Finzel et al., 2011; Wang and Tape, 2014) under a more convergent plate boundary regime after a plate vector change at ca. 25 Ma (more northerly with a ~52% increase in velocity) (Jicha et al., 2018).

The seismically active Denali fault system bisects the suture zone and extends >2000 km from southwestern Alaska to northwestern British Columbia (Fig. 1; Stout and Chase, 1980; Haeussler et al., 2017a). Stress has been transferred inboard of the Yakutat-Alaska trench leading to increased slip rates along the Denali fault and northwest convergence of southern Alaska across the Denali fault since ca. 30 Ma (Benowitz et al., 2012a, Lease et al., 2016; Haeussler et al., 2017a, 2017b). Previous studies infer as much as ~250–450 km of dextral displacement along the eastern part of the fault system during Cretaceous–Cenozoic time (Nokleberg et al., 1985; Lowey, 1998; Roeske et al., 2012; Benowitz et al., 2012b; Riccio et al., 2014). In contrast, other researchers only allow tens of kilometers of dextral offset along the central part of the fault system based on offset of assumed genetically related geologic units resulting in hundreds of kilometers of Neogene missing slip, if these geological correlations are correct (Reed and Lanphere, 1974; Csejtey et al., 1982).

Intriguingly, Pleistocene slip rates derived from offset glacial features decrease westward along the Denali fault from ~13 mm/yr to ~5 mm/yr indicating the potential bleeding off of slip into vertical tectonics and crustal shortening (Matmon et al., 2006; Mériaux et al., 2009; Riccio et al., 2014; Haeussler et al., 2017a) (Fig. 1). Strain is presently accommodated by active faults and fault-related folds located north and south of the Denali fault (Vallage et al., 2014). A north-verging fold-thrust belt along the north flank of the Alaska Range has deformed parts of the foreland basin (Wahrhaftig, 1958; Bemis et al., 2012, 2015; Koehler et al., 2012; Burkett et al., 2016). Along the south side of the Range, south-verging thrust faults generally splay from the Denali fault at acute angles (Fig. 2; Crone et al., 2004; Trop et al., 2004; Haeussler et al., 2017a; Koehler et al., 2012; Vallage et al., 2014; Bemis et al., 2015).

Recent studies document Cenozoic exhumation pulses within the Alaska Range suture zone using thermochronologic data from igneous intrusions (Fitzgerald et al., 1995, 2014; Perry et al., 2010; Benowitz et al., 2011, 2012a, 2012c, 2014; Riccio et al., 2014) and modern river sediments (Lease et al., 2016). Cretaceous–Cenozoic sedimentary and volcanic rocks exposed within the suture zone also record the geodynamic processes that shaped the tectonic development of the suture zone, including magmatism, exhumation, basin subsidence, shortening, and strike-slip faulting (Cole et al., 1999; Ridgway et al., 2002; Ridgway et al., 2007; Benowitz et al., 2011, 2014; Riccio et al., 2014; Burkett et al., 2016). However, much of the geologic history remains loosely constrained owing to a paucity of analytical data.

This study reports new geochemical and geochronologic data from Upper Cretaceous–Oligocene sedimentary and volcanic rocks and Oligocene dike swarms exposed along the Denali fault in the central and eastern Alaska Range. We also report detrital-zircon data from modern rivers that drain the Alaska Range and thermochronology results from a ca. 70 Ma bentonite that was buried and subsequently unroofed. Collectively, these new data sets place improved constraints on the timing and nature of Cretaceous–Oligocene sedimentation, strike-slip motion, deformation, and magmatism within the suture zone.

FOCUS AREAS AND FIELD OBSERVATIONS

This study focuses on Late Cretaceous–Oligocene sedimentary and volcanic products exposed in the central part of the Alaska Range suture zone (Fig. 3), including three bedrock units that are summarized in the following section: (1) Cretaceous–Oligocene sedimentary and volcanic rocks in the Colorado Creek basin along the south flank of the central Alaska Range; (2) Cretaceous bentonites in the Cantwell basin in the central Alaska Range; and (3) Oligocene dike swarms along the Denali fault in the central and eastern Alaska Range. In this paper, the eastern Alaska Range refers to the area where the Nenana River crosses the Denali fault (~148.48°W longitude, NR on Fig. 2) and the Tok River valley (~144°W); the central Alaska Range refers to the area between the area where the Nenana River crosses the Denali fault and the headwaters of the West Fork of the Yentna River (~152°W).

Colorado Creek Basin

Late Cretaceous–Oligocene sedimentary and volcanic rocks crop out in a <50 km^2 area of the headwaters of the Colorado Creek drainage basin along the south flank of the central Alaska Range, several kilometers south of the Denali fault. The well-exposed stratigraphy has been incorporated into a south-verging fold-thrust belt that parallels the Denali fault (Figs. 4 and 5; Csejtey et al.,

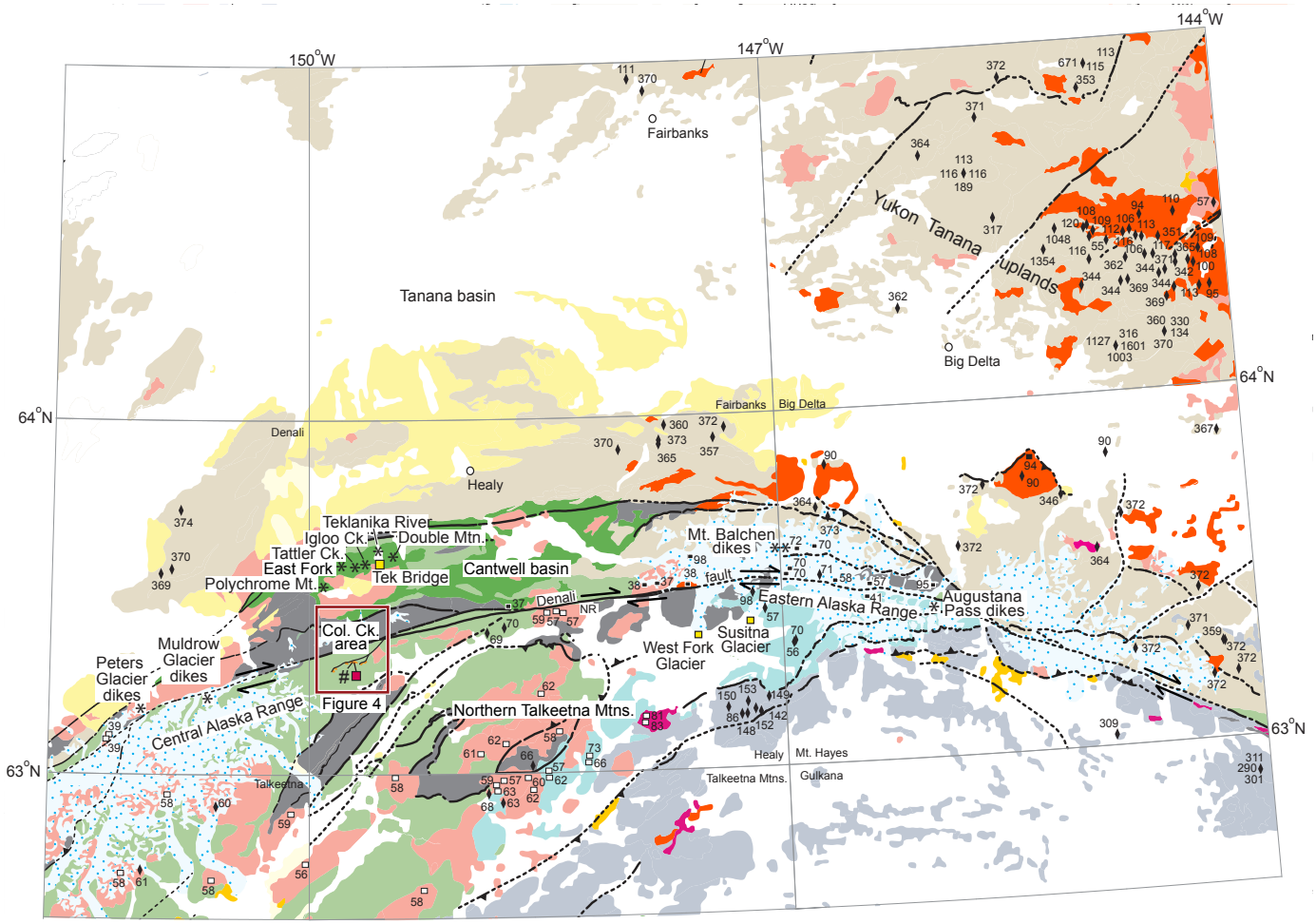

Explanation

- Quaternary deposits/ice
- Neogene nonmarine sed. strata (Usibelli Group, Nenana Gravel)
- Oligocene-Neogene unnamed nonmarine sedimentary strata
- Cretaceous nonmarine sed. strata (lower Cantwell Fm.)
- Jurassic-Cretaceous marine strata (Kahiltna assemblage)
- Paleozoic-Mesozoic sedimentary and igneous rocks (WCT)
- Cretaceous metamorphic and igneous rocks (MGMB)
- Paleozoic-Triassic undifferentiated bedrock
- Paleozoic metamorphic and igneous rocks (YCT)
- Late Cretaceous-Oligocene igneous rocks
- Mid-Cretaceous (Albian-Coniacian, 113-86 Ma) igneous rocks
- Early Cretaceous (Hauterivian-Aptian) igneous rocks

○ Town/City River Fault (exposed) Fault (concealed)

Published geochronologic samples

- 60 ♦ U/Pb bedrock age (Wilson et al., 2015)
- 60 ▪ U/Pb bedrock age (Benowitz et al., 2011; 2016)
- 60 □ U/Pb bedrock age (Cole et al., 2007; 2016)

Geochronologic samples (this study)

- ▫ U/Pb detrital zircon age (river sediment)
- ▪ U/Pb zircon ages (sandstone)
- * Ar/Ar age (Denali fault dikes)
- # Ar/Ar age (Colorado Creek Volcanics - lava)

Figure 2. Generalized geologic map of interior south-central Alaska. Red box highlights Colorado Creek study area. Thin gray lines define 1:250,000 scale quadrangles; quadrangle names are shown in quadrangle corners. U-Pb ages are zircon ages from igneous rocks with the exception of a handful of monazite analyses. Ages of igneous rocks are also constrained by many $^{40}Ar/^{39}Ar$ ages that are not shown for reasons of scale. Refer to Wilson et al. (2015) and references therein for geology and comprehensive database of age data and references.

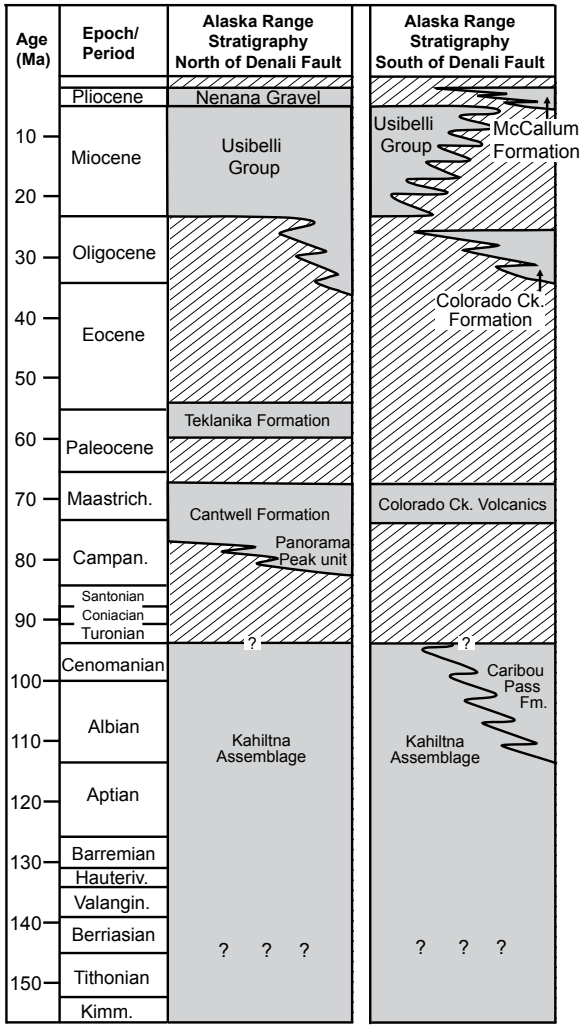

Figure 3. Stratigraphic chart showing age range of Cretaceous–Cenozoic sedimentary and volcanic units in the central and eastern Alaska Range. References: Ridgway et al., 1997, 2002, 2007; Cole et al., 1999; Trop et al., 2004; Hampton et al., 2007; 2010; Hults et al., 2013; Allen, 2016.

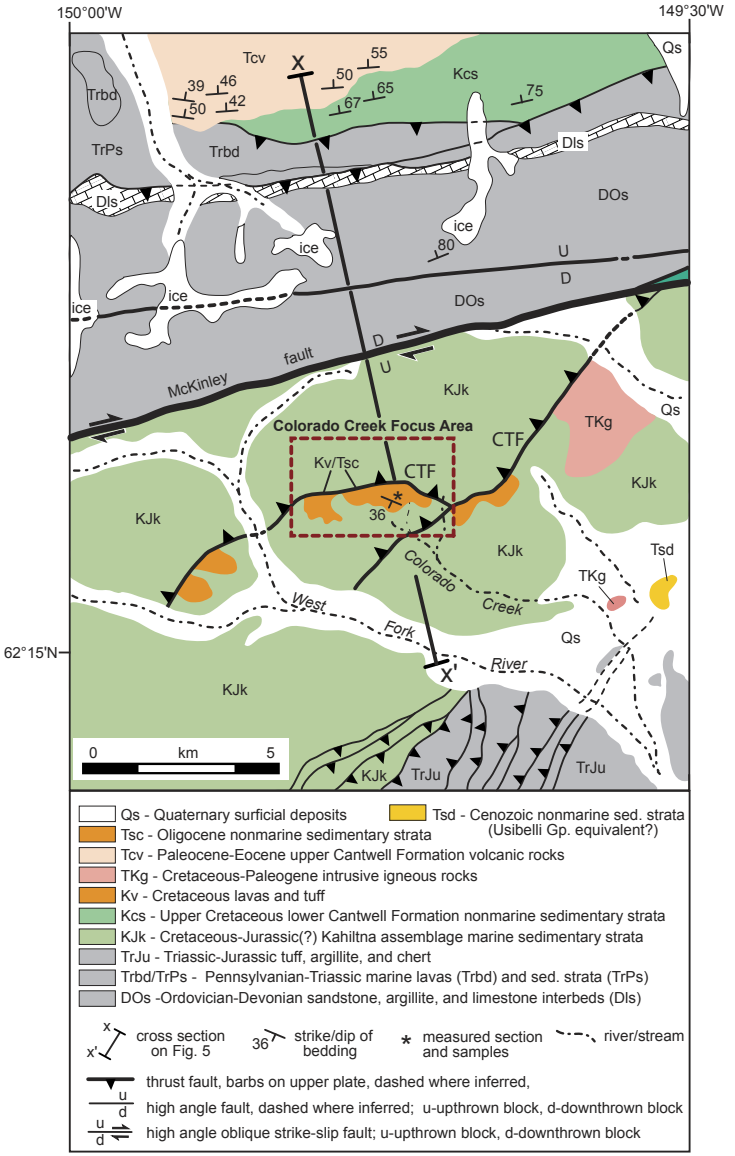

Figure 4. Geologic map of Colorado Creek basin and contiguous area. For reasons of scale, the Colorado Creek volcanics (Kv) and Colorado Creek Formation (Tsc) are combined; refer to Figure 5 for details. CTF—Colorado Creek thrust fault. Geology adapted from Csejtey et al. (1992) and Cole et al. (1999). Refer to Figure 2 for location.

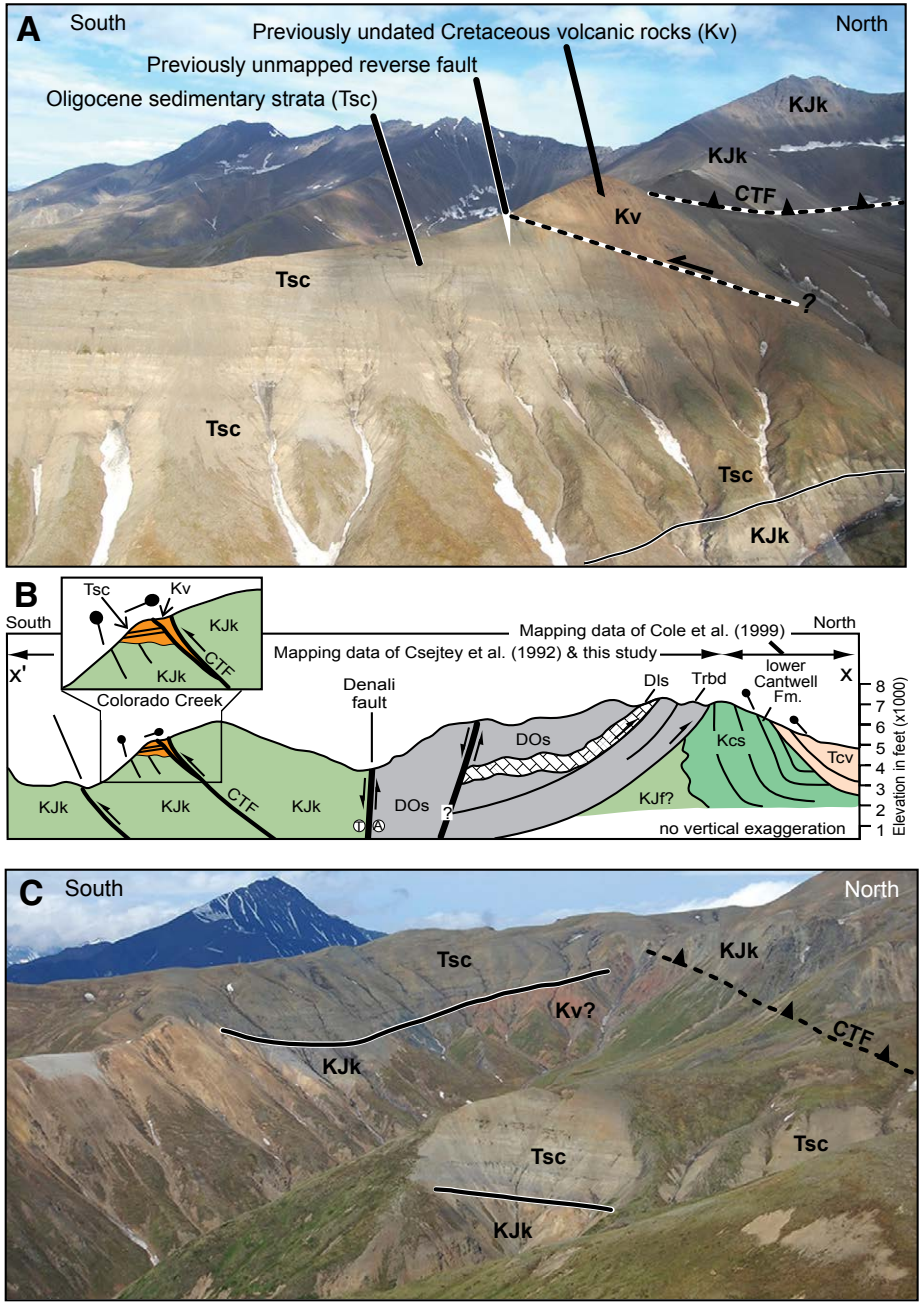

Figure 5. Photographs (A and C) and simplified cross section (B) showing key structural and stratigraphic relationships in the Colorado Creek focus area. Note unconformable relationship between Oligocene sedimentary strata (Tsc) and folded strata of the Cretaceous Kahiltna assemblage (KJk) in the footwall of the Colorado Creek thrust fault (CTF). Also note fault-bound wedge of Cretaceous Colorado Creek volcanics (Kv), which were previously interpreted as Oligocene or younger in age. View is to the west/northwest in both photographs. Refer to Figure 3 for line of cross section and explanation of abbreviations and/or colors. Tadpole symbols on cross section show dip of bedding. Cross section modified from Cole et al. (1999) using field data collected during this study.

1992; Trop et al., 2004). The thrusts occur north of the actively subsiding Susitna basin, which continues to receive sediment eroded from the Alaska Range (Saltus et al., 2016). The oldest stratigraphic succession consists of marine siliciclastic strata assigned to the Cretaceous Kahiltna assemblage. In the Colorado Creek basin (CCB), Kahiltna strata consist of moderately dipping, thin- to thick-bedded, tabular beds of lithic sandstone, pebble-granule conglomerate, and dark-gray to black, mudstone- and shale-bearing marine mollusk fossils (Csejtey et al., 1992; this study; Figs. 6 and 7A–7C). Reconnaissance lithofacies analyses during the present study indicate that these strata were deposited by suspension settling and sediment gravity flows below the routine influence of fairweather waves. This study reports the first detrital geochronologic data from Kahiltna sedimentary strata in the CCB.

Overlying Kahiltna assemblage strata along an angular unconformity is a >300-m-thick succession of gently dipping, siliciclastic sedimentary strata that we refer to in this paper as the Colorado Creek Formation (Fig. 5). These strata consist of amalgamated, lenticular beds of conglomerate and lithic sandstone and more laterally persistent beds of mudstone and carbonaceous shale (Figs. 6 and 7D–7F). Previous lithofacies analyses (Trop et al., 2004) indicate that conglomerate and sandstone lenses were deposited by streamflow in low-sinuosity channel-bar complexes, whereas mudstone and carbonaceous shale record suspension settling, pedogenesis, and accretion of organic matter on bartops and overbank environments. The presence of abundant disseminated organic matter, terrestrial fossil leaves and/or palynomorphs, and minor coal supports deposition in humid fluvial depositional environments. This study reports the first detrital geochronologic data from the Upper Cretaceous–Oligocene sedimentary strata in the CCB.

A >50-m-thick succession of lava and tuff crop out topographically above the Oligocene sedimentary strata along a poorly exposed contact (Figs. 5 and 6). In this report, we refer to the volcanic rocks as the Colorado Creek volcanics. Previous reconnaissance studies inferred that the unnamed volcanic rocks depositionally overlie the topographically lower fluvial strata (Fig. 5; Csejtey et al., 1992; Trop et al., 2004). In this study, we re-interpret the contact as a northwest-dipping thrust fault judging from geological field relationships and new age data that indicate that the volcanic rocks predate the fluvial strata by ~40 m.y. Northwest-dipping thrust faults crosscut all three rock units (Figs. 2–5). The Colorado Creek volcanics consists chiefly of massive, layered, brown-weathering units that locally exhibit vesicular flow tops, indicating emplacement as subaerial lavas. This study provides the first geochronologic and geochemical data from the Colorado Creek volcanics.

Cantwell Basin

The Upper Cretaceous Cantwell Formation is presently exposed along the north flank of the central Alaska Range in a 45-km-wide and 135-km-long outcrop belt referred to as the Cantwell basin (Fig. 2; Ridgway et al., 1997). Most outcrops occur between the Hines Creek fault to the north and the McKinley fault to the south. Cantwell Formation strata unconformably overlie deformed Cretaceous marine strata of the Kahiltna assemblage and older bedrock (Csejtey et al., 1992). The Cantwell Formation consists of two distinct lithologic units, a lower sedimentary unit, and an upper volcanic unit (Wolfe and Wahrhaftig, 1970). The sedimentary unit, sometimes referred to as the lower Cantwell Formation (Ridgway et al., 1997), consists of conglomerate, sandstone, siltstone, mud rock, shale, minor coal, and sparse volcanic rocks that locally exhibit a maximum preserved thickness of ~4000 m (Hickman et al., 1990). Cantwell strata yield diverse fossils, including dinosaur footprints, invertebrate traces, and plant megafossils important for high-latitude ecosystem reconstructions (Fiorillo et al., 2009, 2011, 2012, 2014, 2016; Tomsich et al., 2010, 2014; Fiorillo and Adams, 2012). Lithofacies and paleontological analyses indicate deposition in alluvial, fluvial, lacustrine, and minor marginal marine environments of deposition (Hickman et al., 1990; Ridgway et al., 1997; Tomsich et al., 2014). Biostratigraphic data and U-Pb zircon ages from three volcanic ash layers indicate latest Cretaceous deposition (ca. 80–70 Ma; Ridgway et al., 1997; Tomsich et al., 2014; Salazar-Jaramillo et al., 2016).

Unconformably overlying the Cantwell Formation sedimentary strata is a >3000-m-thick succession of volcanic rocks referred to as the Teklanika Formation (Gilbert et al., 1976) or upper Cantwell Formation (Ridgway et al., 1997; Cole et al. 1999) (Fig. 3). At some locations, the contact between the volcanic and sedimentary successions is an angular unconformity (Gilbert et al., 1976; Cole et al., 1999). The volcanic succession consists of andesite, rhyolite, and basalt flows, subordinate pyroclastic and intrusive rocks, and minor sedimentary rocks. Samples spanning most of the stratigraphic thickness of the succession yield ca. 60 to ca. 55.5 Ma $^{40}Ar/^{39}Ar$ ages, indicating a ca. 10 Ma hiatus during which the Cantwell Formation sedimentary succession was deformed and partly eroded (Cole et al., 1999).

In this paper, we utilize stratigraphic nomenclature proposed by Gilbert et al. (1976) that breaks the Cantwell basin stratigraphy into two formations. The Cretaceous sedimentary strata are referred to as the Cantwell Formation, whereas the overlying Paleocene–Eocene volcanics are referred to as the Teklanika Formation (Fig. 3). Two formations are warranted given that the lithologically distinct and separately mapped volcanic and sedimentary units are separated by an angular unconformity representing millions of years of depositional hiatus (Figs. 3 and 5B; Gilbert et al., 1976, Cole et al., 1999; this study). This study provides geochronologic and thermochronologic data from Cantwell Formation bentonites (Fig. 8) and a modern river that drains Cantwell and Teklanika Formation outcrops (Tek Bridge on Fig. 2).

Denali Fault Mafic Dike Swarms

Mafic dike swarms occur in outcrops along the McKinley segment of the Denali fault in the central and eastern Alaska Range (Fig. 9); most sampled dikes occur within several kilometers of the fault and are truncated by the fault. Sample sites in the central Alaska Range are adjacent to Peter's Glacier and

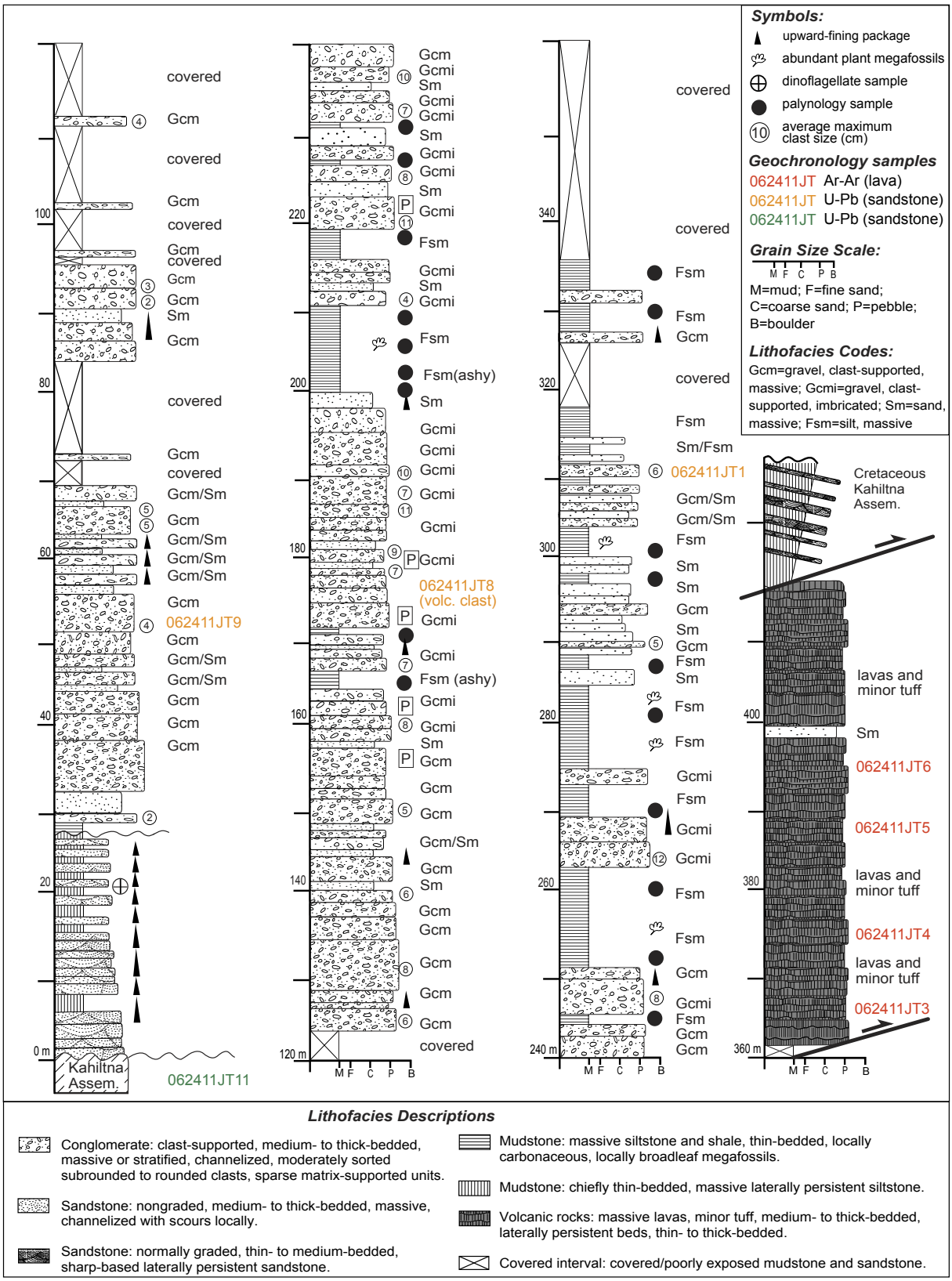

Figure 6. Detailed logs (in meters) of measured stratigraphic section from Colorado Creek showing geochronology and geochemistry samples. Section was measured on a bed-by-bed basis using a Jacob staff. Modified from Trop et al. (2004).

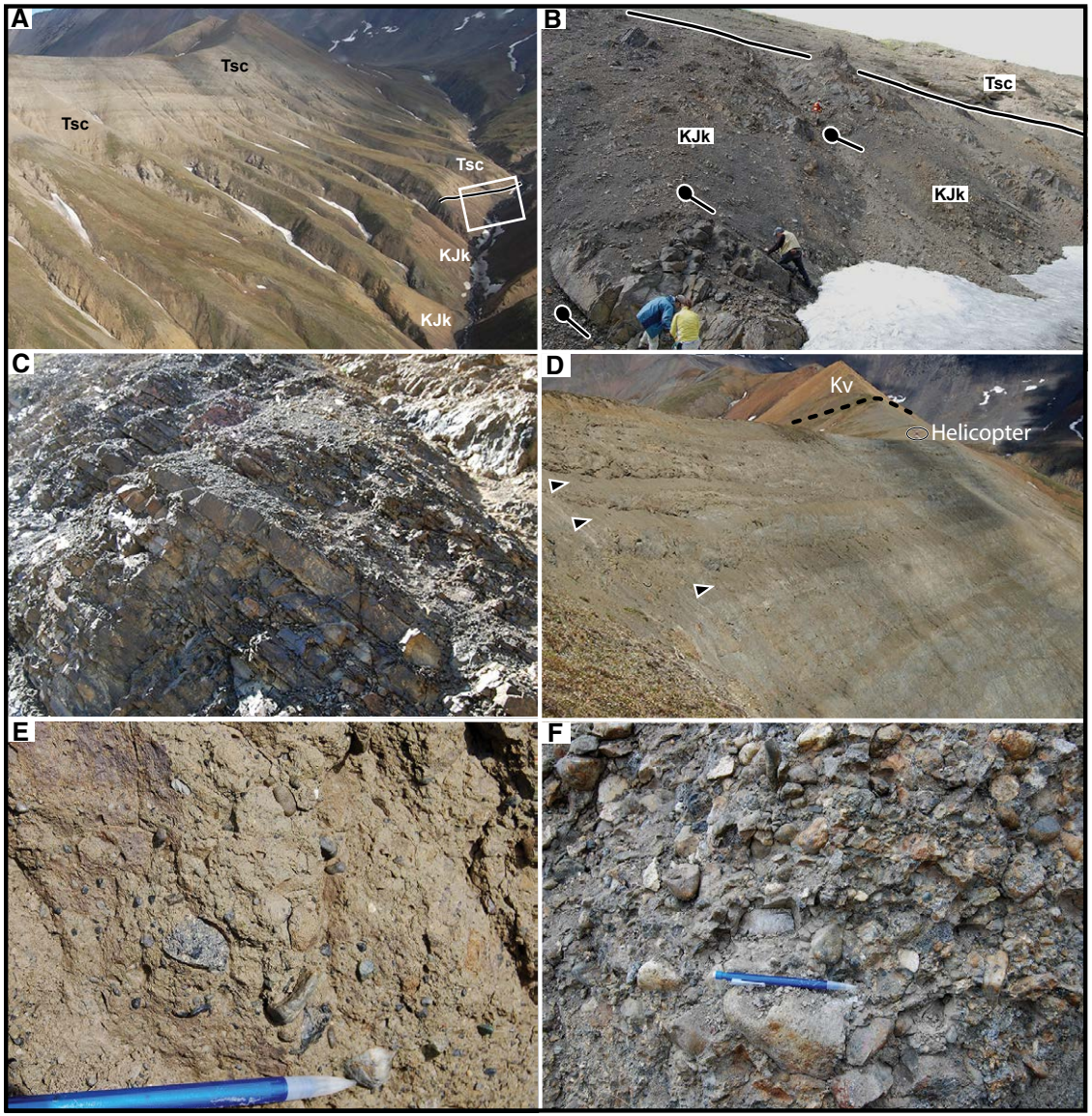

Figure 7. Photographs of Cretaceous Kahiltna assemblage (A–C) and Oligocene Colorado Creek Formation (D–F) in the Colorado Creek area. (A) Unconformable contact between Oligocene fluvial strata (Tsc) and underlying marine strata of the Kahiltna assemblage (KJk). White rectangle (center right) marks contact shown in Figure 7B. View is toward north. (B) Kahiltna assemblage massive sandstone and mudstone unconformably overlain by Oligocene sedimentary strata (Tsc; top right). Black tadpole symbols depict moderate dip of bedding to right (north) in Kahiltna strata. (C) Close-up of interbedded sharp-based sandstone and mudstone in Kahiltna strata shown in Figure 7B. Outcrop is ~2.2 m tall. Strata dip to right (north). (D) Amalgamated packages of broadly lenticular conglomerate and sandstone with sparse mudstone intervals (black arrows). Note irregular bed contacts in conglomerate and sandstone successions that reflect erosive scouring along fluvial channel-bar bases. Helicopter (circled, middle top) for scale. Orange-brown weathering Cretaceous volcanic rocks (Kv) in background. View is toward north. (E) Poorly sorted, matrix-supported conglomerate with subrounded granules and pebbles interpreted as hyperconcentrated flow deposits in shallow, low-sinuosity fluvial channel-bar complexes. (F) Moderately sorted, clast-supported conglomerate with subrounded pebbles and cobbles interpreted as streamflow deposits in shallow, low-sinuosity fluvial channel-bar complexes.

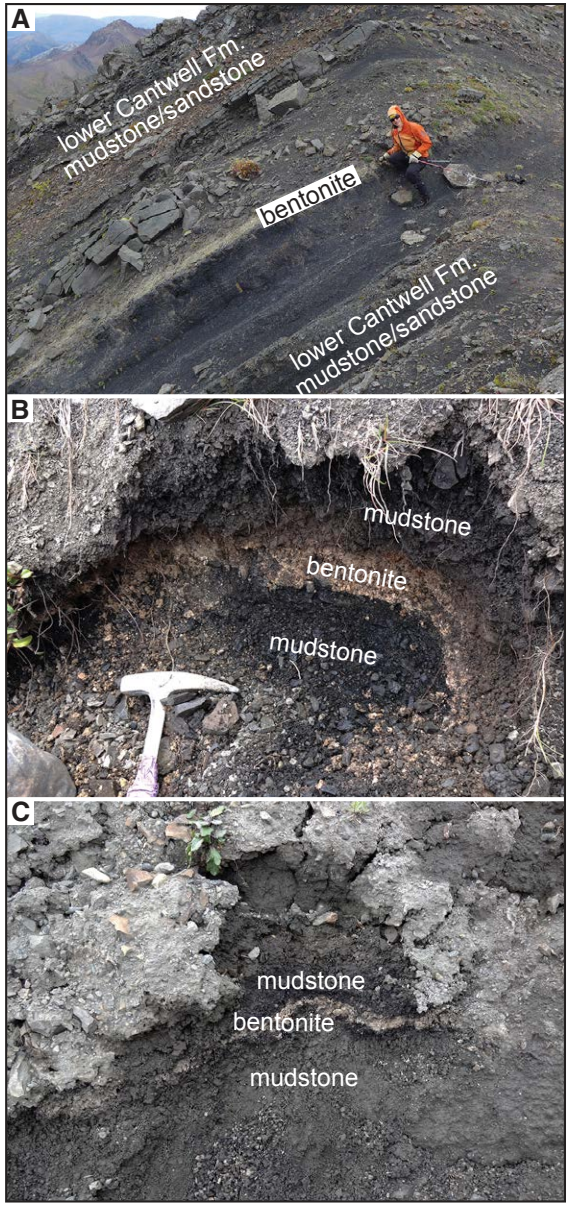

Figure 8. Photographs of thin-bedded, light-colored bentonites sampled for U-Pb zircon geochronology from Cantwell Formation fluvial-lacustrine strata. (A) Igloo Creek. (B) Double Mountain. (C) Polychrome Mountain. Refer to Figure 2 for sample locations.

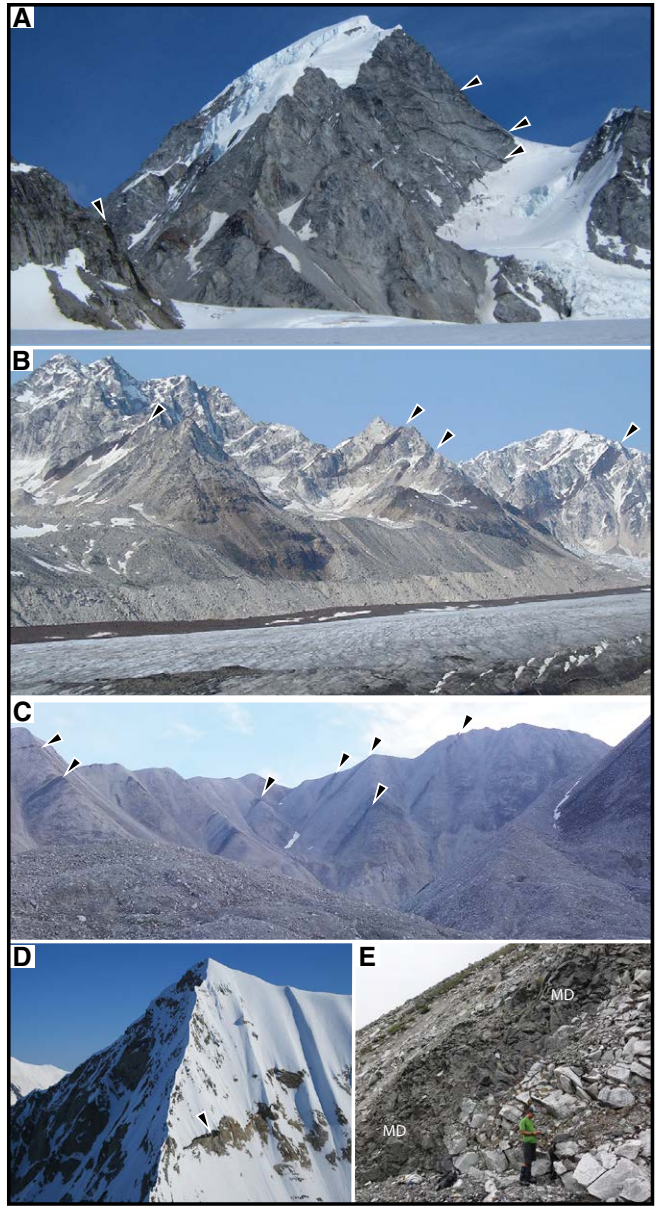

Figure 9. Photographs of mafic dike swarms along the Denali fault in the eastern and central Alaska Range. (A) Mount Balken; (B) Nenana Glacier; (C) Peter's Glacier; (D) Unnamed peak east of Mount Balchen; (E) Gunsight Pass. Black arrows denote the large dikes visible in each photograph. MD—mafic dike.

Muldrow Glacier; sample sites in the eastern Alaska Range are from adjacent to the Nenana Glacier, Mount Balchen, an unnamed peak several kilometers east of Mount Balken, and Augustana Pass (Fig. 2). Although common locally (Fig. 9C), dike swarms are not depicted on published geologic maps for reasons of scale. Generally orientated oblique to and truncated by the Denali fault, individual dikes are <50 m wide and intrude ca. 70–40 Ma plutons (Wilson et al., 2015). This study reports the first geochronologic and geochemical data from these dike swarms.

ANALYTICAL METHODS

Considerable care was taken in the field to collect the freshest possible samples for geochronologic and geochemical analyses. Refer to Supplemental Item A[1] for details on sample sites and Supplemental Item B for details of analytical methods.

For $^{40}Ar/^{39}Ar$ geochronology of lavas and dikes, phenocryst-free whole-rock chips were extracted from samples by traditional methods of crushing, sieving, washing, and handpicking. $^{40}Ar/^{39}Ar$ age determinations were performed by co-author Dr. J. Benowitz at the Geochronology Facility at the University of Alaska Fairbanks. Refer to Supplemental Item B for $^{40}Ar/^{39}Ar$ geochronology methods.

For U-Pb geochronology of bentonite, sandstone, and modern river sand, zircon crystals were extracted from samples by traditional methods of crushing and grinding (for sandstones only), followed by density separation with a Wilfley table and heavy liquids. The resulting heavy-mineral fraction then underwent further separation using a Frantz magnetic separator. Samples were processed such that all zircons were retained in the final heavy-mineral fraction. U-Pb geochronology of individual zircon crystals was conducted by laser ablation–multicollector–inductively coupled plasma mass spectrometry (LA-MC-ICP MS). Zircons from sandstone samples were analyzed by co-author Dr. J. Trop at the Arizona LaserChron Center. Zircons from bentonite and modern river samples were analyzed by co-author Dr. P. O'Sullivan at Washington State University. Refer to Supplemental Item B (footnote 1) for details on U-Pb geochronology methods.

For apatite fission-track analysis (AFT), apatites were separated from a previously dated bentonite (ca. 69.5 Ma U-Pb zircon age; Salazar-Jaramillo et al., 2016) collected along the east side of the East Fork of the Toklat and analyzed by Dr. P. O'Sullivan using the laser ablation–inductively coupled plasma–mass spectrometry (LA-ICP-MS) fission-track method (Hasebe et al., 2004; Donelick et al., 2005) at GeoSep Services. Refer to Supplemental Item B for details on AFT methods. Results were complemented by thermal modeling using the inverse thermal modeling software HeFTy (Ketcham, 2005). HeFTy fits cooling curves to the input criteria using a Monte Carlo randomization. Constraints for modeling the thermal history of the bentonite were the U-Pb zircon time of deposition (ca. 69.5 Ma), burial and resetting during peak Teklanika Formation magmatism (ca. 57 Ma; this study), regional vitrinite reflection analysis (Stanley, 1987), the ZHe and AFT results, and the modern-day temperature. We applied a broad window for the time of burial because we know when the sample was deposited on the surface and when it started to cool rapidly, but we have limited constraints on how deep the sample was buried and for how long.

Zircons were separated from the same previously dated bentonite used for AFT analysis to conduct zircon (U-Th)/He (ZHe). Analysis was performed at the University of Colorado TRAIL laboratory by Dr. J. Metcalf. Refer to Supplemental Item B (footnote 1) for details on AHe methods.

For geochemical analyses of lavas and dikes, fist-sized hand samples were trimmed to remove weathering rinds and powdered using an alumina ceramic mixer mill at Allegheny College. Major-element oxides were determined by X-ray fluorescence and trace elements were determined by inductively coupled plasma mass spectrometry at ALS Global (Vancouver, British Columbia) and Actlabs (Activation Laboratories, Ltd.), Ancaster, Ontario. Major elements were determined on fused glass beads. Trace-element samples were prepared by four-acid digestion and lithium metaborate fusion. The samples with less mineralogical alteration in hand sample were among those selected for geochemical analysis, and these samples typically have less than 5% loss on ignition. But, because there are samples with relatively high loss on ignition (>5%), the major-oxide data presented here are normalized to 100% volatile free (e.g., Johnson et al., 1999).

GEOCHRONOLOGY RESULTS

Colorado Creek Volcanics

We report $^{40}Ar/^{39}Ar$ ages from four lavas spanning the exposed stratigraphic thickness of the Colorado Creek volcanics (Figs. 5 and 6). Sampled lavas are massive, aphanitic, brown-weathering units; some exhibit vesicular-flow tops. The lavas yield $^{40}Ar/^{39}Ar$ ages that range from ca. 68 to ca. 71 Ma (Table 1 and Fig. 10). Refer to Supplemental Items C and D (footnote 1) for analytical data, plots, and details on age determinations. The weighted average age of the four $^{40}Ar/^{39}Ar$ analyses is 68.7 ± 1.8 Ma (mean square of weighted deviates [MSWD] = 3.7) (Fig. 10B). The weighted average age of the youngest three $^{40}Ar/^{39}Ar$ analyses is 68.4 ± 0.9 Ma (MSWD = 1.1) (Fig. 10B). This age best represents the timing of this eruptive volcanic episode.

As outlined above, the Colorado Creek volcanics were previously interpreted as early Oligocene or younger (<34 Ma) based on their position topographically above early Oligocene sedimentary strata. However, the contact between the sedimentary and volcanic units is covered by slumped talus; note the covered interval on the measured stratigraphic section shown in Figure 5. These field relations, together with the latest Cretaceous whole-rock ages, suggest that the contact is northwest-dipping thrust fault (Figs. 5 and 6). The fault may represent an imbricate of a better exposed northwest-dipping thrust that splays from the Denali fault at an acute angle (CTF on Figs. 4 and 5).

Data Repository Item A - Sample location information

Sample name	Sample location	Lat (°N)	Long (°W)	Elevation (meters)
Colorado Creek lavas				
062411JT7	Colorado Creek	63.31595	149.73285	-
062411JT6	Colorado Creek	63.31445	149.73033	-
062411JT5	Colorado Creek	63.31346	149.72993	-
062411JT4	Colorado Creek	63.31253	149.73018	-
062411JT3	Colorado Creek	63.29566	149.73020	-
Cantwell Formation bentonites				
East Fork East Bank	East Fork Toklat River	63.5745	149.8315	956
East Fork West Bank	East Fork Toklat River	63.5961	149.8941	869
East Fork West Bank (Pb loss)	East Fork Toklat River	63.5961	149.8941	869
Brown Ash	Tattler Creek	63.5806	149.6857	1461
White Ash	Tattler Creek	63.5806	149.6857	1464
01LTC	Igloo Creek	63.5733	149.6343	1035
02LTC	Igloo Creek	63.5818	149.6434	1275
03LTC	Igloo Creek	63.5857	149.6606	1504
03POLY	Polychrome Mountain	63.5423	149.9058	1348
01DDB	Double Mountain	63.6104	149.4858	1284
01DDB (Pb loss)	Double Mountain	63.6104	149.4858	1284
03DDB	Double Mountain	63.6088	149.4820	1434
04DDB	Double Mountain	63.6081	149.4819	1450
05DDB	Double Mountain	63.6076	149.4816	1480
Colorado Creek sandstones				
062411JT1	Colorado Creek	63.3067	149.7329	-
062411JT8 (igneous clast)	Colorado Creek	63.3066	149.7318	-
062411JT9	Colorado Creek	63.3067	149.7302	-
062411JT11	Colorado Creek	63.3081	149.7239	-
Mafic dikes near Denali Fault				
28CM20 WRIL1	Foraker Glacier	63.0514	151.3755	2253
03PETER WRIL1	Peter's Glacier	63.1677	151.1632	2472
34PETER WRIL1	Peter's Glacier	63.2052	150.9168	1519
25PETER WRIL1	Peter's Glacier	63.2056	150.9151	1529
30PETER WRIL1	Peter's Glacier	63.2361	150.7383	2002
50NEN WRIL1	Nenana Glacier	63.5268	147.7665	1369
02BAL WRIL1	Mount Balchan	63.6169	146.8887	2273
07BAL WRIL1	Mount Balchan	63.6201	146.9245	2092
28BAL WRIL1	Mount Balchan	63.6139	146.8696	2693
10SIGDIKE WRIL1	Peak east of Mount Balchan	63.6110	146.7878	2825
J809MUD	Muldrow Glacier	63.2054	150.8519	-
J810MUD	Muldrow Glacier	63.2050	150.8382	-
J815AMUD	Muldrow Glacier	63.2436	150.6471	-
J84UG	Augustana Pass	63.4349	145.9843	-
Related, previously dated volcanic rocks				
Sugarloaf volcano rhyolite	Sugarloaf Mountain	63.7517	148.7900	1117
05JNG36A dacite		64.0000	148.5702	970
Modern detrital sand				
01TEK	Teklanika River at Park Road Bridge	63.6357	149.5611	820
Susitna Glacier	Susitna Glacier terminus	63.4191	147.2222	818
West Fork Glacier	West Fork Glacier terminus	63.1496	147.5154	805

Note: datum WGS84 for all samples

[1]Supplemental Items. Sample locations, analytical details, geochronologic data/plots, and geochemical data/plots. Please visit https://doi.org/10.1130/GES02014.S1 or access the full-text article on www.gsapubs.org to view the Supplemental Items.

TABLE 1. SUMMARY OF $^{40}Ar/^{39}Ar$ ANALYTICAL RESULTS FROM COLORADO CREEK VOLCANIC ROCKS

Sample name	Phase analyzed	Integrated age (Ma)	Plateau age (Ma)	Plateau information	Isochron age (Ma)	Isochron information	Supplemental figure (see text footnote 1)
062411JT03	Biotite	69.5 ± 0.7	**69.9 ± 1.1**	3 of 7 fractions 86.6 % ^{39}Ar release MSWD = 2.39	—	—	Item D-A
062411JT04	Whole-rock	67.2 ± 0.5	**68.1 ± 0.7**	3 of 7 fractions 93.1% ^{39}Ar release MSWD = 2.18	—	—	Item D-B
062411JT05	Biotite	70.6 ± 0.8	**70.8 ± 1.2***	6 of 7 fractions 99.4% ^{39}Ar release MSWD = 2.56	71.9 ± 0.9	6 of 7 fractions $^{40}Ar/^{36}Ar_i$ = 305.8 ± 55.0 MSWD = 1.98	Item D-C
062411JT06	Whole-rock	67.0 ± 0.6	**68.2 ± 0.7**	4 of 7 fractions 95.7% ^{39}Ar release MSWD =2.21	—	—	Item D-D

Note: Preferred age determination in bold.
*Does not meet the criteria of a plateau age. Weighted average age reported. MSWD—mean square of weighted deviates.

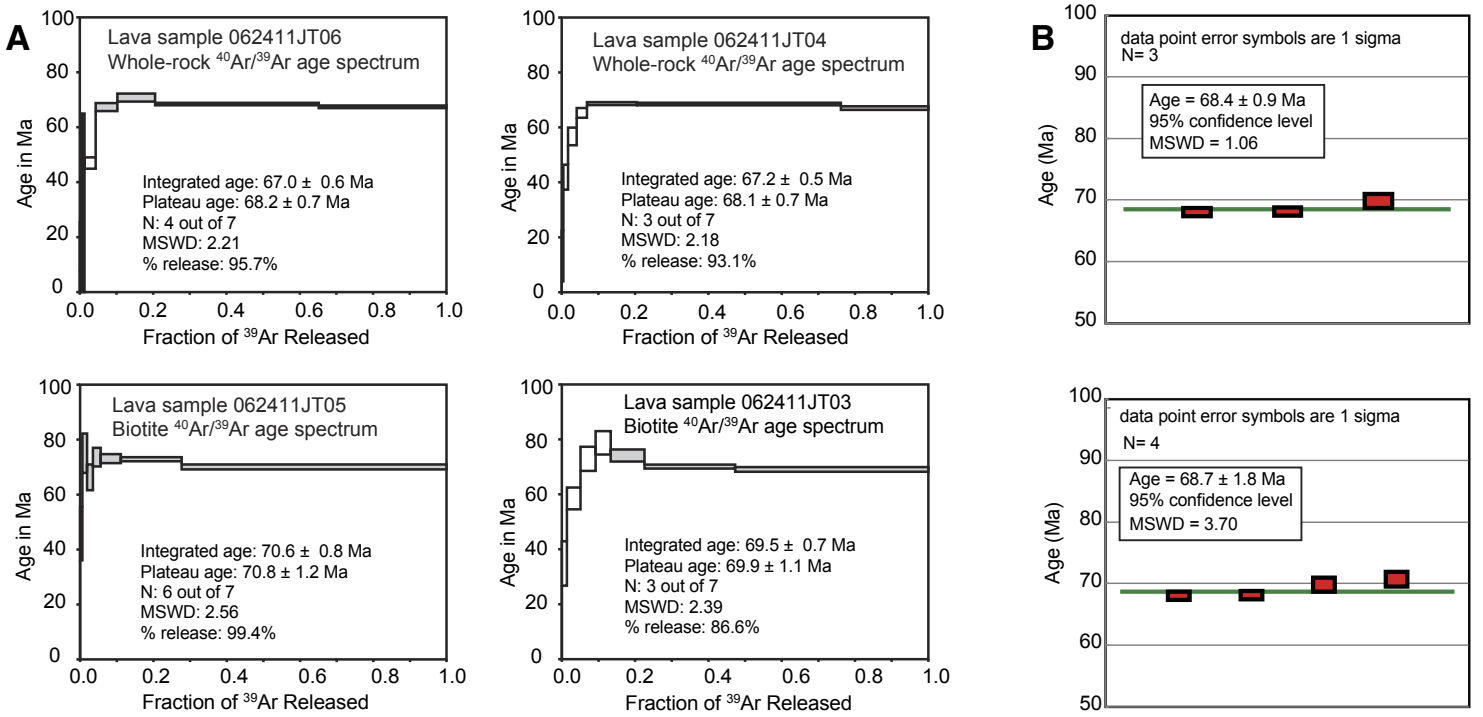

Figure 10. (A) Age spectrum for $^{40}Ar/^{39}Ar$ age samples of Colorado Creek volcanics. Plateau ages (tp) are quoted for all samples. (B) Weighted average plots of $^{40}Ar/^{39}Ar$ age samples of the Colorado Creek volcanics shown in Figure 10A. See text for discussion. MSWD—mean square of weighted deviates.

Cantwell Formation Bentonites

We report geochronologic data from nine bentonite samples from Cantwell Formation strata in the northwestern Cantwell basin (Fig. 2). Sampled bentonites are <5-cm- to ~15-cm-thick, brown- to yellow-weathering altered tuffs. Cantwell Formation bentonites typically consist of clay, mainly montmorillonite with minor illite and chlorite, and minor zircon, apatite, altered feldspars, and volcanic glass (Tomsich et al., 2014; Salazar Jaramillo et al., 2016). Refer to Supplemental Item E for analytical data. Eight of the nine new samples yield U-Pb zircon ages that range from ca. 68 to ca. 71 Ma (Table 2 and Fig. 11). These ages overlap three previously reported ages from Cantwell Formation bentonites (Fig. 12; Tomsich et al., 2014; Salazar-Jaramillo et al., 2016).

A ninth bentonite sample yields a ca. 88 Ma U-Pb zircon age (West Bank of the East Fork River on Fig. 11), which is substantially older than other bentonite ages from this study and previous studies. This older age may indicate a potentially older depositional age for part of the Cantwell Formation; the age of initial deposition has been interpreted as ca. 84 Ma based on the presence of early Campanian pollen and spores at other localities (Ridgway et al., 1997). A lithologically similar but more deformed sedimentary unit near Panorama Mountain (Fig. 2) yielded a maximum depositional age of ca. 84 Ma judging from the youngest detrital-zircon U-Pb ages (Huff, 2008). Alternatively, the ca. 88 Ma zircons could represent recycled grains that are not representative of the timing of primary volcanism and/or deposition.

Two of the Cantwell Formation bentonite samples yield a subset of younger grains indicative of Pb loss at ca. 57 Ma (Figs. 12 and 13). Single-grain ICP-MS analyses permit recognition of Pb loss and resultant younger than depositional ages by the presence of young zircon age tails (Gehrels, 2014). Given that Cantwell Formation bentonites are associated with dinosaur remains (Fiorillo et al., 2014; Tomsich et al., 2014) and other fossils restricted to the Cretaceous (Ridgway et al., 1997; Fiorillo et al., 2009), there is also independent confirmation that ca. 57 Ma zircon grains are younger than the eruptive age for these ash-fall deposits and that Pb loss is likely responsible for the anomalously young single-grain U-Pb zircon ages. Pb loss may occur during fluid flow with temperatures as low as ~300 °C (Cherniak and Watson, 2001), conditions expected in a volcanic province that typified the Cantwell basin during Paleocene–Eocene time (Cole et al., 1999). We have no images of the zircons dated, nor evidence of a correlation between U or Th and age, and concordance cannot be used to determine if Pb loss occurred due to the young age of these samples and the linear nature of the concordia plot for young samples. We infer Pb loss was due to hydrothermal fluid leaching of Pb (Geisler et al., 2002) but acknowledge the anomalously young grains may have defects allowing fast diffusion pathways given our lack of zircon image documentation. Adding further support to these ca. 57 Ma zircon grains reflecting Pb loss related to volcanic processes is the fact that the ca. 57 Ma age represents the time of peak Teklanika Formation magmatism in the Cantwell basin (Cole et al., 1999; this study).

ZHe and AFT Results—Cantwell Formation Bentonite

We present thermochronologic data from a Cantwell Formation bentonite along the East Fork of the Toklat River in the northwestern part of the Cantwell basin (Fig. 2). The bentonite was deposited ca. 69.5 Ma judging from U-Pb zircon data (Table 2). Three single-grain ZHe ages from the bentonite sample yielded an average age of ca. 45.7 Ma with a standard deviation error of 8.76. Apatites

TABLE 2. SUMMARY OF U/Pb ZIRCON ANALYTICAL RESULTS FROM CANTWELL FORMATION BENTONITES

Sample name	Location name	Mean weighted U/Pb age (Ma)	MSWD	No. of zircons used for age calculation	Total no. of zircons analyzed	References
East Fork East Bank	East Fork Toklat River	69.5 ± 0.7	2.0	46	54	Salazar-Jaramillo et al., 2016
East Fork West Bank	East Fork Toklat River	88.0 ± 0.4	1.0	61	112	This study
East Fork West Bank (Pb loss)	*East Fork Toklat River*	*58.2 ± 1.1*	*0.8*	*5*	*112*	*This study*
Brown Ash	Tattler Creek	71.5 ± 0.9	1.3	38	54	Tomsich et al., 2014
White Ash	Tattler Creek	71.0 ± 1.1	1.8	22	54	Tomsich et al., 2014
01LTC	Igloo Creek	68.8 ± 0.5	1.0	42	112	This study
02LTC	Igloo Creek	68.0 ± 0.4	0.8	65	109	This study
03LTC	Igloo Creek	67.8 ± 0.2	1.0	78	100	This study
03POLY	Polychrome Mountain	68.0 ± 0.5	1.0	40	111	This study
01DOB	Double Mountain	69.6 ± 0.7	1.1	31	101	This study
01DOB (Pb loss)	*Double Mountain*	*57.1 ± 1.2*	*1.2*	*7*	*101*	*This study*
03DOB	Double Mountain	70.2 ± 1.0	1.0	10	63	This study
04DOB	Double Mountain	70.4 ± 0.9	1.0	11	102	This study
05DOB	Double Mountain	70.8 ± 0.4	1.0	65	112	This study

Notes: East Fork Toklat (West Bank) and 01DOB1 yield a subset of younger ages interpreted to have experienced lead loss; these younger grains are reported separately and highlighted in italics and gray background.

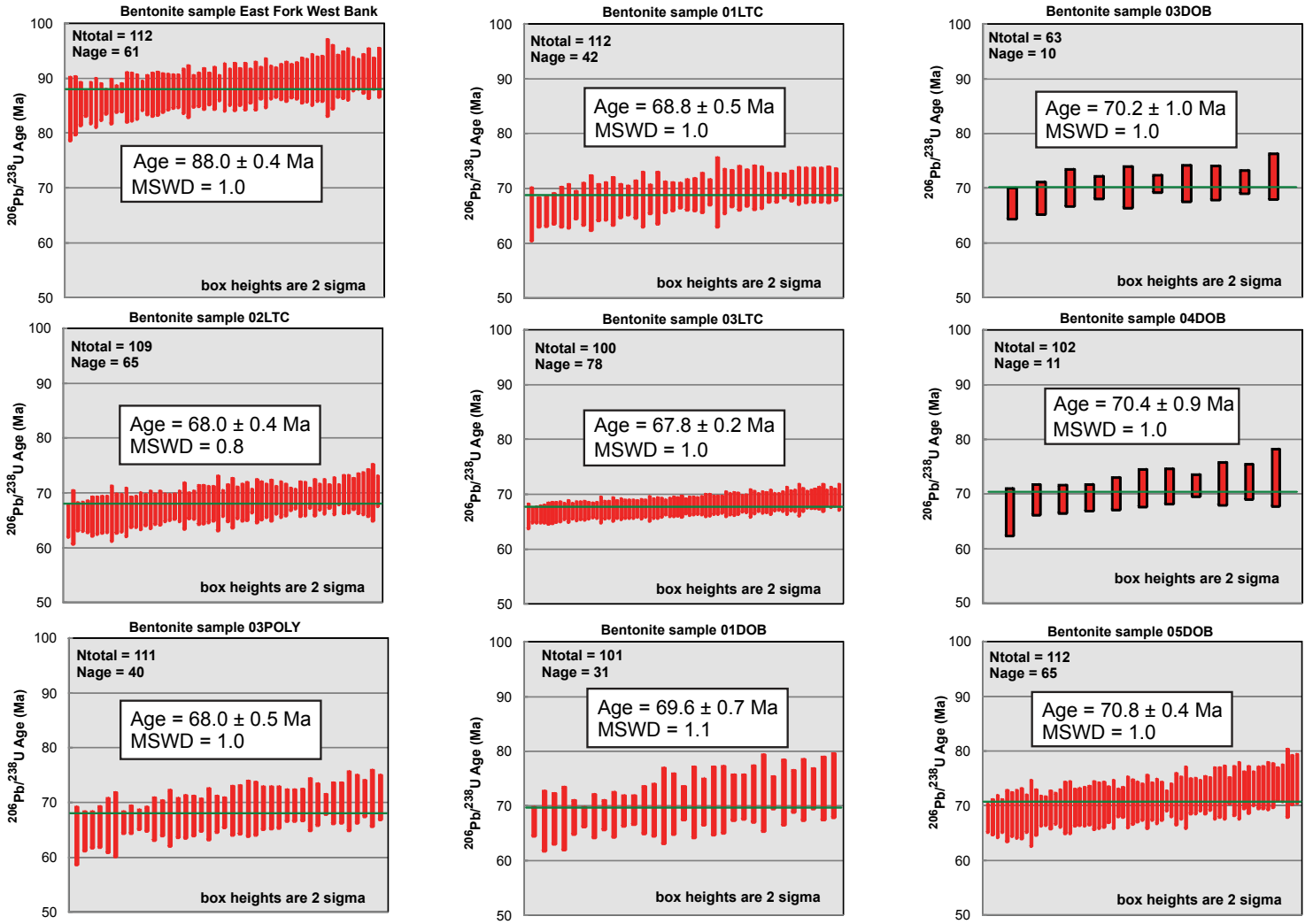

Figure 11. Weighted average plots showing concordant zircons from Cantwell Formation bentonites. Zircons plotted are interpreted as reflecting age of ash eruption/deposition. Age determinations represent laser ablation–inductively coupled plasma–mass spectrometry (LA-MS-ICP) analyses from individual zircons. Green bars represent weighted-mean U-Pb ages. Nage—total number of concordant zircons used for age determination. Ntotal—total number of zircons analyzed in bentonite sample. MSWD—mean square of weighted deviates. Data plotted in Isoplot (Ludwig, 2008).

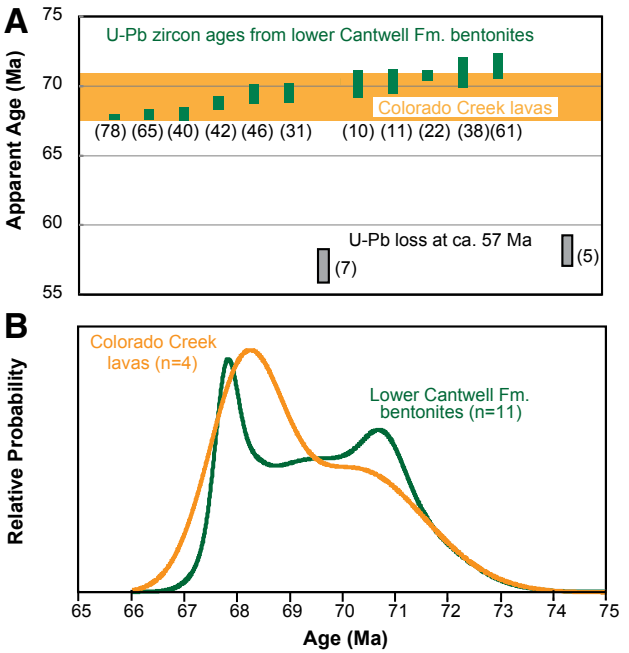

Figure 12. Weighted means (A) and probability plots (B) showing overlapping age range of Cantwell Formation bentonites (green) and Colorado Creek volcanics (orange). Numbers in parentheses represent the number of zircon grains used in the age calculation for bentonites. Refer to Figures 10 and 11 for detailed age plots.

from the bentonite sample yielded an AFT age of 9.42 (–2.9, +4.3) Ma. Refer to Supplemental Items F and G (footnote 1) for analytical data. Figure 14 shows results of HeFTy modeling of the AFT data and other constraints discussed above, providing insight on the history of basin burial and inversion. The sample was at the surface at ca. 69.5 Ma and was buried during Paleocene–Eocene time. Burial temperatures were reached high enough to fully reset the ZHe (~180 °C; Reiners et al., 2005) and AFT (~110 °C; Reiners et al., 2005) systems, implying >6 km of burial assuming a 30 °C/km geothermal gradient. By ca. 46 Ma, the Cantwell basin was inverting or the regional geothermal gradient had dropped significantly enough to close the ZHe system in the bentonite sample. Based on HeFTy modeling of the AFT results, by ca. 20 Ma, the Cantwell basin was being unroofed.

Colorado Creek Formation Detrital Geochronology

We present new detrital-zircon U-Pb ages from two lithic sandstone samples from the Colorado Creek Formation and one lithic sandstone from the underlying Kahiltna Formation. Refer to Figure 15 for age spectra and Supplemental Item H for analytical data. Samples are constrained within the context of targeted field mapping and measured stratigraphic sections (Figs. 2 and 6). Samples 062411JT1 and 062411JT9 are from a ~350-m-thick section of fluvial strata of the Oligocene Colorado Creek Formation. Both samples contain a dominant population of ca. 101–92 Ma grains (59%–82% of ages in two samples) and minor populations of ca. 364 to ca. 462 Ma (8%–10%) and ca. 1234 to ca. 2326 Ma (3%–5%). Sample 062411JT9 also contains minor populations of ca. 67 to ca. 71 Ma (23%) and ca. 29 to ca. 30 Ma (2%). For each sample, a maximum depositional age was calculated in Isoplot (Ludwig, 2008) using the mean weighted age of the youngest significant peak (≥3 zircon ages) whose 1σ errors overlap. The youngest age cluster in sample 062311JT1 includes four ca. 29 to ca. 30 Ma ages that yield a mean weighted average of 29.4 ± 0.8 Ma

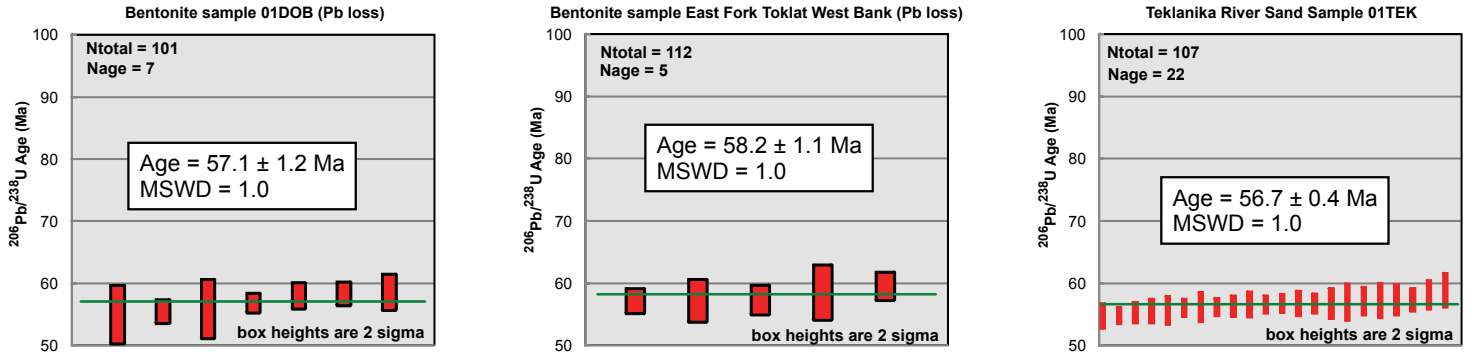

Figure 13. Weighted-means plots showing concordant zircons from Cantwell Formation bentonite samples. Zircons plotted represent a subset of zircons that yield younger ages than the main age population and are interpreted as recording Pb loss after eruption, deposition, and burial of the volcanic ash. Refer to Figure 11 for explanation.

(MSWD = 0.57). This ca. 29 Ma maximum depositional age supports previously reported biostratiographic data diagnostic of early Oligocene deposition (Trop et al., 2004). Sample 062411JT9 only yields Cretaceous and older detrital zircons but is interpreted as early Oligocene given its stratigraphic position above lithologically similar strata that yield early Oligocene palynomorphs and sample 062411JT1, which yields ca. 29 Ma detrital zircons. A volcanic clast sample (062411JT8) from conglomerate in the middle of the section (Fig. 6) yields a U-Pb zircon age of 65.9 ± 0.4 Ma (Fig. 16). For comparative purposes, a sandstone (062411JT11) was sampled from Upper Cretaceous marine strata that unconformably underlie the fluvial strata. This older sample yields a broader distribution of detrital-zircon ages overall, including more abundant Paleozoic and Precambrian ages than the Colorado Creek Formation (Fig. 15).

Denali Fault Dike Swarms

We report geochronologic data from mafic dike swarms that crop out along the McKinley segment of the Denali fault system in the central and eastern Alaska Range (Figs. 2 and 9). Refer to Supplemental Items I and J (footnote 1) for analytical data and additional plots. Ten mafic dikes yield $^{40}Ar/^{39}Ar$ ages that range from ca. 38 to ca. 25 Ma (Table 3 and Figs. 17 and 18). Dikes from Peter's Glacier and Gunsight Pass in the central Alaska Range yield ca. 38 to ca. 27 Ma ages. Samples from the Nenana Glacier and Mount Balchen areas in the eastern Alaska Range yield ca. 32 to ca. 25 Ma ages. These dike ages are all younger than ages reported from plutons that the dikes intrude (Wilson et al., 2015).

Teklanika River Sediment Detrital-Zircon Geochronology

We report detrital-zircon U-Pb age data from a modern stream-sediment sample collected from the Teklanika River (Tek Bridge on Fig. 2). Refer to Supplemental Items A and K for sample location and analytical data. The sample yielded 106 single-grain U-Pb zircon ages ranging from ca. 54 to ca. 2850 Ma (Fig. 15). Precambrian ages make up 49% of the ages. Subordinate Cenozoic ages (24%) range from ca. 64 to ca. 54 Ma and minor Paleozoic ages (~19%) span ca. 333 to ca. 541 Ma, including a major peak at ca. 422 Ma. Mesozoic ages are distinctly sparse (8%), with isolated ages from ca. 84 to ca. 219 Ma.

IGNEOUS GEOCHEMISTRY

Description of Colorado Creek Volcanic Rocks

The Colorado Creek lavas range from basalt to trachyte using the Zr/Ti versus Nb/Y classification of Pearce (1996) (Fig. 19A). These lavas are in the high-K calc-alkaline to shoshonitic series (Fig. 19B), consistent with their relatively high

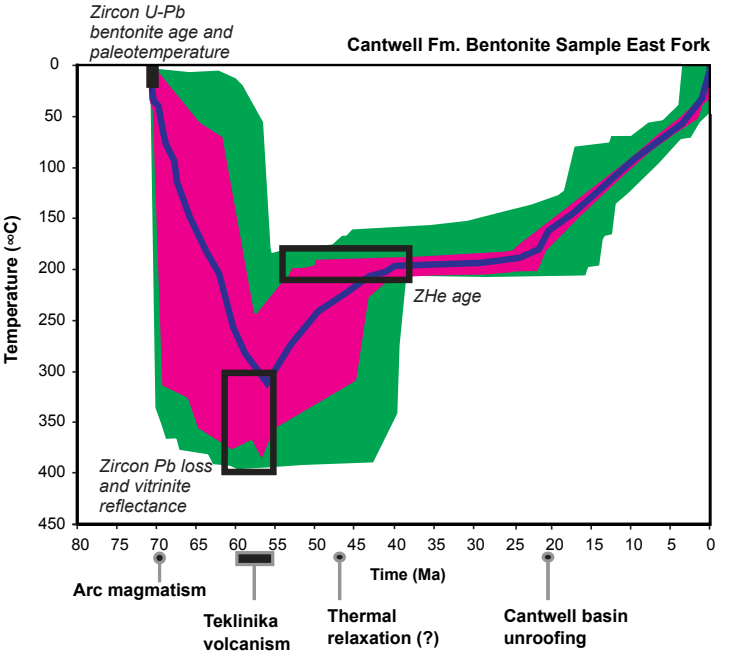

Figure 14. Thermal model generated from analytical results from apatite and zircon grains from Cantwell Formation bentonite sample East Fork Toklat. The magenta band is the 90% confidence interval of the mean, and the green band is the 90% confidence of the distribution. Model generated using HeFTy thermal modeling software (Ketcham, 2005).

Nb/Y ratio (which serves as a proxy for K). None of the Colorado Creek lavas have primitive compositions (they have low MgO, Cr, and Ni) (Supplemental Item L [footnote 1]). The Colorado Creek lava samples have Th/Yb ratios that are elevated above the mantle array (Fig. 19C) and exhibit high ratios of large ion lithophile (LILE) and fluid-mobile elements (FMEs) to less mobile elements including high field strength (HFSE) and heavy rare-earth elements (HREE). For example, Ba/Ta ratios range from 384 to 2842 (all but one sample is >450). Chondrite-normalized rare-earth element plots (Fig. 20) reveal a uniform pattern among the Colorado Creek lava samples with an average $(La/Yb)_N$ ratio of 9.5, with La ranging from 101 to 170 times chondrite. One sample (JT8) exhibits a pronounced negative Eu anomaly, but the remaining samples show small to no negative Eu anomaly (Fig. 20).

Description of Dikes along the Denali Fault

The dikes that crosscut granitic plutons along the Denali fault range from basalt to basaltic andesite (Fig. 19A) and have moderate K_2O content, largely

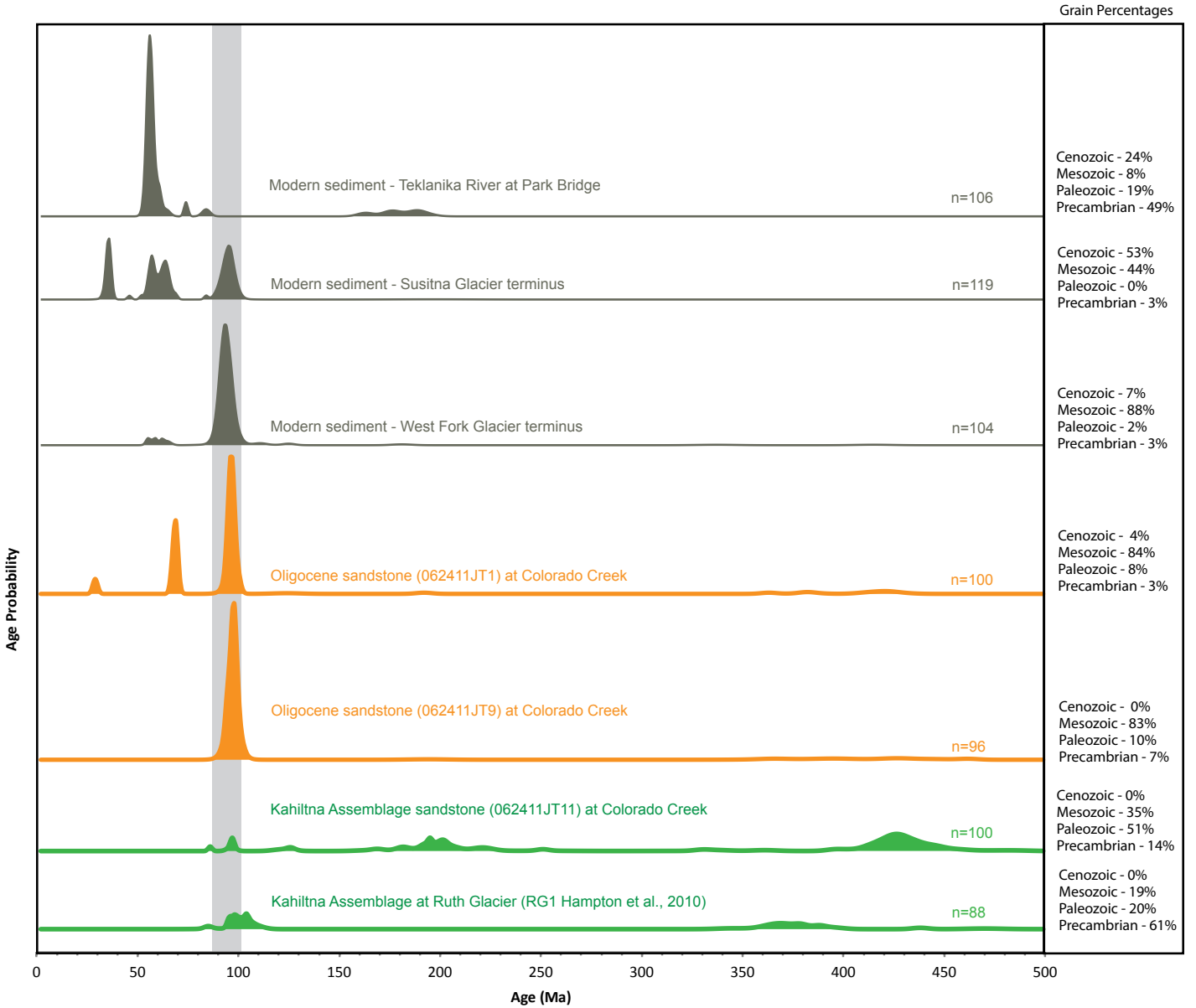

Figure 15. Normalized probability density plots of detrital-zircon U-Pb ages of Phanerozoic grains for Oligocene Colorado Creek Formation sandstone and Cretaceous Kahiltna assemblage sandstone at Colorado Creek. Age determinations represent laser ablation–inductively coupled plasma–mass spectrometry (LA-ICP-MS) analyses from individual zircons. For comparative purposes, data from a Cretaceous Kahiltna assemblage sandstone at Ruth Glacier (Hampton et al., 2010) and eastern Alaska Range modern rivers (this study) are also plotted. Refer to Supplemental Item H (text footnote 1) for geochronologic data.

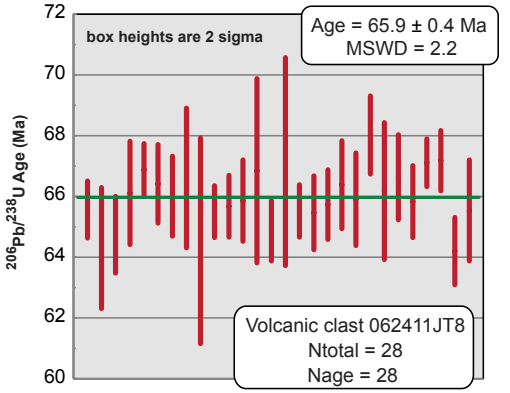

Figure 16. Histograms showing concordant zircons from a felsic volcanic clast from the Colorado Creek Formation. Age determinations represent laser ablation–inductively coupled plasma–mass spectrometry (LA-ICP-MS) analyses from individual zircons. Green bar represents weighted-mean U-Pb age. Nage—total number of concordant zircons used for age determination. Ntotal—total number of zircons analyzed in the sample. MSWD—mean square of weighted deviates. Data are plotted using Isoplot (Ludwig, 2008).

TABLE 3. SUMMARY OF $^{40}Ar/^{39}Ar$ ANALYTICAL RESULTS FROM MAFIC DIKES ALONG THE DENALI FAULT

Sample	Location	Phase analyzed	Integrated age (Ma)	Plateau age (Ma)	Plateau information	Isochron age (Ma)	Isochron or other information	Supplemental figure (text footnote 1)
28CHED WR#L1	Foreaker Glacier	Whole rock	34.3 ± 0.2	**34.0 ± 1.0***	3 of 8 fractions 55.6 % ^{39}Ar release MSWD = 2.70	—	—	Item J, section A
02PETER WR#L1	Peter's Glacier	Whole rock	37.2 ± 0.5	**38.0 ± 0.4**	3 of 8 fractions 87.5% ^{39}Ar release MSWD = 0.59	—	—	Item J, section B
24PETER WR#L1	Peter's Glacier	Whole rock	32.7 ± 0.3	**34.8 ± 0.3**	3 of 8 fractions 83.3% ^{39}Ar release MSWD = 0.37	—	—	Item J, section C
25PETER WR#L1	Peter's Glacier	Whole rock	27.6 ± 0.7	**27.3 ± 0.6**	5 of 8 fractions 88.7% ^{39}Ar release MSWD = 0.50	28.2 ± 0.9	10 steps $^{40}Ar/^{36}Ar_i$ = 292.4 ± 3.8 MSWD 0.31	Item J, section D
30PETER WR#L1	Peter's Glacier	Whole rock	34.2 ± 0.7	**35.7 ± 0.7**	5 of 10 fractions 88.7% ^{39}Ar release MSWD = 0.52	34.9 ± 0.9	10 steps $^{40}Ar/^{36}Ar_i$ = 303.8 ± 7.7 MSWD 0.52	Item J, section E
55NEN WR#L1	Nenana Glacier	Whole rock	25.7 ± 0.1	**25.4 ± 0.1***	4 of 9 fractions 74.2% ^{39}Ar release MSWD = 3.11	—	—	Item J, section F
02BAL WR#L1	Mount Balchen	Whole rock	27.4 ± 0.2	**28.4 ± 0.2**	5 of 13 fractions 64.1% ^{39}Ar release MSWD = 0.79	—	—	Item J, section G
07BAL WR#L1	Mount Balchen	Whole-rock	27.5 ± 0.2	**27.1 ± 0.2**	6 of 12 fractions 78.9% ^{39}Ar release MSWD = 0.71	—	—	Item J, section H
28BAL WR#L1	Mount Balchen	Whole rock	32.2 ± 0.2	**32.1 ± 0.2***	4 of 12 fractions 43.3% ^{39}Ar release MSWD = 0.21	—	—	Item J, section I
10910DIKE WR#L1	Near Mount Balchen	Whole rock	26.2 ± 0.7	**27.6 ± 0.9**	3 of 8 fractions 85.3% ^{39}Ar release MSWD = 1.45	—	—	Item J, section J

Note: Preferred age determination in bold. MSWD—mean square of weighted deviates.
*Does not meet the criteria of a plateau age. Weighted average age reported.

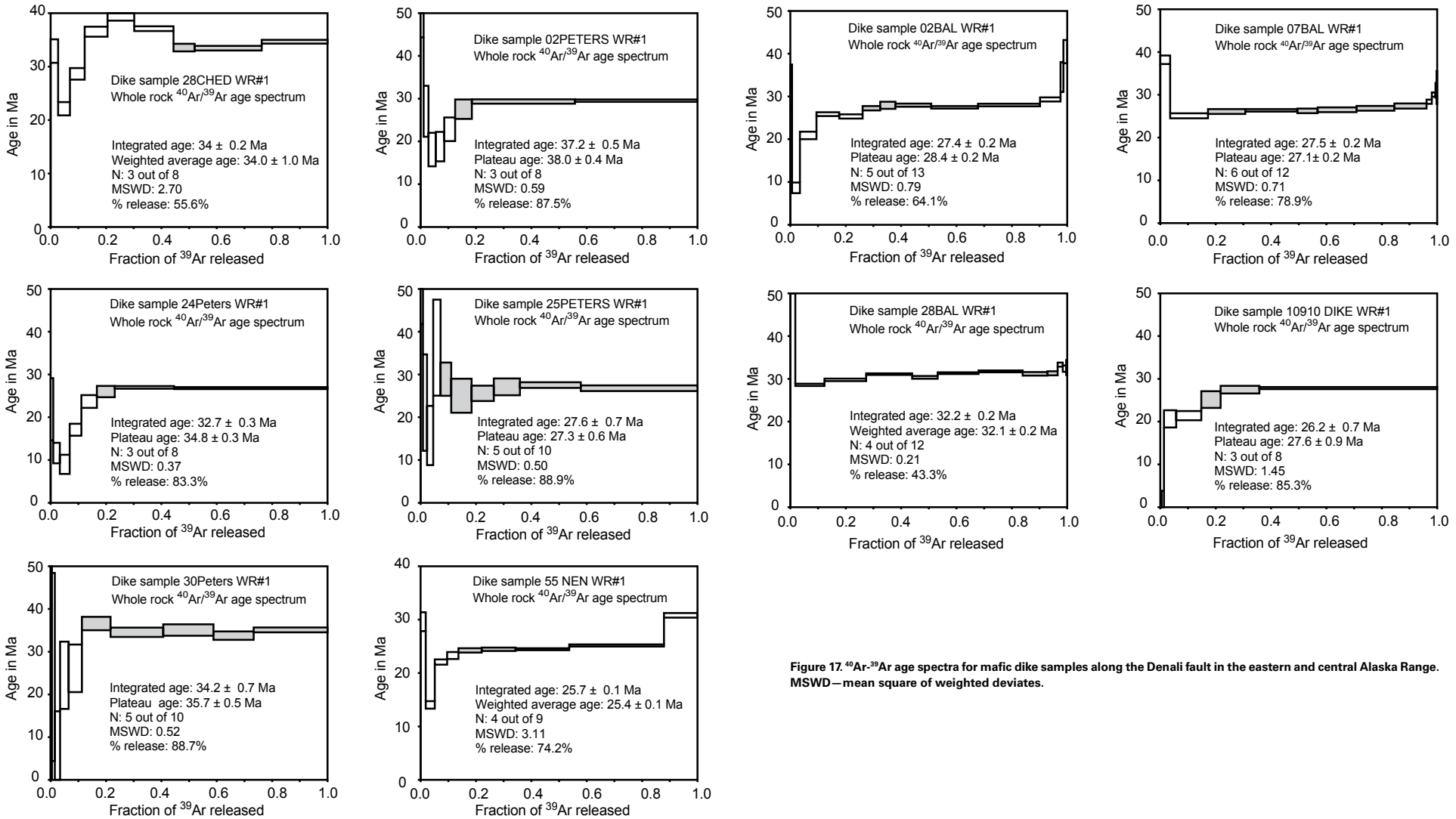

Figure 17. ^{40}Ar-^{39}Ar age spectra for mafic dike samples along the Denali fault in the eastern and central Alaska Range. MSWD—mean square of weighted deviates.

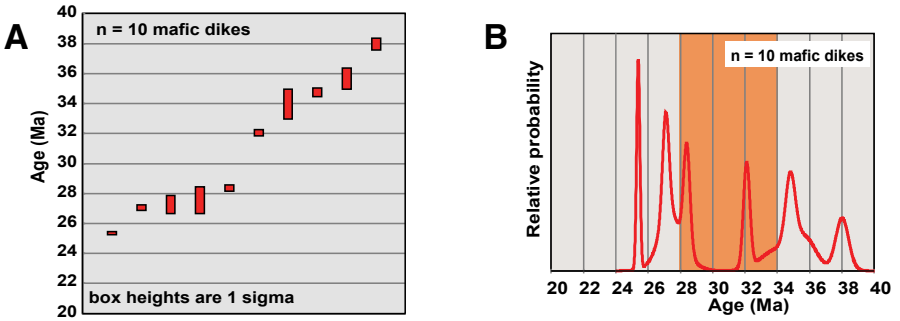

Figure 18. Histograms (A) and probability plot (B) of $^{40}Ar/^{39}Ar$ ages from mafic dike samples along the Denali fault in the eastern and central Alaska Range. Orange rectangle represents age range of Colorado Creek Formation sediment accumulation based on biostratigraphic data (Trop et al., 2004) and the youngest cluster of detrital zircons (this study).

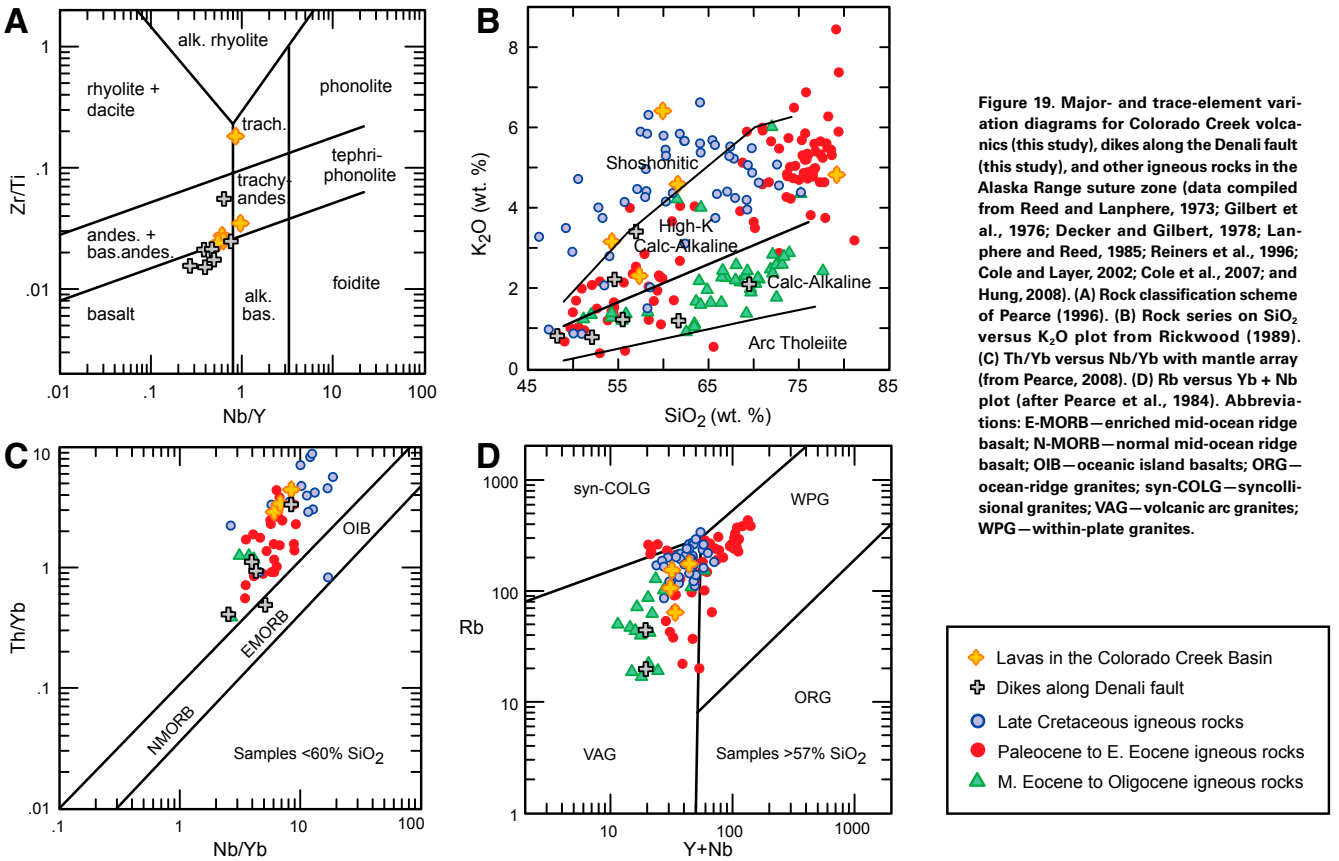

Figure 19. Major- and trace-element variation diagrams for Colorado Creek volcanics (this study), dikes along the Denali fault (this study), and other igneous rocks in the Alaska Range suture zone (data compiled from Reed and Lanphere, 1973; Gilbert et al., 1976; Decker and Gilbert, 1978; Lanphere and Reed, 1985; Reiners et al., 1996; Cole and Layer, 2002; Cole et al., 2007; and Hung, 2008). (A) Rock classification scheme of Pearce (1996). (B) Rock series on SiO_2 versus K_2O plot from Rickwood (1989). (C) Th/Yb versus Nb/Yb with mantle array (from Pearce, 2008). (D) Rb versus Yb + Nb plot (after Pearce et al., 1984). Abbreviations: E-MORB—enriched mid-ocean ridge basalt; N-MORB—normal mid-ocean ridge basalt; OIB—oceanic island basalts; ORG—ocean-ridge granites; syn-COLG—syncollisional granites; VAG—volcanic arc granites; WPG—within-plate granites.

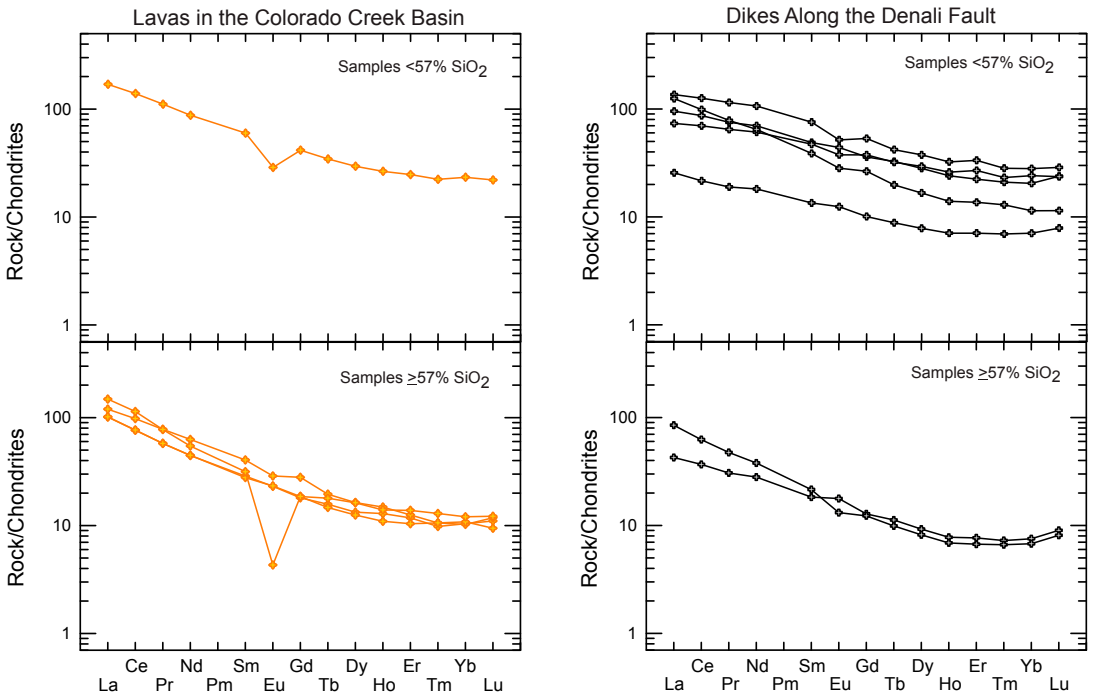

Figure 20. Chondrite-normalized rare-earth element plots for Colorado Creek volcanics and for dikes along the Denali fault. Normalizing values are from Sun and McDonough (1989).

consistent with the calc-alkaline series (Fig. 19B). Most of the dike samples have Th/Yb and Nb/Yb ratios that are in the range of enriched mid-ocean ridge basalt (E-MORB) and lie along or above the mantle array (Fig. 19C). The dike samples exhibit relatively high LILE and FME contents with Ba/Ta ratios ranging from 517 to 2442. Chondrite-normalized rare-earth element plots (Fig. 20) reveal a relatively small degree of light rare-earth element (LREE) enrichment with $(La/Yb)_N$ ratios ranging from 2.9 to 11.9 and La ranging from 25 to 136 times chondrite. The dike samples have smooth REE patterns and show no negative Eu anomalies. The sample with the lowest La/Yb ratio, JB09-MUD, also has relatively high Cr (430 ppm) and Ni (110 ppm) compared to other dike samples (Supplemental Item L), but none of these samples has a primitive composition.

Interpretations and Summary of Alaska Range Suture Zone Cretaceous-Cenozoic Magmatism

The Colorado Creek lava and Denali fault dike samples have geochemical signatures indicative of arc magmatism. The high concentration of LILE and FME is a typical characteristic of arc magmatism when these elements are released from a subducted slab into the overlying mantle wedge (Pearce and Parkinson, 1993; Arculus, 1994). The elevated Th/Yb ratios (above the mantle array) among the more mafic samples (Fig. 19C) are consistent with magma-crust interaction or slab input to the source magma (Pearce, 2008). The more felsic samples of each unit fall within the volcanic arc field on a Rb versus Y + Nb discriminatory plot (Fig. 19D). Given their age and geochemical affinity, we interpret that the Colorado Creek lavas were erupted as part of Alaska Range–Talkeetna Mountains arc magmatism while the Wrangellia composite terrane was shortened and uplifted within the suture zone. The Denali fault dikes were emplaced during the subsequent Alaska-Aleutian Range arc magmatism; however, arc magmatism was essentially shut off in south-central Alaska during progressive flat-slab subduction of the Yakutat plate.

While the Colorado Creek lavas and Denali fault dikes share common traits of arc magmatism, there are important geochemical differences between these two sample sets. Importantly, the Denali fault dikes are more geochemically depleted (e.g., lower K, La/Yb, Th/Yb, and Nb/Yb) than the Colorado Creek lavas (Figs. 19 and 20). From a regional perspective, the Colorado Creek lavas are similar geochemically to other Late Cretaceous volcanic and plutonic rocks, and the Denali fault dikes are similar geochemically to other mid-Eocene to Oligocene volcanic and plutonic rocks in the Alaska Range suture zone (Fig. 19).

While there are no primitive compositions among the Colorado Creek lavas and Denali fault dike samples, these regional observations are suggestive of a change to more depleted magmatism that may reflect a change in mantle source composition beneath the Alaska Range suture zone between Late Cretaceous and mid-Eocene time.

Paleocene to early Eocene volcanic and plutonic rocks within the Alaska Range suture zone have a different geochemical affinity than the Colorado Creek lavas or Denali fault dikes (Fig. 19). Overall, the Paleocene to Early Eocene rocks have a diverse compositional range including A-type granites, adakite, and within-plate to arc affinity that represent an episode of collisional magmatism with less influence of "typical" arc processes (Cole et al., 2007; Carrion et al., 2012; Cole and Chung, 2013). The Paleocene to early Eocene igneous rocks have geochemical compositions (e.g., K_2O, Nb/Yb, and Th/Yb) that lie between the compositions of Late Cretaceous and mid Eocene to Oligocene igneous rocks in the Alaska Range suture zone with some overlap (Fig. 19).

In summary, Late Cretaceous igneous rocks in the Alaska Range suture zone represent Alaska Range–Talkeetna Mountain arc magmatism during suturing of the Wrangellia composite terrane to south-central Alaska, marked by contractional deformation and peak metamorphism between ca. 70 and 60 Ma. Melt-fertile Kahiltna assemblage rocks in the thickened suture zone contributed to the enriched high-alkali magmas that formed at this time and into Paleocene time (Reiners et al., 1996; Cole et al., 2007). Exhumation of early Paleocene plutons by late Paleocene time (Cole and Chung, 2013) indicates that regional uplift followed collision of the Wrangellia composite terrane and accompanied Paleocene magmatism. The more depleted geochemical composition of the mid-Eocene to Oligocene igneous rocks (e.g., lower Nb/Yb, Th/Yb, K_2O) indicate less crustal contamination and/or a more depleted asthenospheric source than was present during Late Cretaceous time (Figs. 19B–C) (Pearce, 2008).

COLORADO CREEK SEDIMENTARY PROVENANCE AND DENALI FAULT DISPLACEMENT

Oligocene Colorado Creek fluvial strata were eroded chiefly from sedimentary and igneous bedrock sources judging from compositional and detrital geochronologic data. Polymictic conglomerate and lithic sandstone clast types dominate conglomerate and sandstone compositions, consistent with recycling of Cretaceous sedimentary strata that crop out along the suture zone (Fig. 21; Trop et al., 2004). The mid-Cretaceous detrital-zircon population that dominates the Oligocene Colorado Creek sandstones (Fig. 15) typifies Cretaceous strata that crop out in the central Alaska Range, including the northern Kahiltna assemblage, lower Cantwell Formation, and Panorama Peak unit (Huff, 2008; Hampton et al., 2010; Hults et al., 2013; Brennan and Ridgway, 2015). Moreover, modern rivers draining these Cretaceous strata yield abundant mid-Cretaceous detrital ages reflecting second-cycle zircons eroded from the Kahiltna assemblage. For example, the modern Chulitna River in the central

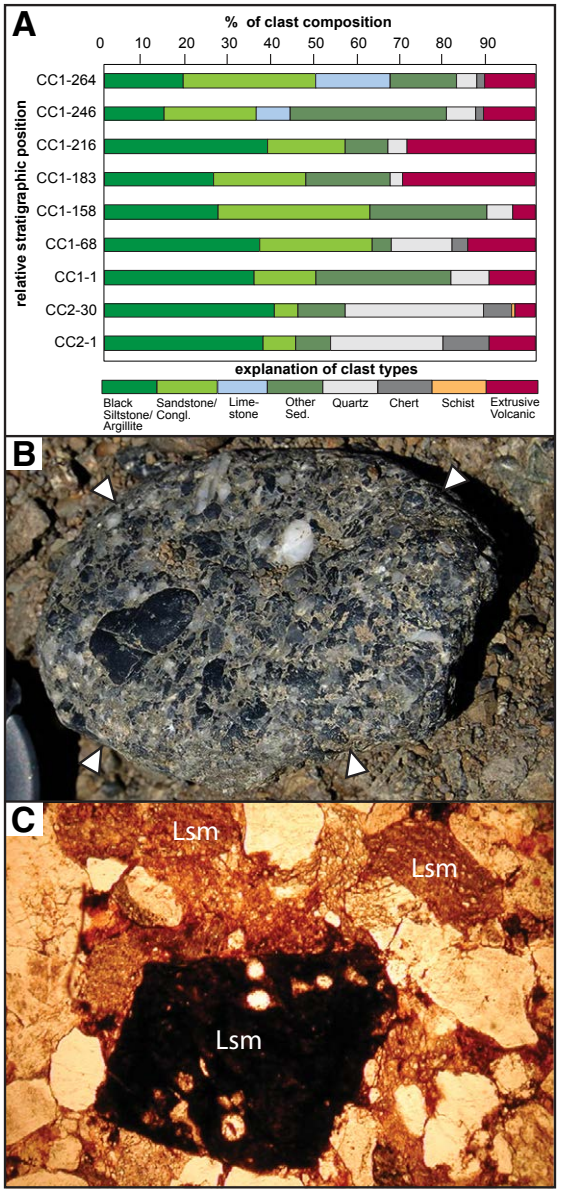

Figure 21. (A) Histograms showing clast dominance of sedimentary lithologies in compositional data from Oligocene Colorado Creek Formation conglomerate. From Trop et al. (2004). (B) Photograph of recycled conglomerate clast common in Oligocene Colorado Creek Formation conglomerate. Clast is ~25 cm long. (C) Photomicrograph of mudstone lithic grains (Lsm) common in Oligocene Colorado Creek Formation sandstone.

Alaska Range yields chiefly ca. 110 to ca. 90 Ma U-Pb detrital-zircon ages (Lease et al., 2016). However, most Kahiltna assemblage strata yield a broader distribution of Cretaceous detrital-zircon ages as well as subordinate Jurassic, Paleozoic, and Precambrian detrital-zircon ages (Huff, 2008; Hampton et al., 2010; Hults et al., 2013) that are not observed in the sampled Colorado Creek Formation sandstones.

In addition to recycling of Cretaceous sedimentary sources exposed in the suture zone, subordinate Oligocene detritus was eroded from igneous sources judging from compositional and detrital geochronologic data. Volcanic clasts are common in the Oligocene sandstone (29% of lithic grains) and conglomerate (15% of all clasts). A volcanic clast from conglomerate yields a ca. 66 Ma U-Pb zircon age, and sandstones yield abundant ca. 71 to ca. 67 Ma detrital-zircon ages, which fall within the ca. 71 to ca. 68 Ma age range of Colorado Creek volcanics (this paper) that are faulted directly against the Oligocene fluvial strata in the study area (Figs. 4 and 5). Notably, Latest Cretaceous, mid-Cretaceous, and Devonian–Mississippian detrital-zircon populations in the Oligocene fluvial strata overlap the ages of igneous rocks presently exposed north of the Denali fault in the eastern Alaska Range. Igneous rocks exposed in that region yield ca. 70–72 Ma, ca. 95–98 Ma, and ca. 330–375 Ma ages based on K-Ar, $^{40}Ar/^{39}Ar$, and U-Pb geochronology (Fig. 2; Nokleberg et al., 1992a, 1992b). Farther north in the Yukon-Tanana Uplands, crystalline rocks yield U-Pb zircon and monazite ages of ca. 120–90 Ma (Fig. 2; Dilworth et al., 2007; Day et al., 2014; Solie et al., 2014) and ca. 375–335 Ma (Aleinikoff et al., 1981, 1984, 1986; Dusel-Bacon et al., 2006; Dusel-Bacon and Williams, 2009; Day et al., 2014). However, derivation from more distant latest Cretaceous igneous sources is possible; latest Cretaceous plutons and sparse volcanic rocks occur throughout the Alaska Range, other parts of southern Alaska, and contiguous areas in Canada (Moll-Stalcup, 1994; Plafker and Berg, 1994; Jones et al., 2014; Wilson et al., 2015).

Sparse ca. 30 to ca. 29 Ma detrital zircons in the fluvial strata likely reflect erosion of the youngest belt of igneous rocks in the Alaska Range. Spatially limited ca. 40 to ca. 25 Ma igneous rocks, mainly dikes and sills, presently crop out in the central and eastern Alaska Range (Reed and Lanphere, 1974; Csejtey et al., 1992; Benowitz et al., 2011; Jones et al., 2014; this study). Modern rivers draining the Alaska Range yield only minor populations of ca. 40 to ca. 25 Ma zircons, consistent with spatially limited magmatism during this interval (Lease et al., 2016). An alternative source of the ca. 30–29 Ma grains is far-traveled volcanic ash air fall from the oldest phase of the Wrangell arc (Richter et al., 1990; Brueseke et al., 2019) or undocumented volcanic edifices related to the Denali fault Oligocene dike swarms (this study).

The paucity of metamorphic clasts in conglomerate and Precambrian and Devonian–Mississippian detrital zircons in sandstone indicates that the Yukon composite terrane was not a major sediment source for Colorado Creek sandstones. Minor Proterozoic and Devonian–Mississippian ages (<15% of samples) overlap zircon ages reported from the late Paleozoic metasedimentary strata in the eastern Alaska Range (Huff, 2008) and the Yukon composite terrane from east-central Alaska (Bradley et al., 2007; Dusel-Bacon and Williams, 2009) to adjacent parts of Yukon Territory, British Columbia, and southeastern Alaska (Gehrels and Kapp, 1998; Gehrels and Ross, 1998). Aerially extensive ca. 216 to ca. 181 Ma plutons intrude the Yukon composite terrane, but only a couple detrital zircons in the Colorado Creek samples match this age population. Proterozoic and Devonian–Mississippian ages may also be accounted for through recycling from Cretaceous strata within the suture zone (Huff, 2008; Hampton et al., 2010).

Carbonate clasts make up <20% of clasts in uppermost conglomerates (Fig. 16; two of nine beds sampled). These clasts have been interpreted as reflecting erosion of Devonian sedimentary strata that crop out north of the Colorado Creek basin immediately north of the Denali fault (Dillinger terrane; unit DLs on Fig. 2; Csejtey et al., 1992). The provenance link between the clasts and the adjacent Dillinger terrane was based on the presence of late Devonian conodonts in limestone clasts that match the age of limestone in the Dillinger terrane (Csejtey et al., 1992). The linkage would limit dextral displacement across the Denali fault to less than tens of kilometers, unless a thrust fault mapped along the north side of the Dillinger terrane (Csejtey et al., 1992) also experienced strike-slip displacement. Alternatively, the limestone clasts may have been eroded from the Devonian Yanert Fork sequence presently exposed along strike to the east in the eastern Alaska Range. There, the Yanert Fork sequence consists of deformed metasedimentary and metavolcanic rocks, and locally contains carbonate strata (Csejtey et al., 1992; Huff, 2008). Another potential source of carbonate clasts is Cretaceous mélange exposed along the Denali fault; the mélange contains outsized carbonate blocks interpreted as displaced fragments of the Dillinger terrane (Csejtey et al., 1992).

Igneous rocks exposed in the southern and/or outboard part of the suture zone apparently were not major sediment sources judging from the paucity of ca. 60 to ca. 50 Ma detrital zircons and ca. 213 to ca. 153 Ma detrital zircons. Intrusive rocks with ca. 60 to ca. 50 Ma ages crop out extensively in the Denali–Ruth Glacier area of the central Alaska Range and the northern Talkeetna Mountains (Fig. 3, Cole et al., 2007; Wilson et al., 2015). Modern rivers draining these bedrock sources yield abundant ca. 60 to ca. 50 Ma detrital zircons (Lease et al., 2016). Moreover, ca. 213 to ca. 153 Ma igneous rocks crop out extensively in the Talkeetna Mountains (Fig. 3; Rioux et al., 2007) that are not evident in detrital geochronologic ages in the sampled Oligocene strata.

In summary, compositional and detrital geochronologic data from Oligocene Colorado Creek strata indicate erosion chiefly of Cretaceous and Oligocene sedimentary and igneous sources presently exposed along the central Denali fault in the central and eastern Alaska Range. The compositional and geochronologic data are best explained by restoration of ~150 km or more of dextral displacement along the Denali fault since deposition ca. 29 Ma, placing the Oligocene fluvial strata adjacent to the eastern Alaska Range. Future studies can evaluate this new hypothesis. This interpretation fits the current model where total Cenozoic slip along the Denali fault decreases from the eastern to central Alaska Range (Reed and Lanphere, 1974; Nokleberg et al., 1985; Benowitz et al., 2012b; Haeussler et al., 2017a) owing to strain partitioning (Bemis et al., 2015).

TECTONIC SYNTHESIS: EVOLUTION OF THE ALASKA RANGE SUTURE ZONE

The following section integrates new geochronologic and geochemical data sets from this study with previous data sets, summarizing constraints on timing and nature of magmatism, sedimentation, and deformation processes that shaped the suture zone and tectonic interpretations.

Late Jurassic–Early Late Cretaceous (ca. 157 to ca. 84 Ma)

Upper Jurassic–Upper Cretaceous marine clastic strata of the Kahiltna assemblage are interpreted by most workers to have accumulated along both the inboard (northern) margin of the Wrangellia composite terrane and the southern margin of the Yukon composite terrane (e.g., Kalbas et al., 2007; Hampton et al., 2010; Hults et al., 2013). The Kahiltna basin was part of a series of marine depocenters along the >2000 km length of the Wrangellia composite terrane (McClelland et al., 1992). Provenance studies indicate that northern Kahiltna strata exposed in the central Alaska Range reflect erosion of bedrock source terranes exposed along the former continental margin to the north (Yukon composite terrane) as well as mid-Cretaceous arc rocks (Kalbas et al., 2007; Huff, 2008; Romero, 2018). Our new detrital-zircon data from northern Kahiltna strata at Colorado Creek provide similar results. In contrast, Kahiltna and coeval marine strata exposed to the south in the Talkeetna and Clearwater Mountains reflect sediment contributions from Mesozoic sources in the Wrangellia composite terrane to the south (Hampton et al., 2010; Hults et al., 2013). Southern Kahiltna strata locally record upsection increases in detritus interpreted by Hampton et al. (2010) as reflecting continental-margin sources, consistent with closure of the suture zone and accretion of the Wrangellia composite terrane during late early to early Late Cretaceous time. In contrast, Hults et al. (2013) interpret provenance differences between the northern and southern Kahilta strata as evidence that the depositional systems were never connected and that the Wrangellia composite terrane was not near the former continental margin until Late Cretaceous time. Thus, the original width of the marine basin during Jurassic–Cretaceous time is controversial. Given that faults with evidence of strike-slip deformation bisect northern and southern Kahiltna outcrop belts, and detailed stratigraphic correlations across the faults are lacking, the two belts of Kahiltna marine strata may have been faulted together and laterally shuffled. Sedimentologic and paleontological data indicate that parts of the Kahiltna and the Nutzotin basin to the southeast were subaerially exposed by early Late Cretaceous time. Spatially restricted Aptian–Cenomanian fluvial strata in the northern Talkeetna Mountains (Caribou Pass Formation) were deposited unconformably upon marine strata of the Kahiltna assemblage in the northern Talkeetna Mountains (Hampton et al., 2007); similar strata crop out locally in the Nutzotin Mountains (Richter, 1976; Fiorillo et al., 2012; Koepp et al., 2017). Provenance data from these sediments indicate sediment derivation from both the Wrangellia and Yukon composite terranes judging from detrital-zircon geochronologic and Hf isotopic data and are interpreted to reflect closure of the marine basin by early Late Cretaceous time (Hampton et al., 2007, 2017).

Interpretations of the Late Jurassic–Early Cretaceous tectonic setting of the marine basins that separated the Wrangellia composite terrane from inboard terranes vary. Several previous studies infer that strata deposited in the southern Kahiltna basin evolved from a backarc basin or remnant ocean basin setting during Late Jurassic to early Cretaceous time to a collisional, compressive basinal setting by early Late Cretaceous time as a result of collision of the Wrangellia composite terrane (Ridgway et al., 2002; Kalbas et al., 2007; Hampton et al., 2010; see Trop and Ridgway, 2007, their figure 4). In these models, northern Kahiltna strata accumulated along the southern margin of the inboard Yukon-Tanana terrane and in a forearc position with respect to arc plutons within the Yukon-Tanana terrane. These previous studies infer an inboard- (north-) dipping subduction zone along the northern margin of the Kahiltna basin that closed during Late Cretaceous time (Hampton et al., 2007; Trop and Ridgway, 2007, their figure 4). This interpretation is supported by the presence of rocks mapped as part of the Kahiltna assemblage; these rocks consist of a lower argillite-dominated mélange and an overlying klippe of older chert-dominated mélange that also includes greenstone and felsic tuff (Bier et al., 2017). Lithologic and structural observations, combined with geochemical analyses of the tuffs, indicate that this mélange is part of a south-facing accretionary wedge consisting of oceanic crust and hemipelagic sediment; this wedge formed prior to the closure of the Kahiltna basin (Bier and Fisher, 2003).

East of the Kahiltna basin in eastern Alaska and the Yukon Territory, the Nutzotin Mountains sequence and the Dezadeash Formation record Late Jurassic to Early Cretaceous deposition of marine siliciclastic strata and mafic-intermediate volcanic rocks. Nutzotin Mountains strata are locally in depositional contact with the Wrangellia-Alexander terrane and in other areas have been thrust southward (present-day coordinates) over Wrangellia along south-verging thrust faults (Richter, 1976; Manuszak et al., 2007). Sedimentological and detrital data from the Nutzotin Mountains sequence and Dezadeash Formation reflect a provenance from sources within the Wrangellia-Alexander terrane (Manuszak et al., 2007; Lowey, 2011; Fasulo et al., 2018; Lowey, 2018), similar to the southern Kahiltna assemblage. Manuszak et al. (2007) infer that the Nutzotin strata accumulated in a compressional basin setting linked to Late Jurassic–Early Cretaceous shortening, uplift, and unconformity development documented in the Wrangellia composite terrane south of the Nutzotin basin (Trop et al., 2002). In contrast, Lowey (2018) infers that the Nutzotin-Dezadeash basin formed in a backarc setting throughout Late Jurassic–Early Cretaceous deposition.

Along strike to the southeast, the outboard (western) portion of the Gravina basin in southeastern Alaska accumulated along the inboard margin of the Alexander-Wrangellia terrane and in a backarc position with respect to the western Coast Mountains batholith, which is built on the Alexander-Wrangellia terrane (Gehrels et al., 2009; Yokelson et al., 2015). These Late Jurassic–Early Cretaceous strata were derived chiefly from sources within the Alexander

terrane (Yokelson et al., 2015), analogous to southern Kahiltna assemblage strata. Late Jurassic–Early Cretaceous strata of the eastern Gravina belt depositionally overlie Middle Jurassic or older rocks of inboard terranes (Taku and Yukon-Tanana terranes) and accumulated in a forearc basin with respect to the eastern Coast Mountains batholith (built on the Stikine and Yukon-Tanana terranes), analogous to the northern Kahiltna strata of the Alaska Range suture zone. The western facies of the Gravina belt are interpreted to have been juxtaposed against the eastern facies of the Gravina belt by Early Cretaceous sinistral strike-slip followed by mid-Cretaceous structural imbrication of the two Gravina basinal segments (Monger et al., 1994; Yokelson et al., 2015).

Although the original width and tectonic framework of the Late Jurassic–Early Cretaceous Kahiltna, Nutzotin-Dezadeash, and Gravina basins remains controversial, there is agreement on the timing of postdepositional deformation. Strata in all these basins were deformed by regional mid-Cretaceous thrust faults, folds, and shear zones within the suture zone separating the Wrangellia composite terrane from inboard terranes (Rubin et al., 1990; Ridgway et al., 2002; Manuszak et al., 2007; Gehrels et al., 2009; Yokelson et al., 2015).

Latest Cretaceous (ca. 84 to ca. 67 Ma)

During latest Cretaceous time, the Alaska Range suture zone was marked by regional shortening and metamorphism that prompted subaerial uplift of marine basinal strata (Kahiltna assemblage) coeval with deposition of nonmarine strata (Cantwell Formation) and arc magmatism. We interpret these processes as reflecting terminal suturing of the oceanic Wrangellia composite terrane against metamorphic rocks of the continental margin. Mid-Cretaceous accretion of the Wrangellia composite terrane followed by latest Cretaceous northward-dipping subduction (modern coordinates) and arc magmatism prompted development of a retroarc thrust belt and attendant thrust-top basin (Cantwell basin; Ridgway et al., 1997; Trop and Ridgway, 2007). Cretaceous Kahiltna assemblage marine strata were subaerially uplifted and deformed by outboard- (south-) dipping thrust faults, folds, and synkinematic intrusions located inboard (north) of coeval arc-related igneous rocks (Csejtey et al., 1982; Davidson et al., 1992; Ridgway et al., 2002). This deformation is attributed to plate convergence outboard (south) of the suture zone, mainly north-dipping subduction (modern coordinates) of oceanic crust that is recorded by Upper Cretaceous arc plutons, forearc basin sedimentary strata, and accretionary prism metasedimentary strata preserved south of the suture zone (e.g., Plafker and Berg, 1994; Trop, 2008; Amato et al., 2013; Stevens Goddard et al., 2018). Along the southern part of the Cantwell basin, syndepositional displacement along south-dipping thrusts prompted deposition of fluvial-lacustrine strata in growth footwall synclines (Ridgway et al., 1997). Southern Cantwell Formation strata were derived chiefly from Mesozoic marine sedimentary and igneous sources within the actively uplifting suture zone, whereas northern strata were derived from Paleozoic–Precambrian metamorphic and igneous sources along the former continental margin (Trop and Ridgway, 1997).

Arc magmatism within the suture zone is reflected by ca. 71 to ca. 68 Colorado Creek lavas (this study) that are correlative with more widespread intrusions (Wilson et al., 2015). These volcanic rocks and coeval intrusions yield arc-affinity geochemical compositions attributable to northward subduction (present coordinates) of oceanic lithosphere beneath the former continental margin (e.g., Moll-Stalcup, 1994; Plafker and Berg, 1994). Cantwell Formation bentonites also record ca. 71 to ca. 68 Ma magmatism. These tephra deposits may record eruptive centers located within the suture zone, or from more distant arc volcanoes that formed outboard (south) of the suture zone. In the Alaska Range–Talkeetna Mountains belt, which spans the suture zone and the Wrangellia composite terrane to the south, ca. 85 to ca. 66 Ma intrusions are common (Moll-Stalcup, 1994; Davidson and McPhillips, 2007; Cole and Chung, 2013; Bleick et al., 2012; Cole et al., 2016; Wilson et al., 2015; Harlan et al., 2017). Cole and Chung (2013) report ca. 84 to ca. 66 Ma U-Pb zircon ages from intrusions with an age peak at ca. 70 to ca. 68 Ma that closely overlaps the ca. 72 to ca. 67 Ma age range of Colorado Creek volcanics and Cantwell Formation bentonites. Less widespread volcanics include ca. 74 Ma tuff in the northern Talkeetna Mountains (Cole et al., 2007) and a small pile of ca. 70 to ca. 67 Ma lavas in the western Alaska Range; this pile of lavas yields geochemical compositions similar to the Colorado Creek volcanics (Jones et al., 2014; J. Jones and E. Todd, 2016, personal commun.).

Latest Cretaceous–Early Paleocene (ca. 67–61 Ma)

Additional shortening, exhumation, and arc magmatism characterized the suture zone during late Maastrichtian–early Paleocene time. Arc magmatism is recorded by granitic plutons, including the ca. 64–60 Ma McKinley sequence plutons in the northern part of the suture zone around Denali (Hung, 2008). In the northern part of the suture zone, Cantwell Formation sedimentary strata were deformed, uplifted, and partly eroded by thrust faults and folds between ca. 67 Ma (age of the youngest dated Cantwell Formation bentonite) and ca. 59 Ma (age of the oldest dated lava in the Teklanika Formation) (Ridgway et al., 1997; Cole et al., 1999; this paper). Metamorphosed rocks exposed in the middle of the suture zone along the Valdez Creek shear zone were uplifted and cooled through the biotite closure temperature by ca. 62 Ma (Davidson et al., 1992; Ridgway et al., 2002). Geologic evidence of Latest Cretaceous–Paleocene shortening and exhumation has been attributed to continued plate convergence and dextral transpression along regional strike-slip faults, including the Denali fault (Plafker and Berg, 1994; Ridgway et al., 2002; Pavlis and Roeske, 2007). Shortening may have been linked to low-angle subduction of juvenile crust, an interpretation consistent with the presence of intrusions attributed to low-angle subduction emplaced far inboard of the margin (Moll-Stalcup, 1994). Low-angle subduction may have been related to the approach of an oceanic spreading ridge that is interpreted to have subducted obliquely beneath southern Alaska ca. 61–50 Ma. This interpretation is based chiefly from a >2000-km-long string of ca. 61–50 Ma "near-trench" intrusions within the

Chugach accretionary prism presently located >250 km south of the suture zone (Bradley et al., 2003). Alternatively, the inferred spreading ridge may not have influenced the suture zone and other parts of interior south-central Alaska, if large-scale (>1000 km) strike-slip translated the prism with respect to inboard terranes (Garver and Davidson, 2015).

Early Paleocene–Early Eocene (ca. 61–50 Ma)

During early Paleocene to early Eocene time, the suture zone experienced episodes of overlapping plutonic and volcanic activity coupled with rapid uplift and exhumation. Volcanic rocks that were erupted during this time (e.g., the Teklanika Formation and those exposed in the Northern Talkeetna Mountains) show geochemical compositions transitional between arc and intraplate characteristics and evolved by assimilation-fractional crystallization from an E-MORB to OIB type mantle source (Cole et al., 2006a; Cole et al., 2007). In addition, peraluminous granitic plutons were emplaced in the suture zone between ca. 62 and ca. 58 Ma, some with intraplate geochemistry (e.g., A-type, ferroan, and adakite geochemical characteristics) (Cole et al., 2007; Cole and Chung, 2013). These plutons mingle with km-wide zones of migmatite and both are crosscut by rhyolite dikes that contain garnet, tourmaline, cordierite, and muscovite (Birsic et al., 2011). These observations indicate melting of high-alumina crustal rocks (e.g., the pelitic Kahiltna assemblage) was involved in the origin of the granitic plutons and the late-stage rhyolite dikes.

The early Paleocene plutons are intruded by basalt, andesite, and rhyolite dikes, one of which yields a zircon U-Pb age of ca. 57 Ma (Carrion et al., 2012). In addition, the plutons are overlapped in places by late Paleocene to early Eocene volcanic deposits that include hundreds of meters of thick piles of andesite and rhyolite lavas and volcaniclastic units that contain clasts of granite and migmatite (Cole et al., 2007; Ceschini et al. 2013). Granitic clasts from the volcaniclastic units yield early Paleocene ages (Cole et al., 2007; Cole and Chung, 2013). The late Paleocene shallow intrusions that crosscut the early Paleocene plutons and the appearance of clasts with the same age as these plutons in early Eocene volcaniclastic units indicate uplift and exhumation of the early Paleocene plutons by the end of Paleocene time (ca. 56 Ma) (Cole et al., 2011).

The intraplate geochemical characteristics of the early Paleocene igneous rocks reveal a change from the more typical arc composition exhibited by Late Cretaceous rocks in the suture zone. This transition in magmatism was accompanied by an episode of regional uplift and exhumation (Benowitz et al., 2012a; Terhune, 2018). These observations are consistent with models of collisional magmatism during which there may be a combination of anatexis of thickened crustal rocks to form granitic magmas and convective removal or delamination of the root of thickened lithosphere in the suture zone resulting in upwelling and partial melting of asthenosphere (e.g., Aldanmaz et al., 2000; Chung et al., 2005; Pang et al., 2013). Further investigation of the igneous rocks in the Alaska Range suture zone is warranted to test these models.

Late Eocene–Late Oligocene (ca. 49–25 Ma)

Exhumation, diking, and localized fluvial sedimentation characterized the suture zone during late Eocene to late Oligocene time. Our ca. 46 Ma ZHe results indicate the ca. 69.5 Ma Cantwell Formation bentonite was buried deep enough to reset the ZHe system (~180 °C; Reiners et al., 2005). Vitrinite reflectance analysis of Cantwell Formation sedimentary strata along the upper East Fork of the Toklat River (Stanley, 1987) indicates a maximum temperature of ~160 °C, consistent with significant burial. We infer total burial of the bentonite was at least ~8 km, consistent with preservation of >4 km of Cantwell Formation sedimentary strata and >3 km of Teklanika Formation volcanic rocks (Gilbert et al., 1976; Ridgway et al., 1997; Cole et al., 1999). By ca. 46 Ma, the Cantwell basin was either exhuming or experienced a drop in regional geothermal gradient resulting in the closure of the ZHe system. We infer relatively slow exhumation and basin inversion during this time interval based on the HeFTy modeling (Fig. 14). Circa 46 Ma is broadly contemporaneous with a significant change in Pacific plate motion (Torsvik et al., 2017), initiation of the Aleutian Arc (Jicha et al., 2006) and renewed arc magmatism in the Alaska Range suture zone (Nokleberg et al., 1992a; Cole and Layer, 2002).

We infer that Oligocene Colorado Creek fluvial strata and dike swarms along the Denali fault record transtensional deformation linked to strike-slip deformation along the Denali fault ca. 38 to ca. 25 Ma. Similar age dikes are not reported distal from the fault zone. The fact that the dikes exist close to and preferentially along the north side of the fault implies a genetic link; transtensional deformation along the fault zone, perhaps by normal faults oriented oblique to the Denali fault, likely provided accommodation space for ascending arc magma. Notably, diking and fluvial sedimentation overlapped temporally and spatially with strike-slip basin development inferred along other segments of the Denali fault (Dickey, 1984; Ridgway and DeCelles, 1993), initial onset of rapid, persistent exhumation in the Alaska Range, and slab-edge volcanism in the Wrangell–St. Elias Range (Figs. 22 and 23; Richter et al., 1990; Trop et al., 2012). Circa 37 to ca. 16 Ma hornblende, muscovite, and biotite cooling ages (K-Ar and $^{40}Ar/^{39}Ar$) from the eastern Alaska Range proximal to the Denali fault are inferred to reflect metamorphism and deformation during lateral migration along the Denali fault (Nokleberg et al., 1992a; Roeske et al., 2012; Tait, 2017). Detrital thermochronologic data from modern rivers draining the Alaska Range reveal widespread late Oligocene to early Miocene cooling ages and suggest exhumation of the central Alaska Range starting ca. 30 Ma in the central Alaska Range (Lease et al., 2016). Bedrock thermochronology performed on granitoid samples from the central Alaska Range supports this interpretation (Benowitz et al., 2012c). Given that magmatism continued from ca. 30 Ma to ca. 25 Ma, this was likely a transition time as convergence of the southern Alaska block with the Denali fault increased with augmented coupling of the subducting Yakutat slab. The limiting of arc magmatism in the Alaska Range suture zone coincides with the initiation of Wrangell arc magmatism (Richter et al., 1990; Trop et al., 2012; Brueseke et al., 2019). Overall, Oligocene to early Miocene Alaska Range deformation and exhumation, localized within the lithological

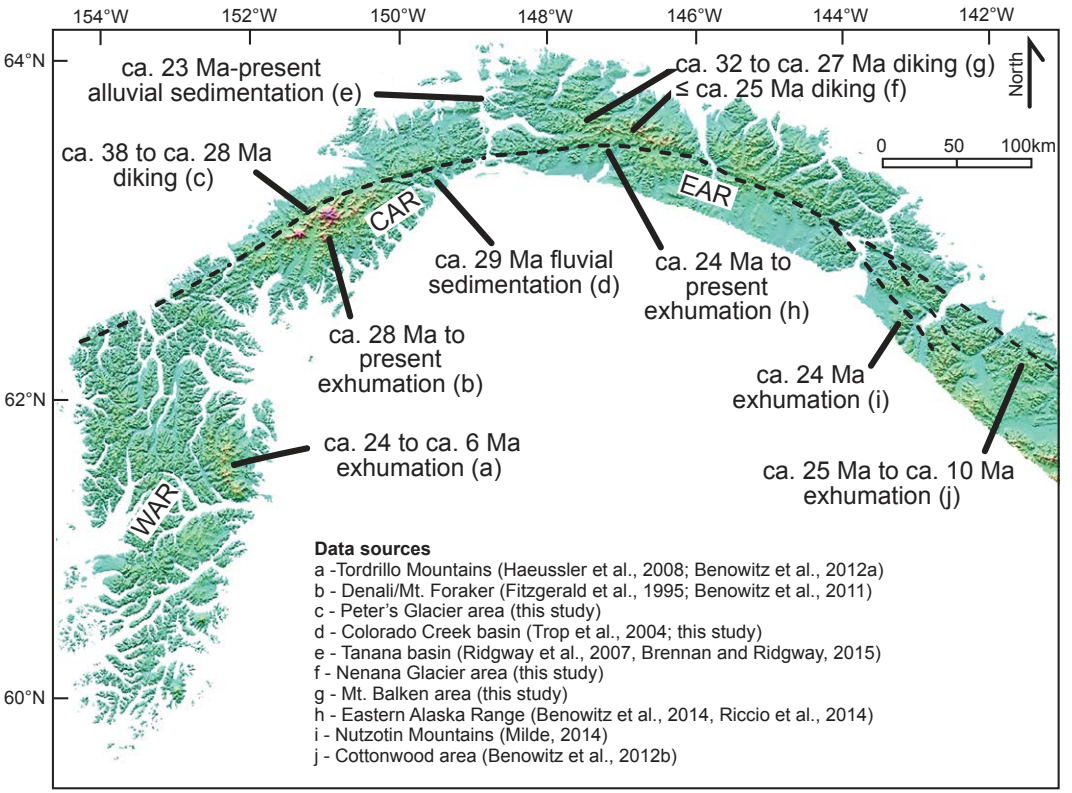

Figure 22. Digital elevation map of the Alaska Range flooded to 800 m to emphasize higher-elevation topography. Dashed black lines denote main segment of Denali fault, including McKinley strand in central Alaska Range (CAR). Other abbreviations: EAR—eastern Alaska Range; WAR—western Alaska Range. Note that emplacement of ca. 38–28 Ma dike swarms and ca. 29 Ma fluvial deposition was coincident with and preceding rapid, persistent exhumation of the Alaska Range (ca. 28 Ma to present) and foreland basin deposition in the Tanana basin (ca. 23 Ma to present). Refer to text for discussion and references.

weak crust comprising the Alaska Range suture zone, are interpreted to reflect partitioned strike-slip motion along the Denali fault driven by the far-field responses to initial Yakutat microplate collision at the plate margin >600 km to the southeast (Jadamec et al., 2013; Fitzgerald et al., 2014; Lease et al., 2016). Additional analysis of the spatially limited Oligocene dikes and sedimentary strata rocks in the Alaska Range suture zone is warranted to carefully evaluate these far-field collisional responses.

Neogene (25 Ma to Present)

Recent bedrock and detrital thermochronologic studies document rapid and persistent exhumation of the entire Alaska Range starting ca. 30–25 Ma (Benowitz et al., 2011, 2012a, 2012c, 2014; Fitzgerald et al., 2014; Riccio et al., 2014; Lease et al., 2016) coincident with and locally proceeding Oligocene fluvial sedimentation in the Tanana foreland basin north of the Range (Ridgway et al., 2007) and the McCallum and Colorado Creek basins south of the range (Allen, 2016; Waldien et al., 2018; this study) as well as arc-related dike swarm emplacement along the Denali fault (this study). Exhumation in the Alaska Range also impacted sedimentary basins positioned farther south of the range. The Susitna and Cook Inlet basins record late Oligocene–Neogene contractile deformation and increased sedimentation, including sediment reflecting erosion of bedrock sources in the central and eastern Alaska Range (Finzel et al., 2015, 2016; Saltus et al., 2016; Bristol et al., 2017; Haeussler et al., 2017b). Overall, the Oligocene–Miocene was a period of major topographic development (e.g., Bill et al., 2018) and regional paleodrainage reorganization across southern Alaska (Davis et al., 2015; Finzel et al., 2016; Benowitz et al., 2019). Oligocene–Holocene deformation, nonmarine sedimentation, magmatism, and paleodrainage reorganization within the suture zone is consistent with oblique plate convergence, including collision and flat-slab subduction of the Yakutat terrane (Ridgway et al., 2007; Trop et al., 2012; Benowitz et al., 2014; Bemis et al., 2015). Geologic and geophysical studies infer that progressive northward subduction of overthickened oceanic crust of the Yakutat terrane transferred compressive stresses inboard to the overriding plate resulting in a zone of broad, diffuse

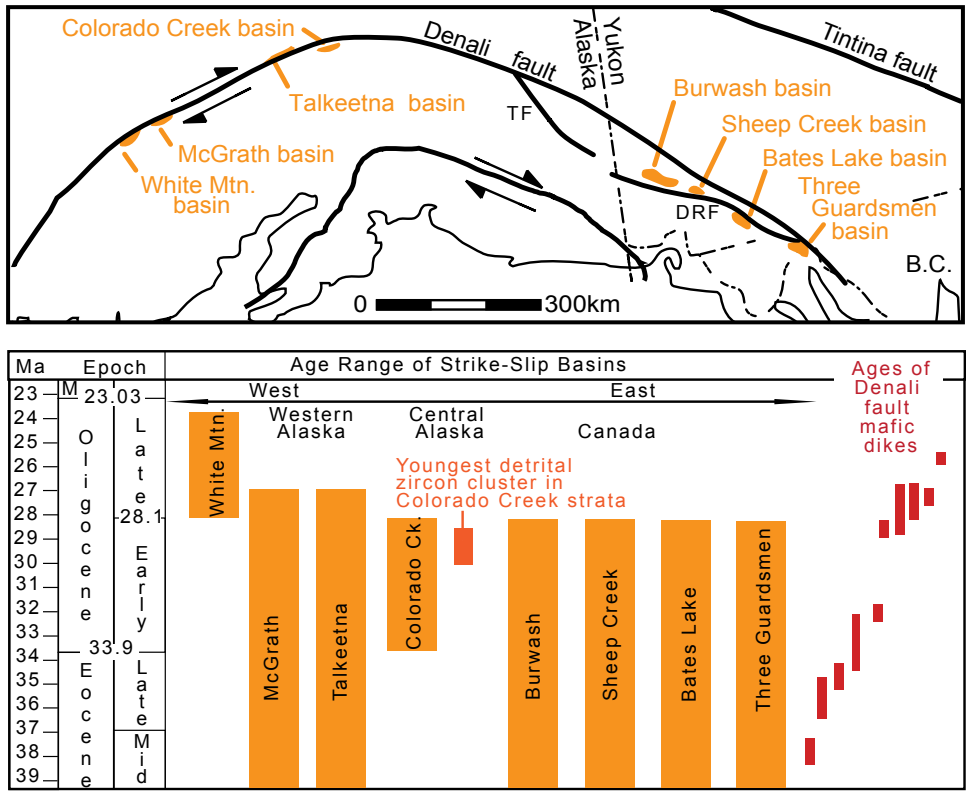

Figure 23. Generalized map (A) and correlation chart (B) showing late Eocene to Oligocene strike-slip–related sedimentary basin fills exposed along the >2000 km length of the Denali fault. Note overlap in timing of Denali fault diking and strike-slip basin development. Refer to Figure 17 for dike ages and Figure 15 for detrital-zircon ages. Strike-slip basin ages summarize palynological data reported by Dickey (1984), Ridgway et al. (1995), Ridgway et al. (1999), and Trop et al. (2004).

deformation and sparse magmatism (e.g., Ferris et al., 2003; Eberhart-Phillips, 2006; Finzel et al., 2011; Trop et al., 2012; Arkle et al., 2013; Jadamec et al., 2013). The essentially shutting off of arc magmatism in the Alaska Range suture zone and syntectonic increase in deformation rates in the region at ca. 25 Ma also coincides with an increase in convergence rate of the Pacific-Yakutat plate with Alaska at ca. 25 Ma (Jicha et al., 2018); this change in convergence may have created a more transpressive environment along this section of the Denali fault and limited the fault zone acting as a conduit for arc magmatism.

The detrital-zircon signature of the Oligocene Colorado Creek Formation is best explained by erosion of bedrock sources presently exposed in the eastern Alaska Range, indicating ~150 km of dextral displacement since deposition ca. 29 Ma. Previous studies infer hundreds to kilometers of dextral displacement along the eastern part of the fault system during Cretaceous–Cenozoic time based on offset geologic features (Nokleberg et al., 1985; Lowey, 1998; Allen, 2016), including ~100 km between 57 and 25 Ma, and ~300 km since ca. 25 Ma (Benowitz et al., 2012b; Roeske et al., 2012; Riccio et al., 2014). A rate of ~300 km in ca. 25 Ma is a long-term horizontal slip rate of ~12 mm/yr, which is similar to the constrained cumulative Pleistocene slip rates (~13 mm/yr, Matmon et al., 2006; Mériaux et al., 2009; Haeussler et al., 2017a) for the eastern Denali fault region (Fig. 1). The long-term average slip rate based on our new offset constraint is ~5 mm/yr, which is remarkably close to and within broad error (~2 mm/yr) of the Pleistocene to present slip rate of ~7 mm/yr (Haeussler et al., 2017a). In contrast, only tens of kilometers of Cenozoic dextral offset are possible along the central part of the fault system in the central Alaska Range, if piercing points reported by other researchers are correct (Reed and Lanphere, 1974; Csejtey et al., 1982). The long-term average slip rate of 1 mm/yr since ca. 38 Ma (Reed and Lanphere, 1974) to the west is in conflict with the Pleistocene slip rate of ~5 mm/yr (Haeussler et al., 2017a). Hence, the often-cited Foraker-McGonagall same-pluton piercing point may be incorrect, and these plutons may not be genetically related. The observed westward decreases in displacement and slip rates, in conjunction with fault geometry and topography, indicate partitioning of fault-normal convergence along the Denali fault in a zone of transpression resulting from increasing obliquity between the fault and plate convergence (Hauessler, 2008; Fitzgerald et al., 2014; Bemis et al., 2015; Waldien et al., 2018).

Changes in basin character along the Denali fault illuminate the overall tectonic setting. Strike-slip basin development along the eastern Denali–Duke River fault (Ridgway and DeCelles, 1993) occurs where "strong" terranes collide and plate motion is oblique to the fault (Fitzgerald et al., 2014). Where the "weak" Alaska Range suture zone occurs, plate motion is more orthogonal to the fault, a broad foreland basin formed along the north flank of the Alaska Range (Tanana basin; Ridgway et al., 2007; Bemis et al., 2015), and smaller transpressional basins formed along the Denali fault within the Alaska Range (Dickey, 1984; Trop et al., 2004). Overall, obliquity of convergence (Vallage et al., 2014) and Oligocene to present-day Wrangell arc magmatism along the Denali fault system (e.g., Brueseke et al., 2019) suggest chiefly transtensional tectonics (along the eastern Denali fault system) that transition to chiefly transpressive shortening along the fault in the Alaska Range. This is consistent with geodynamic modeling of Yakutat collision that produces a kinematic field with chiefly strike slip along the eastern Denali fault and mainly shortening and uplift in the Alaska Range (Koons et al., 2010).

The thermochronologic and geologic record suggest that the overall locus of magmatism uplift, exhumation, and basin formation across southern Alaska has changed substantially during latest Cretaceous–Cenozoic time owing to the changing nature of the plate boundary forces (geometry and coupling of subducting slabs, plate motion change, etc.). However, a relative constant with regard to the formation of the Alaska Range along the Denali fault is that the majority of tectonic uplift forming the high-standing topography (along with related exhumation) has occurred south of the fault in the central Alaska Range and north of the fault in the eastern Alaska Range (Fitzgerald et al., 2014). This has been related to strength contrasts between the Yukon composite terrane (strongest) to the north, the Wrangellia composite terrane to the south, and the intervening suture zone with deformed Mesozoic Kahiltna and Cantwell basins (weakest) (Figs. 1 and 2; Fitzgerald et al., 2014). Preexisting fault geometry (Hines Creek fault on Figs. 1 and 2, in particular) may have also controlled the location where deformation has been focused.

The >70 m.y. record of arc magmatism within the Alaska Range suture zone deserves further investigation. The distance from the trench to the Alaska Range suture zone today is ~500 km; however, active arc magmatism is still occurring locally (Buzzard Marr, Andronikov and Mukasa, 2010). An intrinsic feature of the upper plate is likely driving the location of central Alaska Range arc magmatism, given the significant variations in slab age, slab thickness, and convergence rates over the past ~70 m.y. The deformed Alaska Range suture zone has been thickened to ~45 km (Veenstra et al., 2006) and is likely playing a hydrostatic role in flattening the underlying slabs regardless of slab characteristics, similar to a geodynamic model proposed to explain flat-slab subduction in central Mexico (Ferrari et al., 2012). The Denali fault, at times, has also played a role as a conduit for magma, as demonstrated by the Oligocene dike swarm documented in this study.

The long-lived poly-phase nature of discrete structures is well documented (Oriolo et al., 2016; Betka et al., 2017), but suture zones can provide a greater system-wide perspective on convergent margin processes. Long-lived suture zones can experience numerous episodes of reactivation (Dewey and Burke, 1973), basin subsidence–basin inversion (DeCelles et al., 2011), magmatism (Chung et al., 2005), focused deformation-exhumation (Martin et al., 2015), strike-slip faulting (Peltzer and Tapponnier, 1988), and they play a role in the dip of the underlying slab through crustal thickening (Burg et al., 1987; Manea et al., 2012).

More than 60 years of geologic field studies and research (St. Amand, 1957; Richter and Matson, 1971) have documented the existence and history of the Alaska Range suture zone. We hope our integration of new geochemical, geochronologic, and sedimentological constraints with previous data sets demonstrates the utility of revisiting the Alaska Range suture zone. In summary, the Alaska Range suture zone having originally initiated in Cretaceous time, provides a record of ~120 million years of Northern Cordilleran magmatism and deformation and continues to shape the tectonic-magmatic regime of the interior of Alaska into the Quaternary (Andronikov and Mukasa, 2010).

KEY CONCLUSIONS

(1) Kahiltna assemblage marine strata exposed in the central Alaska Range at Colorado Creek yield a maximum depositional age of ca. 97 Ma and detrital age spectra comparable to previously dated marine strata exposed along strike in the Alaska Range, as well as modern river sediment from the watershed draining the Colorado Creek basin. Compositional data and detrital zircon ages indicate key sediment sources were Cretaceous and Paleozoic–Precambrian igneous and sedimentary rocks located within and inboard of the suture zone in the Alaska Range and Yukon-Tanana uplands.

(2) Latest Cretaceous lavas exposed in the central Alaska Range record arc magmatism within the suture zone. The previously undated lavas (Colorado Creek volcanics) exposed just south of the Denali fault yield ca. 70 to ca. 68 Ma $^{40}Ar/^{39}Ar$ ages and arc-affinity geochemical compositions. Bentonites exposed north of the Denali fault yield ca. 71 to ca. 68 Ma U-Pb zircon ages, reflecting magmatism within the suture zone or from more distant eruptive centers, likely south of the suture zone. Together, these data sets offer relatively rare records of volcanism associated with more widespread Late Cretaceous intrusions that were emplaced in the suture zone and the Wrangellia composite terrane following initial mid-Cretaceous collision.

(3) Detrital-zircon U-Pb ages from a modern river draining the Cantwell basin and Pb-loss constraints on ca. 70 Ma ash-fall zircons delineate ca. 57 Ma as the timing of peak magmatism within the suture zone during early Paleocene to early Eocene time, similar to ca. 61 to ca. 50 Ma magmatic activity documented across southern Alaska. Magmatism during this time included emplacement of granitic plutons with intraplate characteristics in the Alaska Range suture zone.

(4) Oligocene sedimentary strata and Eocene–Oligocene dike swarms exposed along the Denali fault reflect synchronous nonmarine sedimentation and

magmatism along the Denali fault ca. 38 to ca. 25 Ma and may reflect transtensional deformation along the fault. These processes overlapped temporally and spatially with initial onset of rapid, persistent exhumation in the Alaska Range, metamorphism in the Alaska Range, and volcanism in the Wrangell–St. Elias Range. Thermochronologic data from Cantwell Formation bentonites document burial and thermal reheating from ca. 70 to ca. 55 Ma, followed by exhumation through the ZHe closure temperature at ca. 46 Ma and the apatite fission-track closure temperature at ca. 20 to ca. 15 Ma. Collectively, these data sets are interpreted to reflect far-field responses to initial Yakutat microplate collision at the plate margin (ca. 30 Ma) in conjunction with a Pacific-Yakutat plate vector change at ca. 25 Ma, leading to a more convergent regime along the apex of the Denali fault and limiting the fault as a conduit for arc magmatism. Transpressional shortening along the Denali fault resulted in continued postcollisional deformation within the Alaska Range suture zone, a zone of relatively weak crust, above the shallowly subducting Yakutat microplate. Transpressional strike-slip deformation prompted lateral shuffling of Cretaceous–Cenozoic basinal strata and magmatic products. Detrital geochronologic and compositional data from Oligocene fluvial strata at Colorado Creek reflect erosion of Cretaceous igneous and sedimentary bedrock sources that crop out along much of the Denali fault but are best explained by restoration of ~150 km of dextral displacement along the Denali fault since deposition ca. 29 Ma; future studies can evaluate this hypothesis. This interpretation contributes to a number of studies documenting westward increases in strain partitioning along the Denali fault from the eastern to central Alaska Range and continuous Denali fault strike-slip motion from ca. 57 Ma to present.

ACKNOWLEDGMENTS

Our studies in the Alaska Range would not have been possible without earlier geologic mapping studies by U.S. Geological Survey geologists, including B. Csejtey, D. Jones, W. Nokleberg, and C. Wahrhaftig, among many others. Primary funding was provided by the National Science Foundation (NSF) Tectonics Program: NSF grants EAR-1249885 and EAR-1550123 to J. Benowitz and EAR-0910545 to J. Trop. We thank the Alaska Geological and Geophysical Survey for logistical support; Denali National Park and Preserve for facilitating field work; the Arizona LaserChron Center for assisting with geochronological analyses; University of Alaska Fairbanks students K. Davis and P. Terhune and Bucknell University students E. Donaghy and K. Kissock for field assistance; and C. Kirby for GIS assistance developing geologic maps. We thank Steve Box, Jamey Jones, and an anonymous reviewer for constructive feedback.

REFERENCES CITED

Aldanmaz, E., Pearce, J.A., Thirwall, M.F., and Mitchell, J.G., 2000, Petrogenetic evolution of late Cenozoic, post-collision volcanism in western Anatolia, Turkey: Journal of Volcanology and Geothermal Research, v. 102, p. 67–95, https://doi.org/10.1016/S0377-0273(00)00182-7.

Aleinikoff, J.N., Dusel-Bacon, C., and Foster, H.L., 1981, Geochronologic studies in the Yukon-Tanana Upland, east-central Alaska, *in* Albert, N.R.D., and Hudson, T., eds., Accomplishments during 1979: U.S. Geological Survey Circular 823-B, p. 34–37.

Aleinikoff, J.N., Foster, H.L., Nokleberg, W.J., and Dusel-Bacon, C., 1984, Isotopic evidence from detrital zircons for Early Proterozoic crustal materials, east-central Alaska, *in* Coonrad, W.L., and Elliott, R.L., eds., Accomplishments during 1981: U.S. Geological Survey Circular 868, p. 43–45.

Aleinikoff, J.N., Dusel-Bacon, C., and Foster, H., 1986, Geochronology of augen gneiss and related rocks, Yukon-Tanana terrane, east-central Alaska: Geological Society of America Bulletin, v. 97, p. 626–637, https://doi.org/10.1130/0016-7606(1986)97<626:GOAGAR>2.0.CO;2.

Allam, A.A., Schulte-Pelkum, V., Ben-Zion, Y., Tape, C., Ruppert, N., and Ross, Z.E., 2017, Ten kilometer vertical Moho offset and shallow velocity contrast along the Denali fault zone from double-difference tomography, receiver functions, and fault zone head waves: Tectonophysics, v. 721, p. 56–69, https://doi.org/10.1016/j.tecto.2017.09.003.

Allen, W.K., 2016, Miocene–Pliocene strike-slip basin development along the Denali fault system in the eastern Alaska Range: Chronostratigraphy and provenance of the McCallum formation and implications for displacement [M.S. thesis]: West Lafayette, Indiana, Purdue University, 146 p.

Amato, J.M., Pavlis, T.L., Clift, P.D., Kochelek, E.J., Hecker, J.P., Worthman, C.M., and Day, E.M., 2013, Architecture of the Chugach accretionary complex as revealed by detrital zircon ages and lithologic variations: Evidence for Mesozoic subduction erosion in south-central Alaska: Geological Society of America Bulletin, v. 125, p. 1891–1911, https://doi.org/10.1130/B30818.1.

Andronikov, A.V., and Mukasa, S.B., 2010, $^{40}Ar/^{39}Ar$ eruption ages and geochemical characteristics of Late Tertiary to Quaternary intraplate and arc-related lavas in interior Alaska: Lithos, v. 115, p. 1–14, https://doi.org/10.1016/j.lithos.2009.11.002.

Arculus, R.J., 1994, Aspects of magma genesis in arcs: Lithos, v. 33, p. 189–208, https://doi.org/10.1016/0024-4937(94)90060-4.

Arkle, J.C., Armstrong, P.A., Haeussler, P.J., Prior, M.G., Hartman, S.K., Sendziak, L., and Brush, J.A., 2013, Focused exhumation in the syntaxis of the western Chugach Mountains and Prince William Sound, Alaska: Geological Society of America Bulletin, v. 125, p. 776–793, https://doi.org/10.1130/B30738.1.

Bemis, S.P., Carver, G.A., and Koehler, R.D., 2012, The Quaternary thrust system of the northern Alaska Range: Geosphere, v. 8, p. 196–205, https://doi.org/10.1130/GES00695.1.

Bemis, S.P., Weldon, R.J., and Carver, G.A., 2015, Slip partitioning along a continuously curved fault: Quaternary geologic controls on Denali fault system slip partitioning, growth of the Alaska Range, and the tectonics of south-central Alaska: Lithosphere, v. 7, p. 235–246, https://doi.org/10.1130/L352.1.

Benowitz, J., Trop, J.M., Cole, R.B., Layer, P.W., O'Sullivan, P.B., Roeske, S.M., and Brueseke, M., 2016, Mesozoic-Cenozoic magmatic history of the Alaska Range Suture Zone: Geological Society of America, Abstract with Programs, v. 48, no. 7, https://doi.org/10.1130/abs/2016AM-277989.

Benowitz, J.A., Layer, P.W., Armstrong, P.A., Perry, S.E., Haeussler, P.J., Fitzgerald, P.G., and VanLaningham, S., 2011, Spatial variations in focused exhumation along a continental-scale strike-slip fault: The Denali fault of the eastern Alaska Range: Geosphere, v. 7, p. 455–467, https://doi.org/10.1130/GES00589.1.

Benowitz, J.A., Haeussler, P.J., Layer, P.W., O'Sullivan, P.B., Wallace, W.K., and Gillis, R.J., 2012a, Cenozoic tectono-thermal history of the Tordrillo Mountains, Alaska: Paleocene–Eocene ridge subduction, decreasing relief, and late Neogene faulting: Geochemistry, Geophysics, Geosystems, v. 13, Q04009, https://doi.org/10.1029/2011GC003951.

Benowitz, J.A., Vansant, G., Roeske, S., Layer, P.W., Hults, C.P., and O'Sullivan, P., 2012b, Geochronological constraints on the Eocene to present slip rate history of the eastern Denali fault system: Geological Society of America Abstracts with Programs, v. 44, no. 7, p. 634.

Benowitz, J.A., Bemis, S.P., O'Sullivan, P.B., Layer, P.W., Fitzgerald, P.G., and Perry, S.E., 2012c, The Mount McKinley restraining bend: Denali Fault, Alaska: Geological Society of America Abstracts with Programs, v. 44, no. 7, p. 597.

Benowitz, J.A., Layer, P.W., and VanLaningham, S., 2014, Persistent long-term (c. 24 Ma) exhumation in the Eastern Alaska Range constrained by stacked thermochronology, *in* Jourdan, F., Mark, D.F., and Verati, C., eds., Advances in $^{40}Ar/^{39}Ar$ Dating: From Archaeology to Planetary Sciences: Geological Society of London Special Publication 378, p. 225–243, https://doi.org/10.1144/SP378.12.

Benowitz, J.A., Davis, K., and Roeske, S., 2019, A river runs through it both ways across time: $^{40}Ar/^{39}Ar$ detrital and bedrock muscovite geochronology constraints on the Neogene paleodrainage history of the Nenana River system, Alaska Range: Geosphere, v. 15, p. 682–701, https://doi.org/10.1130/GES01673.1.

Beranek, L.P., van Staal, C.R., McClelland, W.C., Joyce, N., and Israel, S., 2014, Late Paleozoic assembly of the Alexander-Wrangellia-Peninsular composite terrane, Canadian and Alaskan Cordillera: Geological Society of America Bulletin, v. 126, p. 1531–1550, https://doi.org/10.1130/31066.1.

Betka, P.M., Gillis, R.J., and Benowitz, J.A., 2017, Cenozoic sinistral transpression and polyphase slip within the Bruin Bay fault system, Iniskin-Tuxedni region, Cook Inlet, Alaska: Geosphere, v. 13, p. 1806–1833, https://doi.org/10.1130/GES01464.1.

Bier, S., and Fisher, D., 2003, Structure and kinematics of a transect across the Kahiltna assemblage, south-central Alaska: Geological Society of America, Abstracts with Programs, v. 35, no. 6, p. 560.

Bier, S.E., Fisher, D.M., Feineman, M., and O'Sullivan, P.B., 2017, Structural fabrics, geochemistry, and geochronology of the Reindeer Hills mélange, a suture zone in south-central Alaska, Geological Society of America Abstracts with Programs, v. 49, no. 6, https://doi.org/10.1130/abs/2017AM-305230.

Bill, N.S., Mix, H.T., Clark, P.U., Reilly, S.P., Jensen, B.J., and Benowitz, J.A., 2018, A stable isotope record of late Cenozoic surface uplift of southern Alaska: Earth and Planetary Science Letters, v. 482, p. 300–311, https://doi.org/10.1016/j.epsl.2017.11.029.

Birsic, E., Stewart, J., and Cole, R.B., 2011, Garnet-bearing granitic pluton in a collisional terrane suture zone, northern Talkeetna Mountains, south-central Alaska: Geological Society of America Abstracts with Programs, v. 43, no. 1, p. 63.

Bleick, H.A., Till, A.B., Bradley, D.C., O'Sullivan, P.B., Wooden, J.L., Bradley, D.B., Taylor, T.A., Friedman, S.B., and Hults, C.P., 2012, Early Tertiary exhumation of the flank of a forearc basin, southwest Talkeetna Mountains, Alaska: U.S. Geological Survey Open-File Report 2012-1232, http://pubs.usgs.gov/of/2012/1232/.

Bradley, D., Kusky, T., Haeussler, P., Goldfarb, R., Miller, M., Dumoulin, J., Nelson, S., and Karl, S., 2003, Geologic signature of early Tertiary ridge subduction in Alaska, *in* Sisson, V.B., Roeske, S., and Pavlis, T.L., eds., Geology of a Transpressional Orogen Developed during Ridge-Trench Interaction along the North Pacific Margin: Geological Society of America Special Paper 375, p. 19–49, https://doi.org/10.1130/0-8137-2371-X.19.

Bradley, D.C., McClelland, W.C., Wooden, J.L., Till, A.B., Roeske, S.M., Miller, M.L., Karl, S.M., and Abbott, J.G., 2007, Detrital zircon geochronology of some Neoproterozoic to Triassic rocks in interior Alaska, *in* Ridgway, K.D., Trop, J.M., Glen, J.M.G., and O'Neill, J.M., eds., Tectonic Growth of a Collisional Continental Margin: Crustal Evolution of Southern Alaska: Geological Society of America Special Paper 431, p. 155–189, https://doi.org/10.1130/2007.2431(07).

Brennan, P.R.K., and Ridgway, K.D., 2015, Detrital zircon record of Neogene exhumation of the central Alaska Range: A far-field upper plate response to flat-slab subduction: Geological Society of America Bulletin, v. 127, p. 945–961, https://doi.org/10.1130/B31164.1.

Brennan, P.R.K., Gilbert, H., and Ridgway, K.D., 2011, Crustal structure across the central Alaska Range: Anatomy of a Mesozoic collisional zone: Geochemistry, Geophysics, Geosystems, v. 12, Q04010, https://doi.org/10.1029/2011GC003519.

Bristol, I.M., Trop, J.M., Benowitz, J., and Davis, K.N., 2017, Major Miocene paleodrainage in south-central Alaska: sedimentology, depositional age, and provenance of strata exposed in the southwestern Talkeetna Mountains: Geological Society of America Abstracts with Programs, v. 49, no. 4, https://doi.org/10.1130/abs/2017CD-292545.

Brueseke, M.E., Benowitz, J.A., Trop, J.M., Davis, K.N., Berkelhammer, S.E., Layer, P.W., and Morter, B.K., 2019, The Alaska Wrangell Arc: ~30 Ma of subduction-related magmatism along a still active arc-transform junction: Terra Nova, v. 31, no. 1, p. 59–66.

Burg, J.P., Leyreloup, A., Girardeau, J., and Chen, G.M., 1987, Structure and metamorphism of a tectonically thickened continental crust: The Yalu Tsangpo suture zone (Tibet): Philosophical Transactions of the Royal Society of London. Series A, Mathematical and Physical Sciences, v. 321, p. 67–86, https://doi.org/10.1098/rsta.1987.0005.

Burkett, C.A., Bemis, S.P., and Benowitz, J.A., 2016, Along-fault migration of the Mount McKinley restraining bend of the Denali fault defined by late Quaternary fault patterns and seismicity, Denali National Park and Preserve, Alaska: Tectonophysics, v. 693, p. 489–506, https://doi.org/10.1016/j.tecto.2016.05.009.

Cameron, C.E., Nye, C., Bull, K.F., and Woods, R.E.F., 2015, Jumbo Dome, Interior Alaska: Whole-rock major- and trace-element analyses: State of Alaska, Department of Natural Resources, Division of Geological and Geophysical Surveys, Raw-Data File 201-14.

Carrion, L., Birsic, E., Cole, R.B., and Chung, S.L., 2012, Bimodal hypabyssal intrusions following granitic pluton emplacement in a collisional terrane suture zone, northern Talkeetna Mountains, South-Central Alaska: Geological Society of America Abstracts with Programs, v. 44, no. 7, p. 544.

Cavazza, W., Albino, I., Zattin, M., Galoyan, G., Imamverdiyev, N., and Melkonyan, R., 2015, Thermochronometric evidence for Miocene tectonic reactivation of the Sevan-Akera suture zone (Lesser Caucasus): A far-field tectonic effect of the Arabia–Eurasia collision?, *in* Sosson, M., Stephenson, R.A., and Adamia, S.A., eds., Tectonic Evolution of the Eastern Black Sea and Caucasus: Geological Society of London Special Publication 428, p. 187–198, https://doi.org/10.1144/SP428.4.

Cawood, P.A., Kröner, A., Collins, W.J., Kusky, T.M., Mooney, W.D., and Windley, B.F., 2009, Accretionary orogens through Earth history, *in* Cawood, P.A., and Kröner, A., eds., Earth Accretionary Systems in Space and Time: Geological Society of London Special Publication 318, p. 1–36, https://doi.org/10.1144/SP318.1.

Ceschini, A., Cole, R.B., and Chung, S.L., 2013, Granitic and volcanic episodes in a collisional setting, Clark Creek igneous field, northern Talkeetna Mountains, Alaska: Geological Society of America Abstracts with Programs, v. 45, no. 7, p. 165.

Cherniak, D.J., and Watson, E.B., 2001, Pb diffusion in zircon: Chemical Geology, v. 172, p. 5–24, https://doi.org/10.1016/S0009-2541(00)00233-3.

Chung, S.L., Chu, M.F., Zhang, Y., Xie, Y., Lo, C.H., Lee, T.Y., Lan, C.Y., Li, X., Zhang, Q., and Wang, Y., 2005, Tibetan tectonic evolution inferred from spatial and temporal variations in post-collisional magmatism: Earth-Science Reviews, v. 68, p. 173–196, https://doi.org/10.1016/j.earscirev.2004.05.001.

Cloos, M., 1993, Lithospheric buoyancy and collisional orogenesis: Subduction of oceanic plateaus, continental margins, island arcs, spreading ridges, and seamounts: Geological Society of America Bulletin, v. 105, p. 715–737, https://doi.org/10.1130/0016-7606(1993)105<0715:LBACOS>2.3.CO;2.

Cole, R., Ridgway, K.D., Layer, P.W., and Drake, J., 1999, Kinematics of basin development during the transition from terrane accretion to strike-slip tectonics, Late Cretaceous–early Tertiary Cantwell Formation, south central Alaska: Tectonics, v. 18, p. 1224–1244, https://doi.org/10.1029/1999TC900033.

Cole, R.B., and Chung, S.L., 2013, Late Cretaceous to Eocene progression of arc and collisional magmatism in south-central Alaska: Geological Society of America Abstracts with Programs, v. 45, no. 7, p. 77.

Cole, R.B., and Layer, P.W., 2002, Stratigraphy, age, and geochemistry of Tertiary volcanic rocks and associated synorogenic deposits, Mount McKinley Quadrangle, Alaska, *in* Wilson, F.H., and Galloway, J.P., eds., Studies by the U.S. Geological Survey in Alaska, 2000: U.S. Geological Survey Professional Paper 1662, p. 19–43.

Cole, R.B., Chung, S.L., Ridgway, K.D., and Shinjo, R., 2006a, Nd-Sr-Pb isotope composition of post-collisional volcanic rocks in front of an accreted terrane suture zone, Cantwell Formation, central Alaska Range: Geological Society of America Abstracts with Programs, v. 38, no. 5, p. 20.

Cole, R.B., Nelson, S.W., Layer, P.W., and Oswald, P.J., 2006b, Eocene volcanism above a depleted mantle slab window in southern Alaska: Geological Society of America Bulletin, v. 118, p. 140–158, https://doi.org/10.1130/B25658.1.

Cole, R.B., Layer, P.W., Hooks, B., Cyr, A., and Turner, J., 2007, Magmatism and deformation in a terrane suture zone south of the Denali Fault, northern Talkeetna Mountains, Alaska, *in* Ridgway, K.D., Trop, J.M., Glen, J.M.G., O'Neill, J.M., eds., Tectonic Growth of a Collisional Continental Margin: Crustal Evolution of Southern Alaska: Geological Society of America Special Paper 431, p. 477–506, https://doi.org/10.1130/2007.2431(19).

Cole, R.B., Stewart, B.W., and Layer, P.W., 2011, Early Cenozoic Talkeetna Mountains Magmatism in south-central Alaska: Record of crust-mantle variations, terrane accretion, and pluton exhumation: Geological Society of America Abstracts with Programs, v. 43, no. 5, p. 553.

Cole, R.B., Chung, S.L., Birsic, E.M., Hung, C.H., Yang, J.H., and Takach, M.K., 2016, Magmatism and orogenic cycles in south-central Alaska: Insights from zircon U-Pb-Hf, whole rock Nd-isotope and geochemical data, and field observations: Geological Society of America Abstracts with Programs, v. 48, no. 7, https://doi.org/10.1130/abs/2016AM-287376.

Condie, K.C., 1998, Episodic continental growth and supercontinents: A mantle avalanche connection?: Earth and Planetary Science Letters, v. 163, p. 97–108, https://doi.org/10.1016/S0012-821X(98)00178-2.

Coney, P.J., Jones, D.L., and Monger, J.W., 1980, Cordilleran suspect terranes: Nature, v. 288, p. 329, https://doi.org/10.1038/288329a0.

Crone, A.J., Personius, S.F., Craw, P.A., Haeussler, P.J., and Staft, L.A., 2004, The Susitna Glacier thrust fault: characteristics of surface ruptures on the fault that initiated the 2002 Denali fault earthquake: Bulletin of the Seismological Society of America, v. 94, p. S5–S22, https://doi.org/10.1785/0120040619.

Csejtey, B., Cox, D.P., Evarts, R.C., Stricker, G.D., and Foster, H.L., 1982, The Cenozoic Denali fault systems and the Cretaceous accretionary development of southern Alaska: Journal of Geophysical Research, v. 87, p. 3741–3754, https://doi.org/10.1029/JB087iB05p03741.

Csejtey, B., Mullen, M.W., Cox, D.P., and Stricker, G.D., 1992, Geology and geochronology of the Healy quadrangle, south-central Alaska: United States Geological Survey Miscellaneous Investigation Series I-1961, 63 p., 2 plates, scale 1:250,000.

Davidson, C., and McPhillips, D., 2007, Along-strike variations in metamorphism and deformation of the strata of the Kahiltna basin, south central Alaska, *in* Ridgway, K.D., Trop, J.M., Glen, J.M.G., and O'Neill, J.M., eds., Tectonic Growth of a Collisional Continental Margin: Crustal Evolution of Southern Alaska: Geological Society of America Special Paper 431, p. 439–453, https://doi.org/10.1130/2007.2431(17).

Davidson, C.M., Hollister, L.S., and Schmid, S.M., 1992, Role of melt in the formation of a deep-crustal compressive shear zone: The Maclaren Glacier metamorphic belt, south-central Alaska: Tectonics, v. 11, p. 348–359, https://doi.org/10.1029/91TC02907.

Davis, K., Benowitz, J.A., and Roeske, S., 2015, $^{40}Ar/^{39}Ar$ dating of detrital micas from paleo and modern basin deposits, interior Alaska: Provenance, paleodrainage history, and constraints on Neogene orogenesis in the Alaska Range: Geological Society of America Abstracts with Programs, v. 47, no. 4, p. 51.

Day, W.C., O'Neill, J.M., Dusel-Bacon, C., Aleinikoff, J.N., and Siron, C.R., 2014, Geologic map of the Kechumstuk fault zone in the Mount Veta area: Fortymile mining district, east-central Alaska: U.S. Geological Society Scientific Investigations Map 3291.

DeCelles, P.G., Kapp, P., Quade, J., and Gehrels, G.E., 2011, Oligocene–Miocene Kailas basin, southwestern Tibet: Record of postcollisional upper-plate extension in the Indus-Yarlung suture zone: Geological Society of America Bulletin, v. 123, p. 1337–1362, https://doi.org/10.1130/B30258.1.

Decker, J.E., and Gilbert, W.G., 1978, The Mount Galen volcanics, a new middle Tertiary volcanic formation in the central Alaska Range: Alaska Division of Geological and Geophysical Surveys Geologic Report no. 59, 11 p.

Dewey, J.F., and Burke, K.C., 1973, Tibetan, Variscan, and Precambrian basement reactivation: products of continental collision: The Journal of Geology, v. 81, p. 683–692, https://doi.org/10.1086/627920.

Dickey, D.B., 1984, Cenozoic non-marine sedimentary rocks of the Farewell fault zone, McGrath Quadrangle, Alaska: Sedimentary Geology, v. 38, p. 443–463, https://doi.org/10.1016/0037-0738(84)90089-7.

Dilworth, K., Mortenson, J.K., Ebert, S., and Tosdal, R.M., 2007, Cretaceous reduced granitoids in the Goodpaster mining district, east-central Alaska: Canadian Journal of Earth Sciences, v, 44, p. 1347–1373.

Donelick, R.A., O'Sullivan, P.B., and Ketcham, R.A., 2005, Apatite fission-track analysis: Reviews in Mineralogy and Geochemistry, v. 58, p. 49–94, https://doi.org/10.2138/rmg.2005.58.3.

Dusel-Bacon, C., and Williams, I.S., 2009, Evidence for prolonged mid-Paleozoic plutonism and ages of crustal sources in east-central Alaska from SHRIMP U-Pb dating of syn-magmatic, inherited, and detrital zircon: Canadian Journal of Earth Sciences, v. 46, p. 21–39, https://doi.org/10.1139/E09-005.

Dusel-Bacon, C., Hopkins, M.J., Mortenson, J.K., Dashevsky, S.S., Bressler, J.R., and Day, W.C., 2006, Paleozoic tectonic and metallogenic evolution of the pericratonic rocks of east-central Alaska and adjacent Yukon Territory, *in* Colpron, M., and Nelson, J.L., eds., Paleozoic Evolution and Metallogeny of Pericratonic Terranes at the Ancient Pacific Margin of North America, Canadian and Alaskan Cordillera: Geological Association of Canada Special Paper 45, p. 25–74.

Eberhart-Phillips, D., Christensen, D.H., Brocher, T.M., Hansen, R., Ruppert, N.A., Haeussler, P.J., and Abers, G.A., 2006, Imaging the transition from Aleutian subduction to Yakutat collision in central Alaska, with local earthquakes and active source data: Journal of Geophysical Research. Solid Earth, v. 111, https://doi.org/10.1029/2005jb004240.

Fasulo, F., Ridgway, K.D., Allen, W.K., Romero, M.C., and Keough, B., 2018, U-Pb and Hf isotope detrital zircon geochronology of the Nutzotin Mountains sequence, south-central Alaska: Implications for the configuration of the Mesozoic convergent margin, NW Cordillera: Geological Society of America, Abstracts with Programs, v. 50, no. 6, https://doi.org/10.1130/abs/2018AM-322455.

Ferrari, L., Orozco-Esquivel, T., Manea, V., and Manea, M., 2012, The dynamic history of the Trans-Mexican Volcanic Belt and the Mexico subduction zone: Tectonophysics, v. 522, p. 122–149, https://doi.org/10.1016/j.tecto.2011.09.018.

Ferris, A., Abers, G.A., Christensen, D.H., and Veenstra, E., 2003, High resolution image of the subducted Pacific (?) plate beneath central Alaska, 50–150 km depth: Earth and Planetary Science Letters, v. 214, p. 575–588, https://doi.org/10.1016/S0012-821X(03)00403-5.

Finzel, E.S., Trop, J.M., Ridgway, K.D., and Enkelmann, E., 2011, Upper-plate proxies for flat-slab subduction processes in southern Alaska: Earth and Planetary Science Letters, v. 303, p. 348–360, https://doi.org/10.1016/j.epsl.2011.01.014.

Finzel, E.S., Ridgway, K.D., and Trop, J.M., 2015, Provenance signature of changing plate boundary conditions along a convergent margin: Detrital record of spreading-ridge and flat-slab subduction processes, Cenozoic forearc basins, Alaska: Geosphere, v. 11, p. 823–849, https://doi.org/10.1130/GES01029.1.

Finzel, E.S., Enkelmann, E., Falkowski, S., and Hedeen, T., 2016, Long-term fore-arc basin evolution in response to changing subduction styles in southern Alaska: Tectonics, https://doi.org/10.1002/2016TC004171.

Fiorillo, A.R., and Adams, T., 2012, A therizinosaur track from the lower Cantwell Formation (Upper Cretaceous) of Denali National Park, Alaska: Palaios, v. 27, p. 395–400, https://doi.org/10.2110/palo.2011.p11-083r.

Fiorillo, A.R., Hasiotis, S.T., Kobayashi, Y., and Tomsich, C.S., 2009, A pterosaur manus track from Denali National Park, Alaska Range, Alaska, United States: Palaios, v. 24, p. 466–472, https://doi.org/10.2110/palo.2008.p08-129r.

Fiorillo, A.R., Hasiotis, S.T., Kobayashi, Y., Breithaupt, B.H., and McCarthy, P.J., 2011, Bird tracks from the Upper Cretaceous Cantwell Formation of Denali National Park, Alaska, USA: A new perspective on ancient northern polar vertebrate biodiversity: Journal of Systematic Palaeontology, v. 9, p. 33–49, https://doi.org/10.1080/14772019.2010.509356.

Fiorillo, A.R., Adams, T.L., and Kobayashi, Y., 2012, New sedimentological, palaeobotanical, and dinosaur ichnological data on the palaeoecology of an unnamed Late Cretaceous rock unit in Wrangell-St. Elias National Park and Preserve, Alaska, USA: Cretaceous Research, v. 37, p. 291–299, https://doi.org/10.1016/j.cretres.2012.04.013.

Fiorillo, A.R., Hasiotis, S.T., and Kobayashi, Y., 2014, Herd structure in Late Cretaceous polar dinosaurs: A remarkable new dinosaur tracksite, Denali National Park, Alaska, USA: Geology, v. 42, p. 719–722, https://doi.org/10.1130/G35740.1.

Fiorillo, A.R., McCarthy, P.J., and Hasiotis, S.T., 2016, Crayfish burrows from the latest Cretaceous lower Cantwell Formation (Denali National Park, Alaska): Their morphology and paleoclimatic significance: Palaeogeography, Palaeoclimatology, Palaeoecology, v. 441, p. 352–359, https://doi.org/10.1016/j.palaeo.2015.05.019.

Fitzgerald, P.G., Sorkhabi, R.B., Redfield, T.F., and Stump, E., 1995, Uplift and denudation of the central Alaska Range—A case study in the use of apatite fission-track thermochronology to determine absolute uplift parameters: Journal of Geophysical Research, v. 100, p. 20,175–20,191, https://doi.org/10.1029/95JB02150.

Fitzgerald, P.G., Roeske, S.M., Benowitz, J.A., Riccio, S.J., Perry, S.E., and Armstrong, P.A., 2014, Alternating asymmetric topography of the Alaska Range along the strike-slip Denali fault: Strain partitioning and lithospheric control across a terrane suture zone: Tectonics, v. 33, https://doi.org/10.1002/2013TC003432.

Foster, H.L., Keith, T.E.C., and Menzie, W.D., 1994, Geology of the Yukon–Tanana area of east-central Alaska, *in* Plafker, G., and Berg, H.C., eds., The Geology of Alaska: Boulder, Colorado, Geological Society of America, Geology of North America, v. G-1, p. 205–240.

Garver, J.I., and Davidson, C.M., 2015, Southwestern Laurentian zircons in Upper Cretaceous flysch of the Chugach-Prince William terrane in Alaska: American Journal of Science, v. 315, p. 537–556, https://doi.org/10.2475/06.2015.02.

Gehrels, G., 2014, Detrital zircon U-Pb geochronology applied to tectonics: Annual Review of Earth and Planetary Sciences, v. 42, p. 127–149, https://doi.org/10.1146/annurev-earth-050212-124012.

Gehrels, G.E., and Kapp, P.A., 1998, Detrital zircon geochronology and regional correlation of metasedimentary rocks in the Coast Mountains, southeastern Alaska: Canadian Journal of Earth Sciences, v. 35, p. 269–279, https://doi.org/10.1139/e97-114.

Gehrels, G.E., and Ross, G.M., 1998, Detrital zircon geochronology of Neoproterozoic to Permian miogeoclinal strata in British Columbia and Alberta: Canadian Journal of Earth Sciences, v. 35, p. 1380–1401, https://doi.org/10.1139/e98-071.

Gehrels, G., Rusmore, M., Woodsworth, G., Crawford, M., Andronicos, C., Hollister, L., Patchett, J., Ducea, M., Butler, R., Klepeis, K., and Davidson, C., 2009, U-Th-Pb geochronology of the Coast Mountains batholith in north-coastal British Columbia: Constraints on age and tectonic evolution: Geological Society of America Bulletin, v. 121, p. 1341–1361, https://doi.org/10.1130/B26404.1.

Geisler, T., Pidgeon, R.T., Van Bronswijk, W., and Kurtz, R., 2002, Transport of uranium, thorium, and lead in metamict zircon under low-temperature hydrothermal conditions: Chemical Geology, v. 191, p. 141–154, https://doi.org/10.1016/S0009-2541(02)00153-5.

Gilbert, W.G., Ferrell, V.M., and Turner, D.L., 1976, The Teklanika Formation: A new Paleocene volcanic formation in the central Alaska Range: Division of Geological and Geophysical Surveys Geologic Report, v. 47, p. 1–16.

Greene, A.R., Scoates, J.S., and Weis, D., 2008, Wrangellia flood basalts in Alaska: A record of plume-lithosphere interaction in a Late Triassic accreted oceanic plateau: Geochemistry Geophysics Geosystems, v. 9, https://doi.org/10.1029/2008GC002092.

Haeussler, P.J., 1992, Structural evolution of an arc-basin: The Gravina Belt in central southeastern Alaska: Tectonics, v. 11, p. 1245–1265, https://doi.org/10.1029/92TC01107.

Haeussler, P.J., O'Sullivan, P.B., Berger, A.L., and Spotila, J.A., 2008, Neogene exhumation of the Tordrillo Mountains, Alaska, and correlations with Denali (Mount McKinley), *in* Freymueller, J.T., Haeussler, P.J., Wesson, R.L., and Ekström, G., eds., Active Tectonics and Seismic Potential of Alaska: American Geophysical Union, Geophysical Monograph Series, v. 179, p. 269–285.

Haeussler, P.J., Matmon, A., Schwartz, D.P., and Seitz, G.G., 2017a, Neotectonics of interior Alaska and the late Quaternary slip rate along the Denali fault system: Geosphere, v. 13, p. 1445–1463, https://doi.org/10.1130/GES01447.1.

Haeussler, P.J., Saltus, R.W., Stanley, R.G., Ruppert, N., Lewis, K., Karl, S.M., and Bender, A.M., 2017b, The Peters Hills basin, a Neogene wedge-top basin on the Broad Pass thrust fault, south-central Alaska: Geosphere, v. 13, https://doi.org/10.1130/GES01487.1.

Hampton, B.A., Ridgway, K.D.O., Neill, J.M., Gehrels, G.E., Schmidt, J., and Blodgett, R.B., 2007, Pre-, syn-, and postcollisional stratigraphic framework and provenance of Upper Triassic-Upper Cretaceous strata in the northwestern Talkeetna Mountains, Alaska, *in* Ridgway, K.D., Trop, J.M., Glen, J.M.G., and O'Neill, J.M., eds., Tectonic Growth of a Collisional Continental Margin: Crustal Evolution of Southern Alaska: Geological Society of America Special Paper 431, p. 401–438.

Hampton, B.A., Ridgway, K.D., and Gehrels, G.E., 2010, A detrital record of Mesozoic island arc accretion and exhumation in the North American Cordillera: U-Pb geochronology of the Kahiltna basin, southern Alaska: Tectonics, v. 29, https://doi.org/10.1029/2009TC002544.

Hampton, B.A., Jacobs, M.R., and Stopka, C.J., 2017, U-Pb detrital geochronology and Hf isotopic analyses from Upper Cretaceous strata of the northern Talkeetna Mountains, southern Alaska: Sediment dispersal and magmatism during the final accretionary phase of the Wrangellia composite terrane: Geological Society of America, Abstracts with Programs, v. 49, no. 6.

Harlan, S.S., Vielreicher, R.M., Mortensen, J.M., Bradley, D.C., Goldfarb, R.J., Snee, L.W., and Till, A.B., 2017, Geology and timing of ore formation in the Willow Creek Gold District, Talkeetna Mountains, southern Alaska: Economic Geology and the Bulletin of the Society of Economic Geologists, v. 112, p. 1177–1204, https://doi.org/10.5382/econgeo.2017.4506.

Hasebe, N., Barbarand, J., Jarvis, K., Carter, A., and Hurford, A.J., 2004, Apatite fission-track chronometry using laser ablation ICP-MS: Chemical Geology, v. 207, p. 135–145, https://doi.org/10.1016/j.chemgeo.2004.01.007.

Hendrix, M.S., Graham, S.A., Amory, J.Y., and Badarch, G., 1996, Noyon Uul syncline, southern Mongolia: Lower Mesozoic sedimentary record of the tectonic amalgamation of central Asia: Geological Society of America Bulletin, v. 108, p. 1256–1274, https://doi.org/10.1130/0016-7606(1996)108<1256:NUSSML>2.3.CO;2.

Hickman, R.G., Sherwood, K.W., and Craddock, C., 1990, Structural evolution of the Early Tertiary Cantwell basin, south central Alaska: Tectonics, v. 9, p. 1433–1449, https://doi.org/10.1029/TC009i006p01433.

Holdsworth, R.E., Handa, M., Miller, J.A., and Buick, I.S., 2001, Continental reactivation and reworking: An introduction, *in* Miller, J. A., Holdsworth, R.E., Buick, I.S., and Hand, H., eds., Continental Reactivation and Reworking: Geological Society of London Special Publication 184, p. 1–12, https://doi.org/10.1144/GSL.SP.2001.184.01.01.

Huff, C.J., 2008, Paleozoic to Neogene stratigraphic and structural history of the Alaska Range suture zone, north of the Denali fault, east central Alaska Range [M.S. thesis]: Davis, California, University of California Davis, 148 p.

Hults, C.P., Wilson, F.H., Donelick, R.A., and O'Sullivan, P.B., 2013, Two flysch belts having distinctly different provenance suggest no stratigraphic link between the Wrangellia composite terrane and the paleo-Alaskan margin: Lithosphere, v. 5, p. 575–594, https://doi.org/10.1130/L310.1.

Hung, C.H., 2008, Zircon U-Pb ages and geochemical characteristics of the McKinley sequence and associated plutons, central Alaska Range [M.S. thesis]: Taiwan, National Taiwan University, 78 p.

Israel, S., Beranek, L., Friedman, R.M., and Crowley, J.L., 2014, New ties between the Alexander terrane and Wrangellia and implications for North America Cordilleran evolution: Lithosphere, v. 6, p. 270–276, https://doi.org/10.1130/L364.1.

Jadamec, M.A., Billen, M.I., and Roeske, S.M., 2013, Three-dimensional numerical models of flat slab subduction and the Denali fault driving deformation in south-central Alaska: Earth and Planetary Science Letters, v. 376, p. 29–42, https://doi.org/10.1016/j.epsl.2013.06.009.

Jicha, B.R., Scholl, D.W., Singer, B.S., Yogodzinski, G.M., and Kay, S.M., 2006, Revised age of Aleutian Island Arc formation implies high rate of magma production: Geology, v. 34, p. 661–664, https://doi.org/10.1130/G22433.1.

Jicha, B.R., Garcia, M.O., and Wessel, P., 2018, Mid-Cenozoic Pacific plate motion change: Implications for the Northwest Hawaiian Ridge and circum-Pacific: Geology, v. 46, p. 939–942, https://doi.org/10.1130/G45175.1.

Johnson, D.M., Hooper, P.R., and Conrey, R.M., 1999, XRF analysis of rocks and minerals for major and trace elements on a single low-dilution Li-tetraborate fused bead: Advances in X-Ray Analysis, v. 41, p. 843–867.

Jones, D., Siberling, N., Gilbert, W., and Coney, P., 1982, Character, distribution, and tectonic significance of accretionary terranes in the central Alaska Range: Journal of Geophysical Research, v. 87, p. 3709–3717, https://doi.org/10.1029/JB087iB05p03709.

Jones, J.V., Todd, E., Box, S., Haeussler, P.J., Holm-Denoma, C.S., Ayuso, R.A., and Bradley, D.C., 2014, Late Cretaceous through Oligocene magmatic and tectonic evolution of the Western Alaska Range: Geological Society of America Abstracts with Programs, v. 46, no. 6, p. 781.

Kalbas, J.L., Ridgway, K.D., and Gehrels, G.E., 2007, Stratigraphy, depositional systems, and provenance of the Lower Cretaceous Kahiltna assemblage, western Alaska Range: Basin development in response to oblique collision, *in* Ridgway, K.D., Trop, J.M., Glen, J.M.G., and O'Neill, J.M., eds., Tectonic Growth of a Collisional Continental Margin: Crustal Evolution of Southern Alaska: Geological Society of America Special Paper 431, p. 307–343, https://doi.org/10.1130/2007.2431(13).

Karabinos, P., Macdonald, F.A., and Crowley, J.L., 2017, Bridging the gap between the foreland and hinterland I: Geochronology and plate tectonic geometry of Ordovician magmatism and terrane accretion on the Laurentian margin of New England: American Journal of Science, v. 317, p. 515–554, https://doi.org/10.2475/05.2017.01.

Ketcham, R.A., 2005, Forward and inverse modeling of low-temperature thermochronometry data: Reviews in Mineralogy and Geochemistry, v. 58, p. 275–314, https://doi.org/10.2138/rmg.2005.58.11.

Koehler, R.D., Farrel, R.E., Burns, P.A.C., and Combellick, R.A., 2012, Quaternary faults and folds in Alaska: A digital database: Alaska Division of Geological and Geophysical Surveys Miscellaneous Publication 141, 31 p., 1 sheet, scale 1:3,700,000.

Koepp, D., Trop, J.M., Benowitz, J.A., Layer, P.W., Zippi, P., and Brueseke, M.E., 2017, Mid-Cretaceous volcanism and fluvial-lacustrine sedimentation in the Alaska Range Suture Zone: Implications for the accretionary history of the Wrangellia composite terrane: Geological Society of America Abstracts with Programs, v. 49, no. 6, https://doi.org/10.1130/abs/2017AM-298406.

Koons, P.O., Hooks, B.P., Pavlis, T., Upton, P., and Barker, A.D., 2010, Three-dimensional mechanics of Yakutat convergence in the southern Alaskan plate corner: Tectonics, v. 29, TC4008, https://doi.org/10.1029/2009TC002463.

Lanphere, M.A., and Reed, B.L., 1985, The McKinley sequence of granitic rocks: A key element in the accretionary history of southern Alaska: Journal of Geophysical Research, v. 90, p. 11,413–11,430, https://doi.org/10.1029/JB090iB13p11413.

Laskowski, A.K., Kapp, P., Ding, L., Campbell, C., and Liu, X., 2017, Tectonic evolution of the Yarlung suture zone, Lopu Range region, southern Tibet: Tectonics, v. 36, p. 108–136, https://doi.org/10.1002/2016TC004334.

Lease, R.O., Haeussler, P.J., and O'Sullivan, P., 2016, Changing exhumation patterns during Cenozoic growth and glaciation of the Alaska Range: Insights from detrital thermochronology and geochronology: Tectonics, v. 35, https://doi.org/10.1002/2015TC004067.

Lowey, G.W., 1998, A new estimate of the amount of displacement on the Denali fault system based on the occurrence of carbonate megaboulders in the Dezadeash Formation (Jura–Cretaceous), Yukon, and the Nutzotin Mountains sequence (Jura–Cretaceous), Alaska: Bulletin of Canadian Petroleum Geology, v. 46, p. 379–386.

Lowey, G.W., 2011, Volcaniclastic gravity flow deposits in the Dezadeash Formation (Jura-Cretaceous), Yukon, Canada: Implications regarding the tectonomagmatic evolution of the Chitina arc in the northern Cordillera of North America: Lithos, v. 125, p. 86–100, https://doi.org/10.1016/j.lithos.2011.01.014.

Lowey, G.W., 2018, Provenance analysis of the Dezadeash Formation (Jurassic–Cretaceous), Yukon, Canada: Implications regarding a linkage between the Wrangellia composite terrane and the western margin of Laurasia: Canadian Journal of Earth Sciences, v. 56, p. 77–100, https://doi.org/10.1139/cjes-2017-0244.

Ludwig, K.R., 2008, Manual for Isoplot 3.7: Berkeley Geochronology Center, Special Publication 4, 77 p.

Manea, V.C., Pérez-Gussinyé, M., and Manea, M., 2012, Chilean flat slab subduction controlled by overriding plate thickness and trench rollback: Geology, v. 40, p. 35–38, https://doi.org/10.1130/G32543.1.

Manuszak, J.D., Ridgway, K.D., Trop, J.M., and Gehrels, G.E., 2007, Sedimentary record of the tectonic growth of a collisional continental margin: Upper Jurassic–Lower Cretaceous Nutzotin Mountains sequence, eastern Alaska Range, Alaska, *in* Ridgway, K.D., Trop, J.M., Glen, J.M.G., and O'Neill, J.M., eds., Tectonic Growth of a Collisional Continental Margin: Crustal Evolution of Southern Alaska: Geological Society of America Special Paper 431, p. 345–377, https://doi.org/10.1130/2007.2431(14).

Martin, A.J., Copeland, P., and Benowitz, J.A., 2015, Muscovite $^{40}Ar/^{39}Ar$ ages help reveal the Neogene tectonic evolution of the southern Annapurna Range, central Nepal, *in* Mukherjee, S., Carosi, R., van der Beek, P.A., Mukherjee, B.K., and Robinson, D.M., eds., Tectonics of the Himalaya: Geological Society of London Special Publication 412, p. 199–220, https://doi.org/10.1144/SP412.5.

Matmon, A., Schwartz, D.P., Haeussler, P.J., Finkel, R.J., Lienkaemper, J., Stenner, H.D., and Dawson, T.E., 2006, Denali fault slip rates and Holocene–late Pleistocene kinematics of central Alaska: Geology, v. 34, p. 645–648, https://doi.org/10.1130/G22361.1.

McClelland, W.C., Gehrels, G.E., and Saleeby, J.B., 1992, Upper Jurassic-lower Cretaceous basinal strata along the Cordilleran margin: Implications for the accretionary history of the Alexander-Wrangellia-Peninsular terrane: Tectonics, v. 11, p. 823–835, https://doi.org/10.1029/92TC00241.

Mériaux, A.S., Sieh, K., Finkel, R.C., Rubin, C.M., Taylor, M.H., Meltzner, A.J., and Ryerson, F.J., 2009, Kinematic behavior of southern Alaska constrained by westward decreasing postglacial slip rates on the Denali fault, Alaska: Journal of Geophysical Research, v. 114, p. B03404, https://doi.org/10.1029/2007JB005053.

Milde, E.R., 2014, Using low-temperature thermochronology to constrain the role of the Totshunda Fault in Southeastern Alaskan tectonics [MS thesis]: Syracuse, New York, Syracuse University, 127 p.

Moll-Stalcup, E.J., 1994, Latest Cretaceous and Cenozoic magmatism in mainland Alaska, *in* Plafker, G., and Berg, H.C., eds., The Geology of Alaska: Boulder, Colorado, Geological Society of America, Geology of North America, v. G-1, p. 589–619, https://doi.org/10.1130/DNAG-GNA-G1.589.

Monger, J.W.H., van der Heyden, P., Journeay, J.M., Evenchick, C.A., and Mahoney, J.B., 1994, Jurassic-Cretaceous basins along the Canadian Coast Belt: Their bearing on pre-mid-Cretaceous sinistral displacements: Geology, v. 22, p. 175–178, https://doi.org/10.1130/0091-7613(1994)022<0175:JCBATC>2.3.CO;2.

Nokleberg, W.J., Jones, D.L., and Silberling, N.J., 1985, Origin and tectonic evolution of the Maclaren and Wrangellia terranes, eastern Alaska Range, Alaska: Geological Society of America Bulletin, v. 96, p. 1251–1270, https://doi.org/10.1130/0016-7606(1985)96<1251:OATEOT>2.0.CO;2.

Nokleberg, W.J., Aleinikoff, J.N., Dutro, J.T., Lanphere, M.A., Silberling, N.J., Silva, S.R., Smith, T.E., and Turner, D.L., 1992a, Map, tables, and summary of fossil and isotopic age data, Mount Hayes quadrangle, eastern Alaska Range, Alaska, U.S. Geological Survey Miscellaneous Investigations Map 1996-D, scale 1:250,000.

Nokleberg, W.J., Aleinikoff, J.N., Lange, L.M., Silva, S.R., Miyaoka, R.T., Schwab, C.E., and Zehner, R.E., 1992b, Preliminary geologic map of the Mount Hayes quadrangle, eastern Alaska Range, Alaska: U.S. Geological Survey Open-File Report 92-594, scale 1:250,000.

Oriolo, S., Oyhantçabal, P., Wemmer, K., Basei, M.A., Benowitz, J., Pfänder, J., Hannich, F., and Siegesmund, S., 2016, Timing of deformation in the Sarandí del Yí Shear Zone, Uruguay: Implications for the amalgamation of western Gondwana during the Neoproterozoic Brasiliano-Pan-African Orogeny: Tectonics, v. 35, p. 754-771.

Pang, K.N., Chung, S.L., Zarrinkoub, M.H., Khatib, M.M., Mohammadi, S.S., Chiu, H.Y., Chu, C.H., Lee, H.Y., and Lo, C.H., 2013, Eocene–Oligocene post-collisional magmatism in the Lut-Sistan region, eastern Iran: Magma genesis and tectonic implications: Lithos, v. 180, p. 234–251, https://doi.org/10.1016/j.lithos.2013.05.009.

Pavlis, T.L., and Roeske, S.M., 2007, The Border Ranges fault system, southern Alaska, *in* Ridgway, K.D., Trop, J.M., Glen, J.M.G., and O'Neill, J.M., eds., Tectonic Growth of a Collisional Continental Margin: Crustal Evolution of Southern Alaska: Geological Society of America Special Paper 431, p. 95–127, https://doi.org/10.1130/2007.2431(05).

Pearce, J.A., 1996, A user's guide to basalt discrimination diagrams, *in* Wyman, D.A., ed., Trace Element Geochemistry of Volcanic Rocks: Applications for Massive Sulphide Exploration: Geological Association of Canada, Short Course Notes, 12, p. 79–113.

Pearce, J.A., 2008, Geochemical fingerprinting of oceanic basalts with applications to ophiolite classification and the search for Archean oceanic crust: Lithos, v. 100, p. 14–48, https://doi.org/10.1016/j.lithos.2007.06.016.

Pearce, J.A., and Parkinson, I.J., 1993, Trace element models for mantle melting—Application to volcanic arc petrogenesis, *in* Prichard, H.M. Alabaster, T., Harris, N.B.W., and Neary, C.R., eds., Magmatic Processes and Plate Tectonics: Geological Society of London Special Publication 76, p. 373–403.

Pearce, J.A., Harris, N.B., and Tindle, A.G., 1984, Trace element discrimination diagrams for the tectonic interpretation of granitic rocks: Journal of Petrology, v. 25, p. 956–983, https://doi.org/10.1093/petrology/25.4.956.

Peltzer, G., and Tapponnier, P., 1988, Formation and evolution of strike-slip faults, rifts, and basins during the India-Asia collision: An experimental approach: Journal of Geophysical Research. Solid Earth, v. 93, p. 15,085–15,117, https://doi.org/10.1029/JB093iB12p15085.

Perry, S., Fitzgerald, P.G., and Benowitz, J., 2010, Thermotectonic evolution of the Eastern Alaska Range: Constraints from low-temperature thermochronology: 12th International Conference on Thermochronology, p. 16–20.

Plafker, G., and Berg, H., 1994, An overview of the geology and tectonic evolution of Alaska, *in* Plafker, G., and Berg, H., eds., The Geology of Alaska: Boulder, Colorado, Geological Society of America, Geology of North America, v. G-1, p. 989–1021, https://doi.org/10.1130/DNAG-GNA-G1.989.

Reed, B.L., and Lanphere, M.A., 1973, Alaska-Aleutian Range batholith; Geochronology, chemistry, and relation to circum-Pacific plutonism: Geological Society of America Bulletin, v. 84, p. 2583–2610, https://doi.org/10.1130/0016-7606(1973)84<2583:ARBGCA>2.0.CO;2.

Reed, B.L., and Lanphere, M.A., 1974, Offset plutons and history of movement along McKinley segment of Denali-fault-system, Alaska: Geological Society of America Bulletin, v. 85, p. 1883–1892, https://doi.org/10.1130/0016-7606(1974)85<1883:OPAHOM>2.0.CO;2.

Reiners, P.W., Nelson, B.K., and Nelson, S.W., 1996, Evidence for multiple mechanisms of crustal contamination of magma from compositionally zoned plutons and associated ultramafic intrusions of the Alaska Range: Journal of Petrology, v. 37, p. 261–292, https://doi.org/10.1093/petrology/37.2.261.

Reiners, P.W., Ehlers, T.A., and Zeitler, P.K., 2005, Past, present, and future of thermochronology: Reviews in Mineralogy and Geochemistry, v. 58, p. 1–18, https://doi.org/10.2138/rmg.2005.58.1.

Riccio, S.J., Fitzgerald, P.G., Benowitz, J.A., and Roeske, S.M., 2014, The role of thrust faulting in the formation of the eastern Alaska Range: Thermochronological constraints from the Susitna Glacier thrust fault region of the intracontinental strike-slip Denali fault system: Tectonics, v. 33, p. 2195–2217, https://doi.org/10.1002/2014TC003646.

Richter, D.H., 1976, Geologic map of the Nabesna quadrangle, Alaska: U.S. Geological Survey Miscellaneous Geological Investigations Series Map I-932, scale 1:250,000.

Richter, D.H., and Matson, N.A., Jr., 1971, Quaternary faulting in the eastern Alaska Range: Geological Society of America Bulletin, v. 82, p. 1529–1540, https://doi.org/10.1130/0016-7606(1971)82[1529:QFITEA]2.0.CO;2.

Richter, D.H., Smith, J.G., Lanphere, M.A., Dalrymple, G.B., Reed, B.L., and Shew, N., 1990, Age and progression of volcanism, Wrangell volcanic field, Alaska: Bulletin of Volcanology, v. 53, p. 29–44, https://doi.org/10.1007/BF00680318.

Rickwood, P.C., 1989, Boundary lines within petrologic diagrams which use oxides of major and minor elements: Lithos, v. 22, p. 247–263, https://doi.org/10.1016/0024-4937(89)90028-5.

Ridgway, K.D., and DeCelles, P.G., 1993, Stream-dominated alluvial-fan and lacustrine depositional systems in Cenozoic strike-slip basins, Denali fault system, Yukon Territory: Sedimentology, v. 40, p. 645–666, https://doi.org/10.1111/j.1365-3091.1993.tb01354.x.

Ridgway, K.D., Sweet, A.R., and Cameron, A.R., 1995, Climatically induced floristic changes across the Eocene–Oligocene transition in the northern high latitudes, Yukon Territory Canada: Geological Society of America Bulletin, v. 107, p. 676–696, https://doi.org/10.1130/0016-7606(1995)107<0676:CIFCAT>2.3.CO;2.

Ridgway, K.D., Trop, J.M., and Sweet, A.R., 1997, Thrust-top basin formation along a suture zone, Cantwell basin, Alaska Range: Implications for development of the Denali fault system: Geological Society of America Bulletin, v. 109, p. 505–523, https://doi.org/10.1130/0016-7606(1997)109<0505:TTBFAA>2.3.CO;2.

Ridgway, K.D., Trop, J.M., and Sweet, A.R., 1999, Stratigraphy, depositional systems, and age of the Tertiary White Mountain basin, Denali fault system, southwestern Alaska, *in* Pinney, D.S., and Davis, P.L., eds., Short Notes on Alaska Geology: Professional Report 119: Alaska Division of Geological and Geophysical Surveys, p. 77–84.

Ridgway, K.D., Trop, J.M., Nokleberg, W.J., Davidson, C.M., and Eastham, K.R., 2002, Mesozoic and Cenozoic tectonics of the eastern and central Alaska Range: Progressive basin development and deformation in a suture zone: Geological Society of America Bulletin, v. 114, p. 1480–1504, https://doi.org/10.1130/0016-7606(2002)114<1480:MACTOT>2.0.CO;2.

Ridgway, K.D., Thoms, E.E., Layer, P.W., Lesh, M.E., White, J.M., and Smith, S.V., 2007, Neogene transpressional foreland basin development on the north side of the central Alaska Range, Usibelli Group and Nenana Gravel, Tanana basin, *in* Ridgway, K.D., Trop, J.M., O'Neill, J.M.,

and Glen, J.M.G., eds., Tectonic Growth of a Collisional Continental Margin: Crustal Evolution of Southern Alaska: Geological Society of America Special Paper 431, p. 507–548, https://doi.org/10.1130/2007.2431(20).

Rioux, M., Hacker, B., Mattinson, J., Kelemen, P., Blusztajn, J., and Gehrels, G., 2007, Magmatic development of an intra-oceanic arc: High-precision U-Pb zircon and whole-rock isotopic analyses from the accreted Talkeetna arc, south-central Alaska: Geological Society of America Bulletin, v. 119, p. 1168–1184, https://doi.org/10.1130/B25964.1.

Roeske, S.M., Benowitz, J.A., and O'Sullivan, P.B., 2012, Late Eocene to Recent record of long-lived dextral slip along the transition from eastern to central Denali fault in the Alaska Range: Geological Society of America Abstracts with Programs, v. 44, no. 7, p. 634.

Romero, M., 2018, Geology, U-Pb geochronology, and Hf isotope geochemistry across the Alaska Range suture zone (South-Central Alaska): Insights to collisional processes and Cordilleran tectonics [MS thesis]: West Lafayette, Indiana, Purdue University.

Rubin, C.M., Saleeby, J.B., Cowan, D.S., Brandon, M.T., and McGroder, M.F., 1990, Regionally extensive mid-Cretaceous west-vergent thrust system in the northwestern Cordillera: Implications for continental-margin tectonism: Geology, v. 18, p. 276–280, https://doi.org/10.1130/0091-7613(1990)018<0276:REMCWV>2.3.CO;2.

Salazar-Jaramillo, S., Fowell, S.J., McCarthy, P.J., Benowitz, J.A., Śliwiński, M.G., and Tomsich, C.S., 2016, Terrestrial isotopic evidence for a Middle-Maastrichtian warming event from the lower Cantwell Formation, Alaska: Palaeogeography, Palaeoclimatology, Palaeoecology, v. 441, p. 360–376, https://doi.org/10.1016/j.palaeo.2015.09.044.

Saltus, R., Hudson, T., and Wilson, F., 2007, The geophysical character of southern Alaska—Implications for crustal evolution, *in* Ridgway, K.D., Trop, J.M., Glen, J.M.G., and O'Neill, J.M., eds., Tectonic Growth of a Collisional Continental Margin: Crustal Evolution of Southern Alaska: Geological Society of America Special Paper 431, p. 1–20, https://doi.org/10.1130/2007.2431(01).

Saltus, R.W., Stanley, R.G., Haeussler, P.J., Jones, J.V., Potter, C.J., and Lewis, K.A., 2016, Late Oligocene to present contractional structure in and around the Susitna basin, Alaska—Geophysical evidence and geological implications: Geosphere, v. 12, p. 1378–1390, https://doi.org/10.1130/GES01279.1.

Solie, D.N., O'Sullivan, P.B., Werdon, M.B., Freeman, L.K., Newberry, R.J., Szumigala, D.J., and Hubbard, T.D., 2014, Zircon U-Pb age data, Alaska Highway Corridor, Tanacross and Nabesna quadrangles: Alaska Division of Geological and Geophysical Surveys, Raw Data File 2014-16, 29 p.

St. Amand, P., 1957, Geological and geophysical synthesis of the tectonics of portions of British Columbia, the Yukon Territory, and Alaska: Geological Society of America Bulletin, v. 68, p. 1343–1370, https://doi.org/10.1130/0016-7606(1957)68[1343:GAGSOT]2.0.CO;2.

Stachnik, J.C., Abers, G.A., and Christensen, D.H., 2004, Seismic attenuation and mantle wedge temperatures in the Alaska subduction zone: Journal of Geophysical Research. Solid Earth, v. 109, https://doi.org/10.1029/2004JB003018.

Stanley, R.G., 1987, Thermal maturity and petroleum-source potential of the Cantwell Formation (Paleocene), Alaska Range: Geologic Studies in Alaska by the U.S. Geological Survey during 1986: U.S. Geological Survey Circular 998, p. 104–107.

Stern, R.J., and Scholl, D.W., 2010, Yin and yang of continental crust creation and destruction by plate tectonic processes: International Geology Review, v. 52, p. 1–31, https://doi.org/10.1080/00206810903332322.

Stevens Goddard, A., Trop, J.M., and Ridgway, K.D., 2018, Detrital zircon record of Mesozoic collisional forearc basin dynamics in south-central Alaska: The tectonic transition from an oceanic to continental arc system: Tectonics, https://doi.org/10.1002/2017TC004825.

Stout, J.H., and Chase, C.G., 1980, Plate kinematics of the Denali fault system: Canadian Journal of Earth Sciences, v. 17, p. 1527–1537, https://doi.org/10.1139/e80-160.

Sun, S., and McDonough, W.F., 1989, Chemical and isotopic systematics of oceanic basalts: Implications for mantle compositions and processes, *in* Saunders, A.D., and Norry, M.J., eds., Magmatism in the Ocean Basins: Geological Society of London, Special Publication 42, p. 313–345, https://doi.org/10.1144/GSL.SP.1989.042.01.19.

Tait, L.D., 2017, Strain and vorticity analysis of mid-crustal rocks exhumed along the Denali Fault in the Eastern Alaska Range [M.S. thesis]: University of California, Davis, 76 p.

Terhune, P., 2018, Cenozoic tectono-thermal history of the southern Talkeetna Mountains, Alaska: Multiple topographic development drivers through time [M.S. thesis]: University of Alaska Fairbanks, 142 p.

Tetreault, J., and Buiter, S., 2014, Future accreted terranes: A compilation of island arcs, oceanic plateaus, submarine ridges, seamounts, and continental fragments: Solid Earth, v. 5, p. 1243–1275, https://doi.org/10.5194/se-5-1243-2014.

Tomsich, C.S., McCarthy, P.J., Fowell, S.J., and Sunderlin, D., 2010, Paleofloristic and paleoenvironmental information from a Late Cretaceous (Maastrichtian) flora of the lower Cantwell Formation near Sable Mountain, Denali National Park, Alaska: Palaeogeography, Palaeoclimatology, Palaeoecology, v. 295, p. 389–408, https://doi.org/10.1016/j.palaeo.2010.02.023.

Tomsich, C.S., McCarthy, P.J., Fiorillo, A.R., Stone, D.B., Benowitz, J.A., and O'Sullivan, P.B., 2014, New zircon U-Pb ages for the Lower Cantwell Formation: Implications for the Late Cretaceous paleoecology and paleoenvironment of the Lower Cantwell Formation near Sable Mountain, Denali National Park and Preserve, central Alaska Range, USA: St. Petersburg, Proceedings, VI International Conference on Arctic Margins (ICAM), VSEGEI, p. 19–60.

Torsvik, T.H., Doubrovine, P.V., Steinberger, B., Gaina, C., Spakman, W., and Domeier, M., 2017, Pacific plate motion change caused the Hawaiian-Emperor Bend: Nature Communications, v. 8, no. 15660, https://doi.org/10.1038/ncomms15660.

Trop, J.M., 2008, Latest Cretaceous forearc basin development along an accretionary convergent margin: South-central Alaska: Geological Society of America Bulletin, v. 120, p. 207–224, https://doi.org/10.1130/B26215.1.

Trop, J.M., and Ridgway, K.D., 1997, Petrofacies and provenance of a Late Cretaceous suture zone thrust-top basin, Cantwell Basin, central Alaska Range: Journal of Sedimentary Research, v. 67, p. 469–485.

Trop, J.M., and Ridgway, K.D., 2007, Mesozoic and Cenozoic tectonic growth of southern Alaska: A sedimentary basin perspective, *in* Ridgway, K.D., Trop, J.M., Glen, J.M.G., and O'Neill, J.M., eds., Tectonic Growth of a Collisional Continental Margin: Crustal Evolution of Southern Alaska: Geological Society of America Special Paper 431, p. 55–94, https://doi.org/10.1130/2007.2431(04).

Trop, J.M., Ridgway, K.D., Manuszak, J.D., and Layer, P.W., 2002, Mesozoic sedimentary basin development on the allochthonous Wrangellia composite terrane, Wrangell Mountains basin, Alaska: A long-term record of terrane migration and arc construction: Geological Society of America Bulletin, v. 114, p. 693–717, https://doi.org/10.1130/0016-7606(2002)114<0693:MSBDOT>2.0.CO;2.

Trop, J.M., Ridgway, K.D., and Sweet, A.R., 2004, Stratigraphy, palynology, and provenance of the Colorado Creek basin: Oligocene transpressional tectonics along the central Denali fault system: Canadian Journal of Earth Sciences, v. 41, p. 457–480, https://doi.org/10.1139/e04-003.

Trop, J.M., Hart, W.K., Snyder, D., and Idleman, B., 2012, Miocene basin development and volcanism along a strike-slip to flat-slab subduction transition: Stratigraphy, geochemistry, and geochronology of the central Wrangell volcanic belt, Yakutat-North America collision zone: Geosphere, v. 8, p. 805–834, https://doi.org/10.1130/GES00762.1.

Vallage, A., Deves, M.H., Klinger, Y., King, G.C.P., and Ruppert, N.A., 2014, Localized slip and distributed deformation in oblique settings: The example of the Denali fault system, Alaska: Geophysical Journal International, v. 197, no. 3, p. 1284–1298, https://doi.org/10.1093/gji/ggu100.

Veenstra, E., Christensen, D.H., Abers, G.A., and Ferris, A., 2006, Crustal thickness variation in south-central Alaska: Geology, v. 34, p. 781–784, https://doi.org/10.1130/G22615.1.

Wahrhaftig, C., 1958, Quaternary geology of the Nenana River valley and adjacent part of the Alaska Range, *in* Wahrhaftig, C., and Black, R.F., eds., Quaternary and Engineering Geology in the Central Part of the Alaska Range: U.S. Geological Survey Professional Paper 293, 73 p.

Waldien, T.S., Roeske, S.M., Benowitz, J.A., Allen, W.K., Ridgway, K.D., and O'Sullivan, P.B., 2018, Late Miocene to Quaternary evolution of the McCallum Creek thrust system, Alaska: Insights for range-boundary thrusts in transpressional orogens: Geosphere, v. 14, p. 2379–2406, https://doi.org/10.1130/GES01676.1.

Wang, Y., and Tape, C., 2014, Seismic velocity structure and anisotropy of the Alaska subduction zone based on surface wave tomography: Journal of Geophysical Research. Solid Earth, v. 119, p. 8845–8865, https://doi.org/10.1002/2014JB011438.

Wilson, F.H., Hults, C.P., Mull, C.G., and Karl, S.M., 2015, Geologic map of Alaska: U.S. Geological Survey Scientific Investigations Map 3340, pamphlet, 196 p., 2 sheets, scale 1:1,584,000, https://doi.org/10.3133/sim3340.

Wolfe, J.A., and Wahrhaftig, C., 1970, The Cantwell Formation of the central Alaska Range, *in* Cohee, G.V., Bates, R.G., and Wright, W.B., eds., Changes in Stratigraphic Nomenclature by the U.S. Geological Survey, 1968: U.S. Geological Survey Bulletin 1294-A, p. A41–A46.

Worthington, L.L., Van Avendonk, H.J., Gulick, S.P., Christeson, G.L., and Pavlis, T.L., 2012, Crustal structure of the Yakutat Terrane and the evolution of subduction and collision in southern Alaska: Journal of Geophysical Research, v. 117, B01102, https://doi.org/10.1029/2011JB008493.

Yokelson, I., Gehrels, G.E., Pecha, M., Giesler, D., White, C., and McClelland, W.C., 2015, U-Pb and Hf isotope analysis of detrital zircons from Mesozoic strata of the Gravina belt, southeast Alaska: Tectonics, v. 34, p. 2052–2066, https://doi.org/10.1002/2015TC003955.